

2-18-2021 2:00 PM

## Finite Element Analysis of Assembly for Warped Composite Automotive Components

Theogenes De Oliveira Maia, *The University of Western Ontario*

Supervisor: Tutunea-Fatan, Ovidiu-Remus, *The University of Western Ontario*

A thesis submitted in partial fulfillment of the requirements for the Master of Engineering Science degree in Mechanical and Materials Engineering

© Theogenes De Oliveira Maia 2021

Follow this and additional works at: <https://ir.lib.uwo.ca/etd>



Part of the [Computer-Aided Engineering and Design Commons](#), and the [Manufacturing Commons](#)

---

### Recommended Citation

De Oliveira Maia, Theogenes, "Finite Element Analysis of Assembly for Warped Composite Automotive Components" (2021). *Electronic Thesis and Dissertation Repository*. 7664.  
<https://ir.lib.uwo.ca/etd/7664>

This Dissertation/Thesis is brought to you for free and open access by Scholarship@Western. It has been accepted for inclusion in Electronic Thesis and Dissertation Repository by an authorized administrator of Scholarship@Western. For more information, please contact [wlsadmin@uwo.ca](mailto:wlsadmin@uwo.ca).

## **Abstract**

One of the most used processes in the automotive industry is the moulding of parts made of thermoplastics filled with glass fibers. This research focused on a specific material: long fiber thermoplastics (LFT). On the one hand, the performance gain, in terms of lightweighting and the strength of final components, justifies its wide use. On the other hand, due to the intrinsic characteristics of part manufacturing, warpage is evident and can influence or even compromise subsequent stages of production.

This research has three main objectives: recreate in the most faithfully way, in Abaqus<sup>TM</sup> environment, the conditions that precede the welding of LFT parts manufactured by moulding; compare gap distances between the assembly fixture and each part, due to their warpage, with the distances provided in the simulation; and finally, allow the prediction of the force acting on the welder head while the welding is performed.

## **Keywords**

LFT; warpage; simulation; Abaqus; welding.

## Summary for Lay Audience

The automotive industry adopts many strategies to produce more efficient vehicles in terms of fuel consumption. Some strategies include hybrid technology (electrical and fossil fuel engines working in parallel), engine power-efficiency and lightweight, which is the attempt to reduce the total mass of the vehicle, impacting and reducing its fuel consumption. On the latter, it is possible to simplify some vehicle systems or, instead, change the material of some components, opting for less dense alternatives, for instance, plastics and composite materials.

The composite material is a promising avenue in terms of technological development. It allows the engineering of parts, combining properties of different materials trying to reach a more efficient use of them with either the same or better performance. However, such a technological option presents its inherent challenges, being the prominent ones the dimensional reliability and precision along its manufacturing process. Dimensional variability observable at each intermediate step involve, for instance, shrinkage, expansion and warpage.

Parallel to it, joining parts is a technique that allows the production of parts with more complex geometries when the material change is not a good option. In some cases, both (change of materials and joining techniques) opens new developmental avenues. One of the joining techniques applicable to composite materials and one of the most efficient is ultrasonic welding, where parts are bonded by heating produced by friction and vibration.

This work tries to recreate the welding process of specific parts to measure the pressure (or force) imposed on each of them, producing data to estimate the force level during the process.

## Acknowledgments

Firstly, I would like to thank my supervisor, Dr. Remus Tutunea-Fatan, who offered me the opportunity to work on this project and oriented me to explore new avenues for my master's degree. The value of your comments, direct and indirect, draw new horizons in my academic, professional and even personal life. Usually, the impact we cause in others' lives passes either little or unnoticed, and I hope this is not the case. You introduced me to all persons available at Western University that could offer a helping hand and share knowledge. For all your effort, I thank you.

Secondly, I would like to acknowledge Ryan Gergely and Dave Okonski, from General Motors Company. All our discussions, meetings, and insightful questions helped pave the way for what is written here. I also would like to thank you for the availability of tools, possible through your additional work, to permit this work's proper conclusion. Thank you.

Next, I would like to thank Stanislav Ivanov and Navraj Singh for the prompt effort to put my contribution into context. Your project's handling oriented my academic work to reach expectations from different project-steps. It helped me recognize where to put more effort and make it more straightforward and accessible in ampler contexts. I also would like to thank Dominic Doer for all contributions and scrutiny over my simulation work. Without a doubt, I owe you a lot for insightful solutions adopted inside Abaqus<sup>TM</sup>. For all your orientations, questions and valuable knowledge, I thank you.

Finally, I would like to acknowledge my research colleagues, family and friends. To Eric, Brody, Thomas, David and Marco, my great thanks not only for your close help and technical knowledge but also for building a friendly environment during the time we had the chance to work side-by-side. To my wife, family and friends, you are a cornerstone for all I do, where I can find a haven to explore further. My most sincere thanks.

# Table of Contents

Abstract .....	ii
Summary for Lay Audience .....	iii
Acknowledgments .....	iv
Table of Contents .....	v
List of Tables .....	viii
List of Figures .....	ix
List of Abbreviations .....	xv
Chapter 1 : Introduction .....	1
1.1 Overview .....	1
1.2 State of the Art .....	1
1.2.1 Composite Materials and Lightweight in Automotive Industry .....	1
1.2.2 Compression Moulding Composites .....	2
1.2.3 Ultrasonic Welding .....	3
1.3 Motivation .....	4
1.4 Research Objectives .....	5
1.5 Contributions .....	8
1.6 Thesis Overview .....	8
Chapter 2 : Pre-processing and Warping Simulations .....	10
2.1 Overview .....	10
2.2 Pre-processing and Mesh Creation .....	11
2.1.1 Element Type .....	13
2.1.2 Meshing in HyperMesh .....	15
2.3 Warping Field .....	16
2.4 Seat Back Outer Warping Model .....	21

2.5 Seat Back Inner Warping Model.....	25
2.6 Chapter Summary.....	28
Chapter 3 : Pre-Clamping Simulations .....	29
3.1 Overview .....	29
3.2 Two-Part Simulation .....	29
3.3 Three-Part Simulation .....	38
3.4 Chapter Summary.....	42
Chapter 4 : Clamping and Welding Simulations .....	43
4.1 Overview .....	43
4.2 Clamping Pattern and Sequence.....	43
4.3 Clamping Simulations .....	46
4.3.1 First Clamping Simulation .....	46
4.3.2 Second Clamping Simulation .....	50
4.3.3 Third Clamping Simulation .....	53
4.3.4 Gap Comparison after Clamping .....	55
4.4 Welding Simulations.....	56
4.4.1 Possible Welding Points .....	57
4.4.2 Welding Simulation Set-up.....	58
4.5 Chapter Summary.....	61
Chapter 5 : Analysis of Welding Measurements .....	62
5.1 Overview .....	62
5.2 Pressure vs. Displacement curves .....	62
5.2.1 Sections of Pressure vs. Displacement Curves .....	65
5.3 Experimental Data and Comparisons.....	72
5.3.1 Comparison of Pressure vs. Displacement curves .....	72
5.4 Chapter Summary.....	76

Chapter 6 : Parametric Studies.....	78
6.1 Overview .....	78
6.2 Parametric Studies Description .....	78
6.3 Change in Material Properties.....	80
6.4 Change in Warped and Not Warped Parts .....	94
6.5 Change in Clamping Pattern .....	106
6.6 Chapter Summary.....	116
Chapter 7 : Conclusion and Future Work .....	117
7.1 Conclusions .....	117
7.2 Future Work .....	119
References .....	121
Appendices.....	123
Appendix A: Mid-surface Meshing Method .....	123
Mid-surface Simplification .....	123
Appendix B: Top-surface Meshing Method .....	123
Top-surface Simplification .....	123
Appendix C: MATLAB scripts .....	124
C.1 - TxtWork.m script.....	124
C.2 - Nset.m script .....	125
C.3 - CompCopy.m script .....	126
C.4 - WriteNset.m script .....	127
C.5 - BcWrite.m script .....	127
CurriculumVitae .....	130

# **List of Tables**

Table 2.1: Resulting overlay for SBO.....	24
Table 2.2: Resulting overlay for SBI .....	27
Table 4.1: Clamping Points coordinates .....	44
Table 4.2: Measures and BC for Clamps 1, 2, and 3 .....	48
Table 4.3: Measures and BC for Clamps 4 and 5 .....	51
Table 4.4: Measures and BC for Clamps 6 and 7 .....	53
Table 4.5: Gap Measurements .....	56
Table 4.6: Maximum Force Measured at Welding Points .....	60
Table 4.7: Welding Simulation Time.....	61
Table 5.1: Estimate of vertical displacement required.....	64
Table 6.1: Parametric Study summarized .....	79
Table 6.2: Material Properties for parametric study .....	81
Table 6.3: Comparison Simulation Time (LFT-Anisotropic).....	87
Table 6.4: Comparison Simulation Time (GMT-Isotropic).....	93
Table 6.5: Summary of Warpage Change.....	94
Table 6.6: Comparison Simulation Time (1st Case-WIO) .....	98
Table 6.7: Comparison Simulation Time (2nd Case-IWO) .....	102
Table 6.8: Comparison Simulation Time (3rd Case-IO) .....	105



# List of Figures

Figure 1.1: Schematic of compression moulding (adapted from Ketabchi et al., [3]).....	3
Figure 1.2: Ultrasonic Welding – Schematic (adapted from Roos and Kalas, [4]) .....	4
Figure 1.3: (a) Seatback Inner (SBI) and (b) Seatback Outer (SBO) .....	6
Figure 1.4: Theoretical Assembly SBO + SBI.....	6
Figure 1.5: Pre-welding Assembly with fixture, SBO and SBI (clamps closed).....	7
Figure 2.1: Warped Mesh creation.....	10
Figure 2.2: Laser scanned data for SBO .....	12
Figure 2.3: Imprecise geometry detected in Abaqus™ .....	12
Figure 2.4: Linear and Quadratic elements in Abaqus™ (adapted from Abaqus/CAE User’s Manual, Dassault Systems, 2010 [12]) .....	14
Figure 2.5: PolyWorks alignment after HyperMesh surface extraction .....	17
Figure 2.6: Disagreements along principal axes .....	17
Figure 2.7: Points in z-group being measured .....	20
Figure 2.8: (a) Boundary Conditions to deform SBO and (b) Resulting mesh, displacement (mm).....	23
Figure 2.9: Colour Map after deforming SBO CAD mesh – Distance in mm.....	24
Figure 2.10: (a) Boundary Conditions to deform SBI and (b) Resulting mesh, displacement (mm).....	26
Figure 2.11: Colour Map after deforming SBI CAD mesh – Distance in mm .....	27
Figure 3.1: Assembly fixture after simplification.....	30

Figure 3.2: Fixture meshed with Reference Point defined .....	31
Figure 3.3: Surfaces defined on the fixture mesh .....	31
Figure 3.4: Surfaces defined on the SBO mesh .....	32
Figure 3.5: (a) Surface-to-surface and (b) Node-to-surface discretization (adapted from Abaqus Analysis User's Guide version 6.14, Dassault Systems [12]) .....	34
Figure 3.6: Regions with the smallest gap in the actual assembly: (a) between SBO and fixture; (b) between SBI and SBO. ....	36
Figure 3.7: Boundary condition for SBO placement over the fixture.....	37
Figure 3.8: 2-part result z-displacement (mm) .....	38
Figure 3.9: Additional surfaces defined on the SBO mesh.....	40
Figure 3.10: Surfaces defined on the SBI mesh.....	40
Figure 3.11: Boundary condition for SBI placement over SBO.....	41
Figure 3.12: 3-part result z-displacement (mm) .....	42
Figure 4.1: Clamping points .....	44
Figure 4.2: Measurement locally done at Clamp 1 position .....	47
Figure 4.3: BC for Clamps 1, 2 and 3 .....	49
Figure 4.4: Stress distribution after Clamps 1, 2, and 3 – (MPa) .....	50
Figure 4.5: BC for Clamps 1 through 5 (Clamps 4 and 5 highlighted) .....	52
Figure 4.6: Stress Distribution after Clamps 4 and 5 – (MPa) .....	52
Figure 4.7: BC for Clamps 1 through 7 (Clamps 6 and 7 highlighted) .....	54
Figure 4.8: Stress distribution after Clamps 6 and 7 – (MPa) .....	54

Figure 4.9: Gap Measuring Points .....	55
Figure 4.10: Possible welding points .....	57
Figure 4.11: Welding Head model (touching surface highlighted) .....	59
Figure 4.12: Area selected .....	59
Figure 4.13: Welding boundary condition (purple arrow) and clamps.....	60
Figure 5.1: Pressure vs. Displacement plot for welding point A.....	62
Figure 5.2: Pressure vs. Displacement plot for welding point AA.....	63
Figure 5.3: Pressure vs. Displacement plot for welding point S.....	63
Figure 5.4: Contact distribution before welding point A (mm): (a) SBI and SBO; (b) SBO and fixture .....	65
Figure 5.5: Pressure versus Displacement for welding point A (increments numbered) .....	66
Figure 5.6: Contact closure at welding point A during Increment 2 (mm): (a) SBI and SBO; (b) SBO and fixture.....	66
Figure 5.7: Contact closure at welding point A during Increment 7 (mm): (a) SBI and SBO; (b) SBO and fixture.....	67
Figure 5.8: Contact closure at welding point A between SBI and SBO (mm): (a) Increment 2; (b) Increment 7.....	67
Figure 5.9: Contact closure at welding point A during Increment 16 (mm): (a) SBI and SBO; (b) SBO and fixture.....	68
Figure 5.10: Contact closure at welding point A during Increment 18 (mm): (a) SBI and SBO; (b) SBO and fixture.....	69
Figure 5.11: Contact closure at welding point A between SBO and fixture (mm): (a) Increment 16; (b) Increment 18 .....	69

Figure 5.12: Gap measurement at welding point S .....	70
Figure 5.13: Experimental Pressure versus Displacement plot: (a) welding point A, (b) welding point AA, (c) welding point S .....	73
Figure 5.14: Comparison plots: (a) welding point A, (b) welding point AA, (c) welding point S .....	74
Figure 6.1: Pressure-displacement curve comparing Isotropic and Anisotropic LFT – point A .....	81
Figure 6.2: Pressure-displacement curve comparing Experimental and Anisotropic LFT – point A .....	82
Figure 6.3: Pressure-displacement curve comparing Isotropic and Anisotropic LFT – point AA.....	83
Figure 6.4: Pressure-displacement curve comparing Experimental and Anisotropic LFT – point AA.....	84
Figure 6.5: Pressure-displacement curve comparing Isotropic and Anisotropic LFT – point S .....	85
Figure 6.6: Pressure-displacement curve comparing Experimental and Anisotropic LFT – point S .....	86
Figure 6.7: Pressure-displacement curve comparing LFT-Isotropic and GMT-Isotropic – point A .....	88
Figure 6.8: Pressure-displacement curve comparing Experimental data and GMT-Isotropic – point A .....	89
Figure 6.9: Pressure-displacement curve comparing LFT-Isotropic and GMT-Isotropic – point AA.....	89
Figure 6.10: Pressure-displacement curve comparing Experimental data and GMT-Isotropic – point AA.....	90

Figure 6.11: Pressure-displacement curve comparing LFT-Isotropic and GMT-Isotropic – point S .....	91
Figure 6.12: Pressure-displacement curve comparing Experimental data and GMT-Isotropic – point S .....	92
Figure 6.13: Pressure-displacement comparing the base-case with 1st Case - point A.....	95
Figure 6.14: Pressure-displacement comparing the base-case with 1st Case - point AA.....	96
Figure 6.15: Pressure-displacement comparing the base-case with 1st Case - point S .....	97
Figure 6.16: Pressure-displacement comparing the base-case with 2nd Case - point A .....	99
Figure 6.17: Pressure-displacement comparing the base-case with 2nd Case - point AA ...	100
Figure 6.18: Pressure-displacement comparing the base-case with 2nd Case - point S .....	101
Figure 6.19: Pressure-displacement comparing the base-case with 3rd Case - point A.....	102
Figure 6.20: Pressure-displacement comparing the base-case with 3rd Case - point AA ....	103
Figure 6.21: Pressure-displacement comparing the base-case with 3rd Case - point S.....	104
Figure 6.22: New Clamping Patterns: (a) 5 clamps, (b) 3 clamps .....	106
Figure 6.23: Pressure-displacement plot comparing LFT-Isotropic (base-case) with 2nd clamping pattern – point A .....	107
Figure 6.24: Pressure-displacement plot comparing LFT-Isotropic (base-case) with 2nd clamping pattern – point AA.....	108
Figure 6.25: Pressure-displacement plot comparing LFT-Isotropic (base-case) with 2nd clamping pattern – point S .....	109
Figure 6.26: Pressure-displacement plot comparing LFT-Isotropic (base-case) with 3rd clamping pattern – point A .....	110

Figure 6.27: Pressure-displacement plot comparing 2nd with 3rd clamping patterns – point A .....	111
Figure 6.28: Pressure-displacement plot comparing LFT-Isotropic (base-case) with 3rd clamping pattern – point AA.....	112
Figure 6.29: Pressure-displacement plot comparing 2nd with 3rd clamping patterns – point AA.....	113
Figure 6.30: Pressure-displacement plot comparing LFT-Isotropic (base-case) with 3rd clamping pattern – point S .....	114
Figure 6.31: Pressure-displacement plot comparing 2nd with 3rd clamping patterns – point S .....	115

## List of Abbreviations

FRC	Fibre Reinforced Composites
LFT	Long Fibre Thermoplastic
GMT	Glass Mat Thermoplastic
LFT-D	Long Fibre Thermoplastic – Direct
SBI	Seatback Inner
SBO	Seatback Outer
CAD	Computer Aided Design
STL	Standard Tessellation Language (stereolithography)
CAE	Computer Aided Engineering
FEM	Finite Elements Method
TM	Trade mark
RF	Reference Point
BC	Boundary Condition

# Chapter 1 : Introduction

## 1.1 Overview

This chapter presents a summary and description of all the subjects covered in this thesis. Then, literary references, motivation, and objectives will be presented. Finally, the general structure of the chapters of this thesis is briefly presented.

## 1.2 State of the Art

### *1.2.1 Composite Materials and Lightweight in Automotive Industry*

Given the vast literature on the subject, composite materials can be defined as the combination of two or more materials or phases to achieve properties synergically that could not be achieved by using them alone. These are materials in which a discontinuous phase (particles, fibres or laminates) impregnates a continuous phase (matrix). Depending on the application and the properties to be optimized, the type of matrix and filler differs. In general terms, the gain in specific strength represents the goal of optimization. This gain means efficient use of the mass regarding the stresses and forces to which the components are subjected.

Within the scope of the project "Process Evaluation of Long-glass Fibre Reinforced Polyamides by Compression Moulding", a partnership between General Motors Company, Fraunhofer Project Centre for Composites Research and Western University, two composites were researched: long fibre thermoplastic (LFT) and glass mat thermoplastic (GMT).

Long fibre thermoplastic (LFT) consists of randomly oriented fibres, with high tensile modulus and tensile strength, impregnating a polymeric matrix. Some applications of such material can be found in seat structures, dashboards carriers and spare-wheel wells. Parts made of LFT can be manufactured either by direct compounding or using pre-compounded pellets, which already contain fibres and matrix combined. When produced



by direct compounding of fibres, the material is called LFT-D. More detailed descriptions of these processes and the justifications for their adoption can be found in the literature [1]. However, the main motives for the use of LFT-D to the pre-compounds pellets are the moulding's thermal cycle, the risk's reduction of degradation of the polymer matrix, and reduced energy consumption.

Glass mat thermoplastic (GMT) consist of a fiber mat combined with a thermoplastic polymer matrix. While for LFT parts, the manufacturing processes used range from injection moulding to compression moulding, allowing the combination of both, for GMT parts, the most common manufacturing process is compression moulding (or flow moulding). Depending on the fibres' length used in the sheets (chopped or continuous), GMT can present greater or lesser isotropy [2].

Although both materials were used in the project's broader scope, we used data from components manufactured in LFT-D to investigate the simulations of assembly and welding processes.

### *1.2.2 Compression Moulding Composites*

The compression moulding process can be applied to both thermoplastic and thermosetting matrix composites. When moulding thermoplastics, the material is often pre-heated to a specified temperature, while thermosettings do not require it. For both cases, the tool itself is pre-heated. Once the material is positioned, the press is closed. As pressure is applied to the material, it flows, filling the mould. The press keeps the pressure until the final part reaches thermal equilibrium with the mould when the upper half of the tool can be opened, and the part removed.

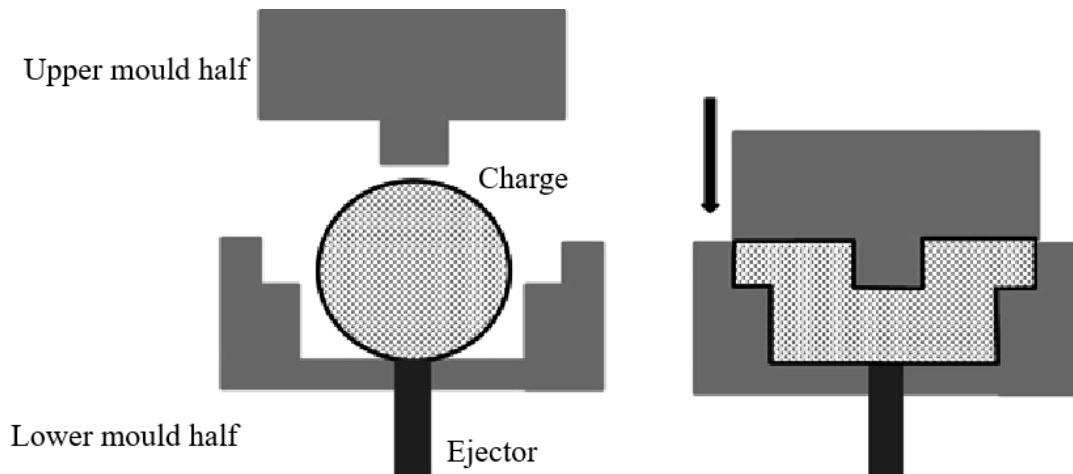


**Figure 1.1: Schematic of compression moulding (adapted from Ketabchi et al., [3])**

Among the advantages of using such a process can be mentioned: high quality of the surface finishing, productivity (especially when using constant temperature) and high fibre volumetric density is achieved (which improves part performance). Among the disadvantages can be cited: significantly costly for small production, certain geometrical features cannot be achieved without tooling modification and variable consolidation depending upon the surface's direction (with parallel or perpendicular to closure direction).

All data used in the simulations of this work were obtained from parts manufactured by compression moulding.

### *1.2.3 Ultrasonic Welding*

Ultrasonic welding consists of a joining technique that applies high-frequency sound waves combined with local pressure to bond materials together, requiring relatively less energy than alternative methods. As a brief description of the ultrasonic welding:

1. The parts to be welded are placed in a fixture;
2. The vertical horn contacts the upper part with pressure being applied to keep the contact;

3. Ultrasonic vibrations are delivered through the horn, heating both materials. The vibrations can be either up-and-down or side-to-side;
4. The materials melt, joining the parts together.

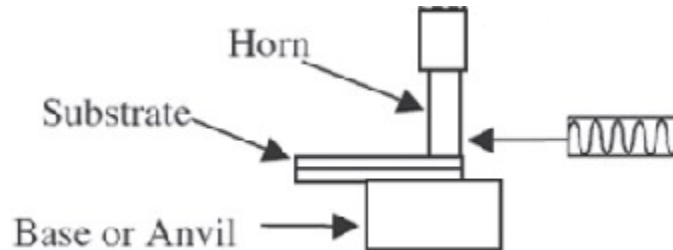


**Figure 1.2: Ultrasonic Welding – Schematic (adapted from Roos and Kalas, [4])**

Figure 1.2 shows a schematic of the procedure. Ultrasonic welding represents one of the most cost-efficient because of not using an open flame, torch or excessive heating. This work will pay special attention to the final assembly steps, in which the components are positioned in the fixation by clamps and further welded together.

### 1.3 Motivation

In the automotive industry, lightweight techniques correspond to efforts to optimize the use of materials in the efficient manufacture of products. In the past, these techniques were used to reduce production costs and promote the vehicles' sales by appealing to consumers' subjective values, such as emotions and images. The same techniques currently start to consider environmental aspects (materials' disposal and life cycle, for instance) and product performance, without losing sight of standards already reached [5].

The same industry still seeks techniques and materials that allow high productivity, besides those mentioned above. In this context, composite materials correspond to a possible solution due to versatility and economy (both in performance and manufacturing process). One of these composite materials that meet these requirements is the fibre-reinforced composites (FRC). However, some disadvantages arise from the manufacturing process of these composites, which must be addressed [6].

Compression moulding, one of the most widely used in the automotive industry and one of the most common processes applied to thermoplastic-matrix composite, forces the material's flow in-mould. As the part's geometry becomes more complex, fibre concentration and orientation are more affected, causing local changes in mechanical properties and surface and volume defects (geometric inaccuracy). Examples of such defects are shrinkage and warpage [7].

Once the moulding is done, those defects affect the next assembly steps, mainly joining processes because additional forces and stresses should be applied to put parts in place. In ultrasonic welding, the welding quality is directly related to the pressure applied by the welding machine's horn and the initial gap between the parts to be bonded. Besides, the welding machine itself encounters limitations on the maximum applied force to the welding horn [8].

If we have in mind the objective of accurately predict the pressure (or force) required to put both parts in-position for ultrasonic welding, the use of non-deformed CAD-parts will massively induce errors in final values because considerable warpage is detected. To overcome this hurdle, a procedure whose outcome is a warped mesh, starting from as-designed parts, is necessary. If this method can include some consistency across batches with different warping patterns, such a procedure will be an additional tool to analyze moulded samples.

## **1.4 Research Objectives**

This research aims to investigate the pressure (or force) required to close gaps of two warped parts in the welding assembly stage, as a function of the gap between them. Such an investigation will be carried out using suggested geometries for two components that form a vehicle's seatback. Figure 1.3 represents proposed geometries for each seatback components.

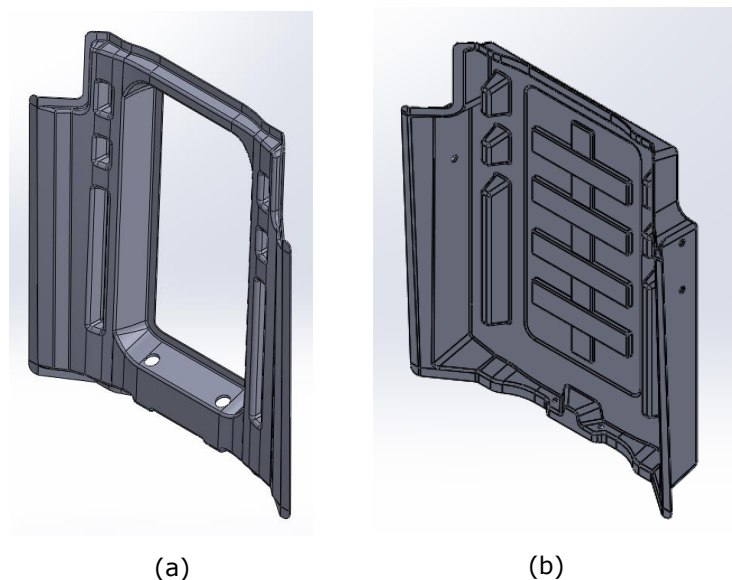


**Figure 1.3: (a) Seatback Inner (SBI) and (b) Seatback Outer (SBO)**

The final assembly of the whole seatback involves the overlapping of these components, being welded by ultrasonic welding. Figure 1.4 shows the theoretical assembly after welding. Both components are manufactured by compression moulding in the same material, LFT. Due to the fibre's orientation of the material used and limitations of the moulding process itself, both parts are produced without geometric precision, warpage being the most evident defect in our particular case.

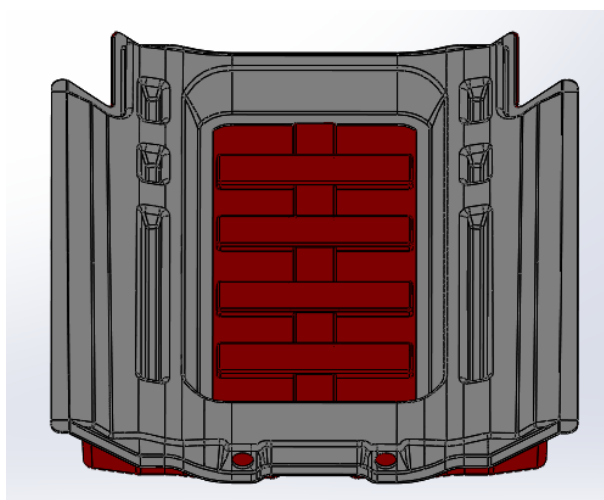


**Figure 1.4: Theoretical Assembly SBO + SBI**

In the real assembly, after moulding, the subsequent step is fixing both parts to a fixture by clamps. Figure 1.5 shows the real pre-welding set-up.

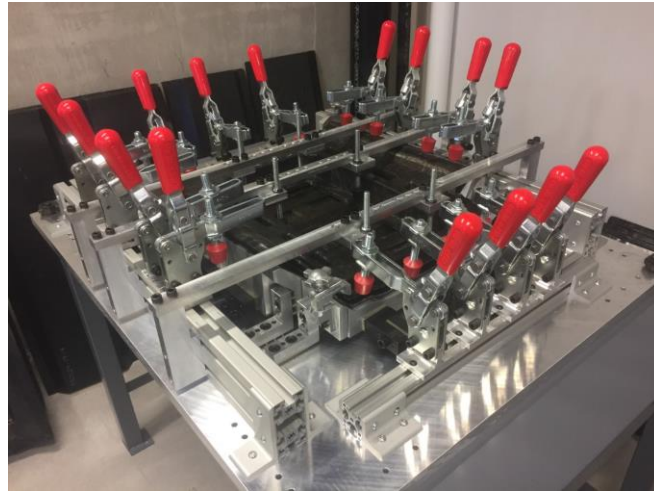


**Figure 1.5: Pre-welding Assembly with fixture, SBO and SBI (clamps closed)**

Due to this geometrical inaccuracy in both parts, gaps appear along the flanges where the welding must occur. However, to ensure the proper formation of the weld spots and the welding quality in the final product, such gaps must be closed by the welding machine itself, through the pressure applied by the horn.

In this context and given the research general objective, the following aims can be outlined:

- Propose types of elements to be used in the finite element method (FEM), considering computational resources, efficiency and precision of the final results;
- Propose a method of mapping the actual part's warpage to simulate, not components with ideal theoretical geometries, but real warped parts (warping method);
- Evaluate how efficient the warping method is within a pre-established acceptability criterion;

- Simulate the pre-welding stage, allowing to extract data of forces (pressure) and local stress to which the parts are subjected due to their warpage;
- Simulate the welding of the first weld spot after clamping, comparing the pressure (convertible to force) required to close the gap between parts in this location;
- Conduct the same set of simulations without the simplifying hypothesis of isotropic properties; thus, considering some anisotropic effect of local fibre concentration and local fibre orientations;
- Conduct the same set of simulations using new clamping patterns.

## 1.5 Contributions

As a consequence of the proposed intermediate objectives, this work aims to contribute by:

- Presenting the element's type to be used in the FEM of the suggested geometry, without shying away from discussing the non-use of alternative elements;
- Presenting an efficient warping method, using standard CAD tools, and applicable to different components, not only the geometry in question;
- Assessing the impact of the simplifying hypothesis of isotropic properties concerning the forces required for closing gaps during welding;
- Assessing the impact of clamping-welding relative position into the pressure (force) required to close gaps locally;
- Digitally predicting the pressure (force) exerted by the head of the welding machine (horn) as a function of the gap between the considered parts.

## 1.6 Thesis Overview

This section intends to present a summary of the following chapters.

Chapter 2 describes and discusses the pre-processing and warping procedures. The pre-processing branch will discuss the element's types available in Abaqus<sup>TM</sup> and how each of them fits the problem. The warping method branch will discuss the warping field's definition and its application to a CAD-based mesh. It will be discussed further how effective this method was for the geometries in question.

Chapter 3 describes the use of warped parts in the pre-clamping context. It will describe the whole set-up of a model involving two parts, SBO and fixture, recreating the situation in which this component is placed on the fixture. It will further describe the whole model's set-up involving three parts: SBI, SBO and fixture. Such simulation recreates the pre-clamping conditions.

Chapter 4 describes the clamping and welding simulations. The clamping scope describes how the clamping sequence is recreated in terms of boundary conditions adopted and parameters involved. The welding model deals with the simulation after all clamps are closed, in which the welder's horn welds a spot.

Chapter 5 discusses some measures made on the welding simulation. Pressure vs. displacement curves are extracted from the result and analyzed at each section. Later on, the same curves are compared with experimental data at the same points.

In Chapter 6 we conduct a parametric study, changing some parameters and analyzing their effect on the pressure vs. displacement curves produced. Such a study covers material properties, the use of warped and not warped parts and the clamping patterns.



## Chapter 2 : Pre-processing and Warping Simulations

### 2.1 Overview

In this chapter, the warpage pattern from a manufactured part is reproduced into a meshed solid and intrinsic details for this model are addressed. In next chapters, the warped mesh produced in such a way will be used in the clamping and welding simulations. Inevitably, it was necessary to manufacture batches of parts, which was done using a hydraulic compression press from Dieffernbacher on the premises of Fraunhofer Project Centre for Composites Research, to detect how each part warped after moulding conditions.

A brief overview of the method can be described consisting of:

1. Scanning of the top surface of each replica manufactured;
2. Meshing of the CAD geometry;
3. Reproduction of the warpage pattern of both SBO and SBI, by deforming specific nodes;
4. Comparison between the resulting solid mesh with scanned surface data.

The next figure pictures the whole method of creation of a warped mesh to be used in following simulations. Each process will be further described in next sections.

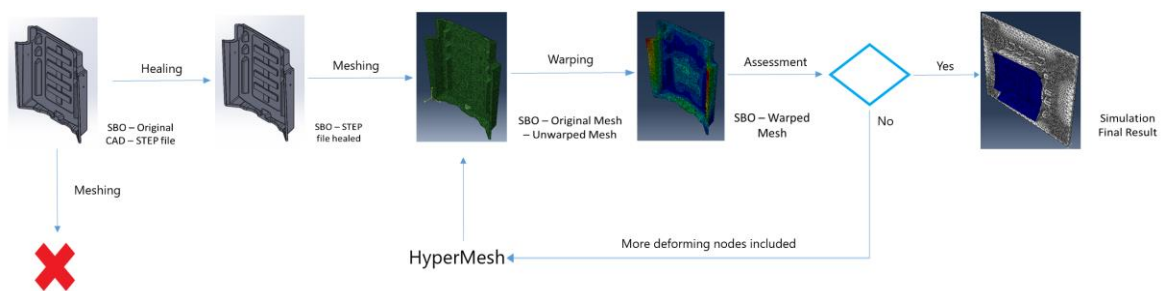


**Figure 2.1: Warped Mesh creation**

## 2.2 Pre-processing and Mesh Creation

Once the parts were produced, having reached thermal equilibrium, they were laser scanned to capture digitally the warpage pattern resulting from the manufacturing process. For this scanning activity, we used data produced at parallel branches of the same project. The data correspond to the laser-scanned surface of only one side of each replica manufactured.

For pre-processing, the creation of the mesh and the reproduction of the warping pattern the following software will be used:

1. PolyWorks Inspector
2. Autodesk Moldex<sup>TM</sup> Studio 2017 version;
3. HyperMesh
4. Abaqus/CAE 2017;
5. MATLAB R2019b;
6. Microsoft Office Applications (namely, Notepad and Excel)

For the sake of the description of the mesh creation, the pictures obtained for the Seat Back Outer (SBO) will be considered. Figure 2.2 shows the tessellated data (STL) produced by laser scanning, imported into Polyworks<sup>TM</sup> and correctly aligned to the coordinate system adopted throughout our method.

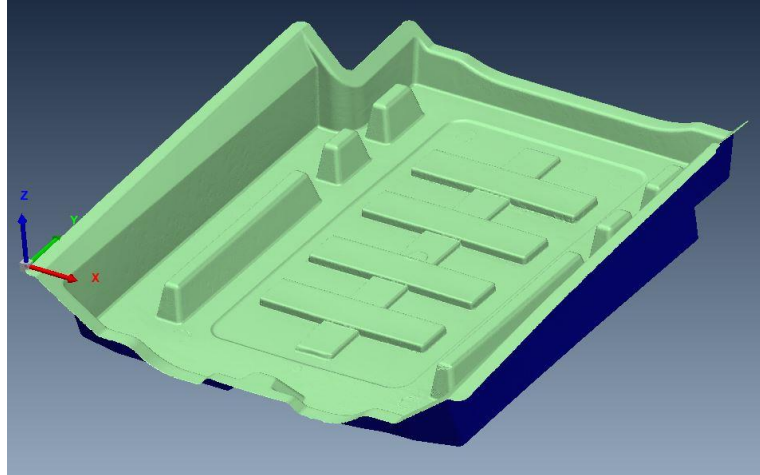


**Figure 2.2: Laser scanned data for SBO**

In parallel, Abaqus™ was initially employed to create the finite element mesh for the undistorted state of the part (CAD). However, in this attempt, the software automatically identifies imprecise geometry for both parts, SBO and SBI. The software also suggests alternative methods, like partitioning quad/hex elements for mesh creation. Figure 2.3 shows, in red, the location of such imprecise geometry for the SBO.

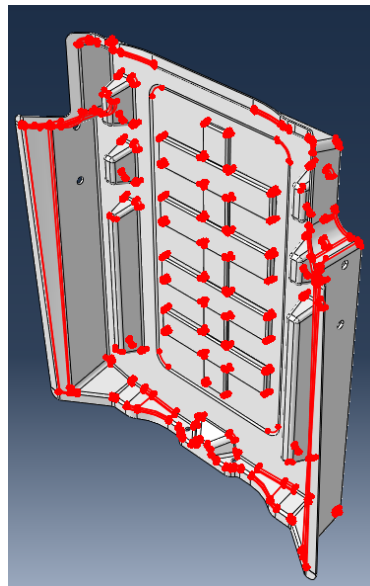


**Figure 2.3: Imprecise geometry detected in Abaqus™**

The presence of these regions of imprecise geometry could influence the quality or even the conclusion of the meshing process. A possible solution, to avoid not meshing or the generation of mesh elements with errors, was geometry simplification by removing fillets with reduced radius ( $r \leq 2.5 \text{ mm}$ ). The removed fillets represent most of the red regions identified in the previous figure. We employed Moldex<sup>TM</sup> to fix any eventual error of agreement between surfaces and remove fillets with reduced radii.

For the specific case of SBI, there was a severe disagreement between surfaces in the original CAD file. The solution adopted was to fill the gap between surfaces up to the point in which it would be possible to create a watertight CAD, allowing the mesh creation.

At this moment, it is essential to discuss which kind of element is most suitable to be used in our problem.

### *2.1.1 Element Type*

In this subsection, the possible choices of elements to be used are discussed for the correct representation of the results taking into consideration the options available in Abaqus<sup>TM</sup>.

Some attempts were made using two-dimensional elements. The use of either a mid-surface or the top surface representing the whole geometry showed to be cumbersome and not agreeing with the warping method further adopted. For more information, the Appendices section brings the initial development of both strategies (Appendices A and B).

Hence, given the geometric difficulties involved, it was opted to use three-dimensional elements. Within the category of three-dimensional elements, the following types can be enumerate: hexahedral-shaped (hex), triangular prism (wedge) and tetrahedral (tet). Figure 2.4 shows each previous element type, divided into linear and quadratic geometric orders.

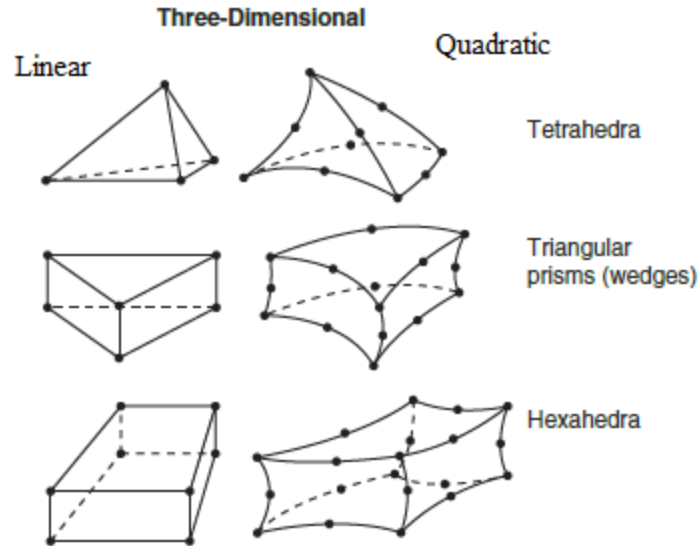


**Figure 2.4: Linear and Quadratic elements in Abaqus<sup>TM</sup> (adapted from Abaqus/CAE User's Manual, Dassault Systems, 2010 [12])**

Diving deeper into the options available for quadratic tetrahedral elements (tet), Abaqus<sup>TM</sup> presents four (4) different mathematical formulation options: regular (C3D10), modified (C3D10M), hybrid (C3D10H) and improved (C3D10I) [9].

The regular formulation (C3D10) is a textbook formulation for a second-order element. The main issue in the use of such elements occurs when applying uniform pressure to its face, producing zero nodal force at corner nodes. As a consequence, such elements are not suitable in simulations involving contact, as is the case. However, we can avoid such insufficiency by defining finite sliding in a surface-to-surface formulation.

The modified formulation (C3D10M) uses bilinear interpolation; then they cannot be called “true” second-order elements. Consequently, such elements are unable to produce quadratic curves as smooth as those produced by the regular formulation. The hybrid formulation (C3D10H) is mainly used in simulations involving incompressible materials, which does not correspond to the material in question.

Finally, the improved formulation (C3D10I) uses integration points coinciding with regular nodes. It presents promising results for stresses and strains being an excellent option for problems involving surface stresses and fatigue.

In conclusion, C3D10 elements will be employed when meshing both SBI and SBO accounting for finite sliding when defining contact between all parts involved in the final simulation [10].

The next subsection is going to describe how a mesh generated from a CAD model can be deformed, using the scanned data as its final target. This method allow to use consistently the same mesh (set of nodes and elements) changing the scanned data depending on the respective replica.

### *2.1.2 Meshing in HyperMesh*

For the creation of the meshes, Abaqus<sup>TM</sup> and HyperMesh<sup>TM</sup> were available. According to practice and tools available in both, HyperMesh<sup>TM</sup> allowed to edit nodes and meshes more directly and applies a more extensive range of criteria to assess and verify the resulting mesh. In the next paragraphs, the whole meshing method is described and all parameters selected are made explicit.

Once selected file is imported it into HyperMesh<sup>TM</sup>, the **3D** table is used, selecting to mesh the geometry as a **tetramesh**. On this option, a whole set of parameters are settable which were used to produce meshes acceptable in Abaqus<sup>TM</sup>. The set of parameters used are the following: in Volume tetra, 2D elements-triangles, 3D elements-tetrahedron, second-order elements, minimum element size-2.0, element size-4.0, use proximity, and use curvature.

Later on, the resulting mesh is Exported in the format of an Abaqus<sup>TM</sup> INP file. Note that, at this point, the final mesh still does not represent the actual warped component.

## 2.3 Warping Field

For clarification purposes, a warping field can be understood as a deformation field (coordinate-based) applied to a set of nodes contained in a mesh, which was generated from a CAD model, trying to coincide the position of such nodes with the scanned data from the warped component. It is a species of space correspondence between nodes of a undeformed geometry and a deformed one [11]. Such definition and its application will be better illustrated below.

Initially, the INP file generated by the last method was imported into HyperMesh™. The initial objective is to extract the mesh surface corresponding to surface scanned, presented, for instance, in Figure 2.2. The process of extraction consists of selecting faces, under lower panel of tools available, and configuring the option to select elements. Once this is done, the whole mesh in the visualization window is selected and picked and it is possible do find all faces. After that, a different configuration is created to receive all faces contained in the mesh.

In the entities tree, all components should be toggled off, except the last created component containing only faces. A new configuration is created to receive only the faces of interest in. In the viewing window, the option to select only faces is selected now. Under the same lower panel of tools, we should organize the chosen and selected elements in the view window to a specific destination component. For this, a single face is chosen in viewing window and, expanding the selection type using other faces as a criteria. By doing so, it will automatically select all faces adjacent to the single one chosen. If the software is not able to highlight all elements wanted, it is always possible to add those not highlighted.

Finally, it is possible to export the resulting component in the **STL** format. Later on, this file is imported into PolyWorks™ together with the original scanned surface for the replica SBO (190318-4-4). After some pre-alignment is done, the discernment of some disagreement between them is possible to be made. It was naturally expected since a

theoretical CAD surface mesh (extracted in HyperMesh™) is compared against a warped scanned surface. Figure 2.5 shows the resulting overlay after pre-alignment.

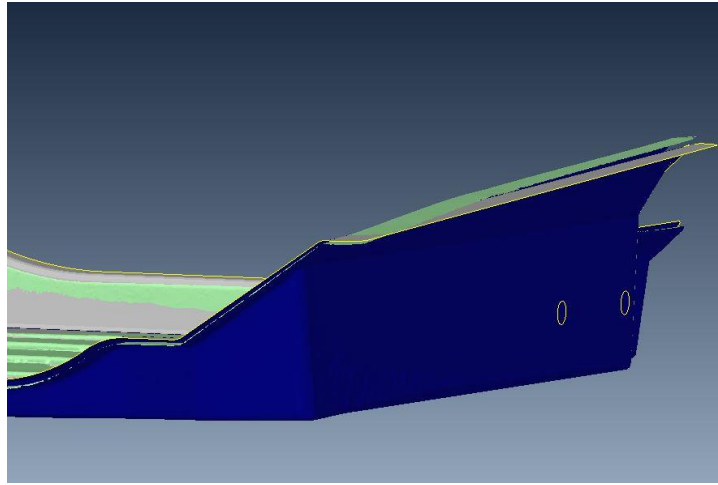


**Figure 2.5: PolyWorks alignment after HyperMesh surface extraction**

Both surfaces can be differentiated by the lateral holes, present in the CAD model and not produced by the manufacturing process so far. As a consequence of the complex geometry and the alignment initially chosen, in some regions, the disagreement between surfaces is evident along the principal axis. Next figure tries to illustrate it.

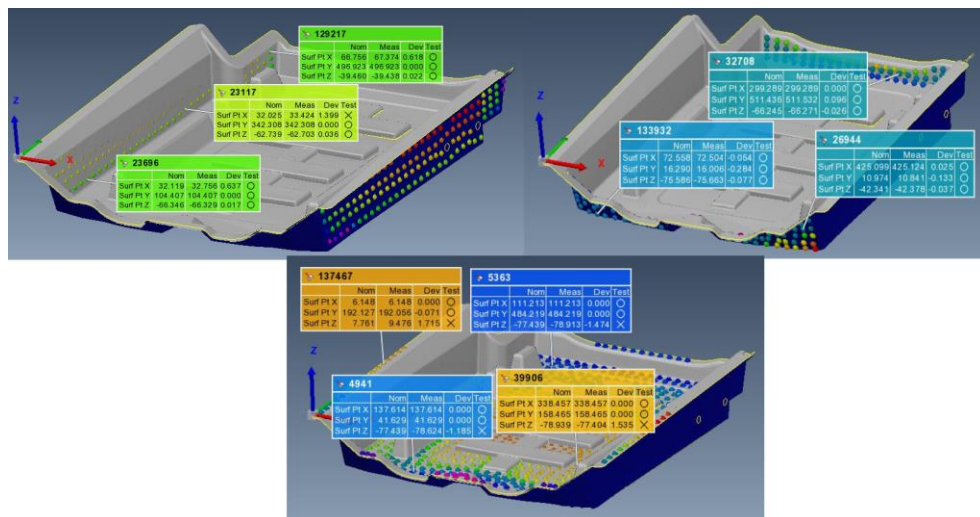


**Figure 2.6: Disagreements along principal axes**



It is evident that to make both surfaces to coincide, the CAD surface should be moved up to the scanned surface position, applying some displacement to points where those disagreements were detected. In HyperMesh<sup>TM</sup>, using the option to create sets of new entities, three groups of nodes were created: one for each principal axis. As a matter of best-practice, it was attempted to keep the density of nodes chosen as uniform as possible across the planes on which they were. Besides, it was avoided selecting points too close to fillets transitioning from one surface to another. It was found that points picked along fillet either did not contribute to adequate warped final mesh or added excessive distortion. Finally, in the case of the SBO, no nodes were chosen in ribs, letting these nodes free to move instead.

The next step should be to measure, automatically in PolyWorks<sup>TM</sup>, the distance between each node and the scanned surface. It is expected that measurements obtained by such process correspond to three-component vectors. However, depending on the position of the node, it is always possible to identify the largest vector component. For instance, consider points positioned in the flat plane of the ribs in Figure 2.6. When the distance between nodes and the scanned surface is measured, the largest component will be aligned with the z-axis.

Once all three sets are created in Hypermesh<sup>TM</sup>, an INP file is exported from it. This file can be open in a text editing tool giving access to all nodes selected under the Header **NSET**. The next bullet points describe how to manipulate the lists of nodes and import it into Polyworks<sup>TM</sup>. MatLab<sup>TM</sup> was used extensively at this stage because of its efficiency in dealing with txt (ASCII text) and xlsx (Excel) files. All scripts employed are available in the Appendices section (Appendix C):

- First, the original INP file is saved with a TXT extension, enabling it to be read by MatLab<sup>TM</sup>. This TXT file will be called *unwarped original file*;
- Next, a separated TXT files is created, one for each group, containing the number of nodes. These files are called *group files*;

- Run *TxtWork.m* which reads the *unwarped original file* with all nodes of the unwarped part. This script creates an XLSX sheet with four columns: node number, x, y, and z coordinates. This file is called *nodes*;
- Open *Nset.m* which reads each *group file*. This script creates three other sheets (inside file *nodes*) with only nodes identification. Before running it, it is necessary to check and adjust the number of nodes selected (necessary for reshaping in MatLab<sup>TM</sup>). After running it, empty lines should be deleted in each new sheet in *nodes* (not always the number of nodes picked in each group has a multiplicity of 8);
- Run *CompCopy.m* which reads two sheets in *nodes* (all nodes and one group), comparing node's identification and, in every match, copying coordinates from the original set (all nodes) to the second sheet (group chosen). After this step, the second sheet is changed, including all coordinates besides the original column;
- Run *WriteNset.m* which writes the second sheet in a TXT format (necessary for Comparison Points step in Polyworks<sup>TM</sup>).

At the end of such a procedure, a TXT file is produced containing node number and its coordinates. In Polyworks<sup>TM</sup>, the node number will work as a “tag” since the software only needs the coordinates to create **Comparison Points**. When proceeding with the method, three separate groups will be needed, one for each principal deformation direction. Using the alignment presented in the Figure 2.5, Comparison Points are created importing the previous TXT files.

Once the **Comparison Points** is imported, the parameters of interest to be extracted are set. The next figure shows points belonging to z-group, and the distance of them to the scanned face.

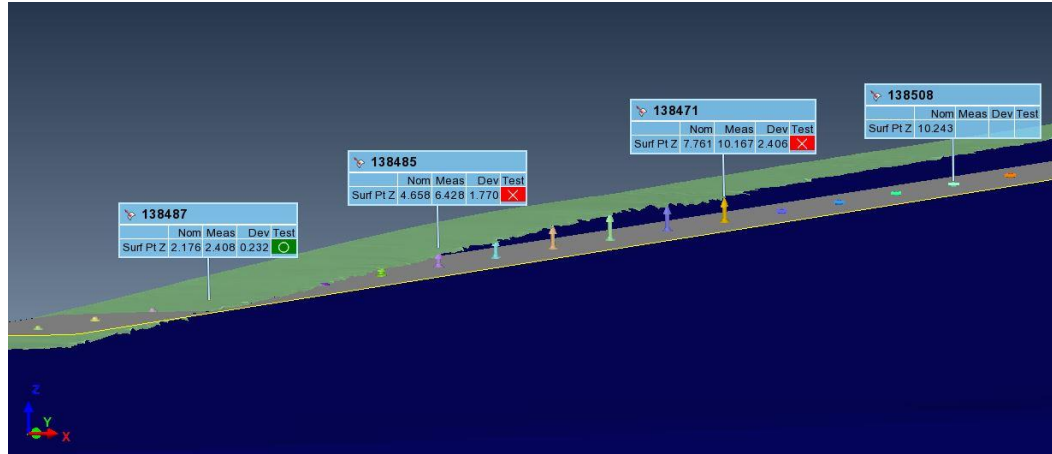


**Figure 2.7: Points in z-group being measured**

Figure 2.7 presents the scanned face in green, the extracted CAD face in grey, with points placed on it. Each point belonging to the z-group receives a tag (being the node number of the original mesh) and have some parameters automatically calculated. The column **Nominal** shows the z component of the Comparison point (original mesh), the column **Measured** shows the z component of the point on the target surface (scanned) and finally, the column **Deviation** the subtraction between both previous values. The column **Test** shows whether or not the Deviation surpasses a set threshold value (in this case, 0.5 mm).

It is also noted some arrows pointing upward (138485 and 138471), downward and even no arrow been drawn (138508). The direction of the arrow depends on the warpage of the scanned face to the CAD surface after pre-alignment. Some points will be above the CAD surface, others below it. For the case in which no arrow is drawn since the measured is calculated automatically, the software only draws an arrow and measures the distance between surfaces locally when it finds a corresponding point in the target surface. Thus, when it is not capable of finding such corresponding point, the arrow is consequently not drawn.

Points which no arrow was drawn were removed from our final report as well as columns with information not necessary for the mesh deformation. Once we export the final report in CSV format (Excel<sup>TM</sup>), we execute a new script in MatLab<sup>TM</sup>:

- Run **BcWrite.m**. It writes two TXT files: 1) definition of sets in Abaqus<sup>TM</sup>, one set for each node number to be deformed, consistent with the INP format. This file is called **Sets**; 2) definitions of each boundary conditions (BC's), translating each node the amount measured in PolyWorks<sup>TM</sup>, and in a way consistent with the INP format. This file is called **BC**.

After this, the same mesh created in HyperMesh<sup>TM</sup> is open in Abaqus<sup>TM</sup>, guaranteeing the same labelling. At this point, it can be said that the deformation field is already wholly defined: all nodes to be deformed are registered in the **Sets** file, and the deformation value to be applied to each one of them written in the **BC** file. It is necessary only to insert such boundary conditions in an appropriate model.

## 2.4 Seat Back Outer Warping Model

In this section, the model in which the previous section warping field is applied is described. For the sake of clarity, the definitions adopted will follow the sequence of Abaqus<sup>TM</sup> modules.

The file produced in the Hypermesh meshing procedure (Sub-section 2.1.2) is initially imported. The whole mesh is picked (region selected), creating and defining a solid and homogeneous section. For the material assigned to it, the following properties were defined, making use of parameters specified for an LFT with 40% weight in fibres by the material characterization research:

- General Property – Density:  $1.45 \times 10^{-9} \text{ ton/mm}^3$ , Uniform distribution;
- Mechanical Property – Elastic – Young's Modulus:  $14300 \text{ MPa (N/mm}^2\text{)}$ , Poisson's Ratio: 0.35, Isotropic type.

At this point, the following comment can be made. Although a composite material made of a matrix impregnated with fibres is used, in which it is known that there is no uniform distribution of such fibres, the chosen parameters implicitly adopt simplifying hypotheses. Presently assumed uniform and isotropic, the properties would vary depending on the fibres' amount and their orientations. In this sense, a possible model's

development can be done by mapping how the fibres are oriented locally in each part, allowing a non-uniform and anisotropic behaviour to occur.

Another simplifying hypothesis, implicitly adopted, is that the stresses involved in the warping of all parts and assembly of the set do not reach the material's elasticity limit. It means that there is no need to define plasticity parameters.

In module assembly, an instance is created, keeping the proper alignment adopted in the meshing procedure. A general static step is defined with a simulation time of one second, and NIgeom turned on. All other parameters are kept in the default option. At this stage, no set of points or deformations to be applied were defined. This step's creation is done so that a header is available in Abaqus' written file to include the text of the warping field generated previously. The NIgeom setting, cited above, takes into account possible geometric nonlinearities present in the step.

Finally, a job is created requesting the input to be written (INP file). Opening the last file on Notepad<sup>TM</sup>, we have access to all headers of an Abaqus<sup>TM</sup> job. Under the header “NSET”, the file Sets’ text is included and under the header “BOUNDARY CONDITIONS”, the file BC’s text is included saving the resulting file in the INP format. This inclusion is repeated for each group created (x,y and z).

The next figure shows the resulting Abaqus<sup>TM</sup> job after loading the resulting INP file with all boundary conditions included for the Seatback Outer (SBO) and the resulting mesh after simulation.

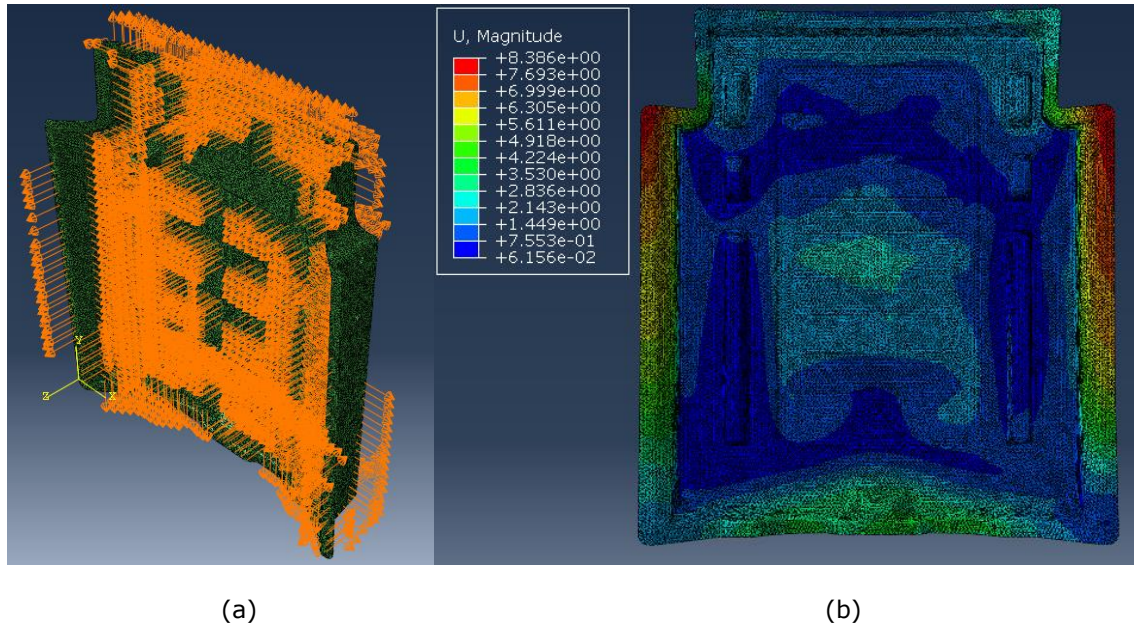


**Figure 2.8: (a) Boundary Conditions to deform SBO and (b) Resulting mesh, displacement (mm)**

To give an idea of the number of nodes selected and distance measured, the previous figure presents 1990 boundary conditions (and nodes selected) applied simultaneously. The resulting mesh is later exported in the STL and its top surface extracted in HyperMesh<sup>TM</sup>. The top surface is overlaid against the scanned surface in PolyWorks<sup>TM</sup> to assess how good the correspondence between deformed mesh and scanned surface is. The next figure shows the final colour map describing qualitatively the result produced.

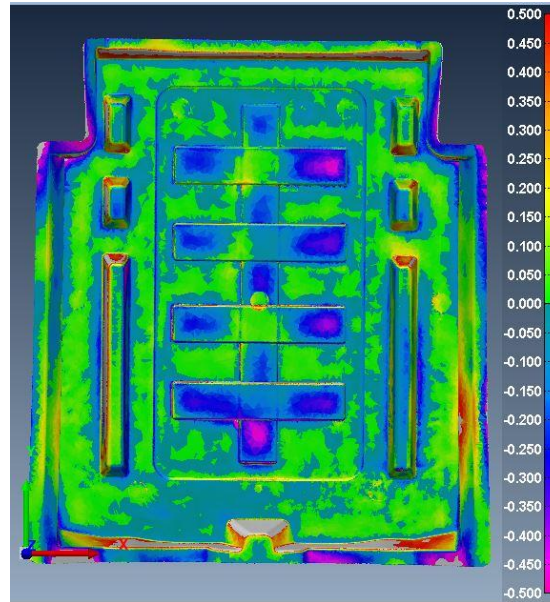


**Figure 2.9: Colour Map after deforming SBO CAD mesh – Distance in mm**

The next table shows quantitatively the deviation still existing after the deformation.

#Points	281887
Dev Mean	-0.015
StdDev	0.185
Pts within +/- (1 * StdDev)	199896 (70.914%)
Pts within +/- (2 * StdDev)	263300 (93.406%)
Pts within +/- (3 * StdDev)	281887 (100.000%)
Pts within +/- (4 * StdDev)	281887 (100.000%)
Pts within +/- (5 * StdDev)	281887 (100.000%)
Pts within +/- (6 * StdDev)	281887 (100.000%)
Surface Out of Tol	0.000%

**Table 2.1: Resulting overlay for SBO**

The distance between nodes and warped surface initially intended was of  $\pm 0.5$  mm. Accordingly, the table shows a mean close to zero ( $-0.015$  mm) and 93.4% of nodes inside the range of  $\pm 2$  standard deviations, which numerically represents points at a distance between  $-0.385$  mm and  $0.355$  mm to the target surface. If the range is extended further, including  $\pm 3$  standard deviations, 100% of nodes are found at a distance between  $-0.57$  mm and  $0.54$  mm. This is considered a good result, proper to use in following clamping and welding simulations.

Besides, it is possible to assess how effective the method is. Despite the cumbersome process of manual selection of points to be displaced, a good result is achieved in reproducing the warpage by selecting only 0.7% of all nodes in the mesh ( $1990/281887 = 0.705 \times 10^{-2} \rightarrow 0.705\%$ ). In terms of simulation time, the time required to conclude the whole process was 28 seconds.

## 2.5 Seat Back Inner Warping Model

In this section, particularities applied to the model of SBI are described. The sequence of Abaqus<sup>TM</sup> modules will be adopted as well.

The file produced in the Hypermesh<sup>TM</sup> meshing procedure (Sub-section 2.1.2) is initially imported. The whole mesh is picked (SBI), creating and defining a solid and homogeneous section. For the material, the same previous properties were defined, making use of parameters specified for an LFT with 40% weight in fibres.

In module assembly, an instance is created, keeping the same alignment adopted in the meshing procedure in Hypermesh<sup>TM</sup>. A new step is defined, keeping the same definitions: a static step, simulation time of one second, Nlgeom on. All other parameters are kept in the default option. Again, neither set of points nor boundary conditions were defined at this stage.

At the end, a job is created requesting the input to be written (INP file). Under the heading “NSET”, the file **Set**’ text is included and under the heading “BOUNDARY CONDITIONS”, the file **BC**’s text is included saving the resulting file in the INP. This



inclusion is repeated for each group created (x,y, z and xz). For the SBI case, points with significant deformations in x- and z-axes simultaneously (inclined planes) had two boundary conditions defined for each node.

The next figure shows the resulting Abaqus™ job after loading the resulting INP file with all boundary conditions included for the Seatback Inner (SBI) and the resulting mesh after simulation.

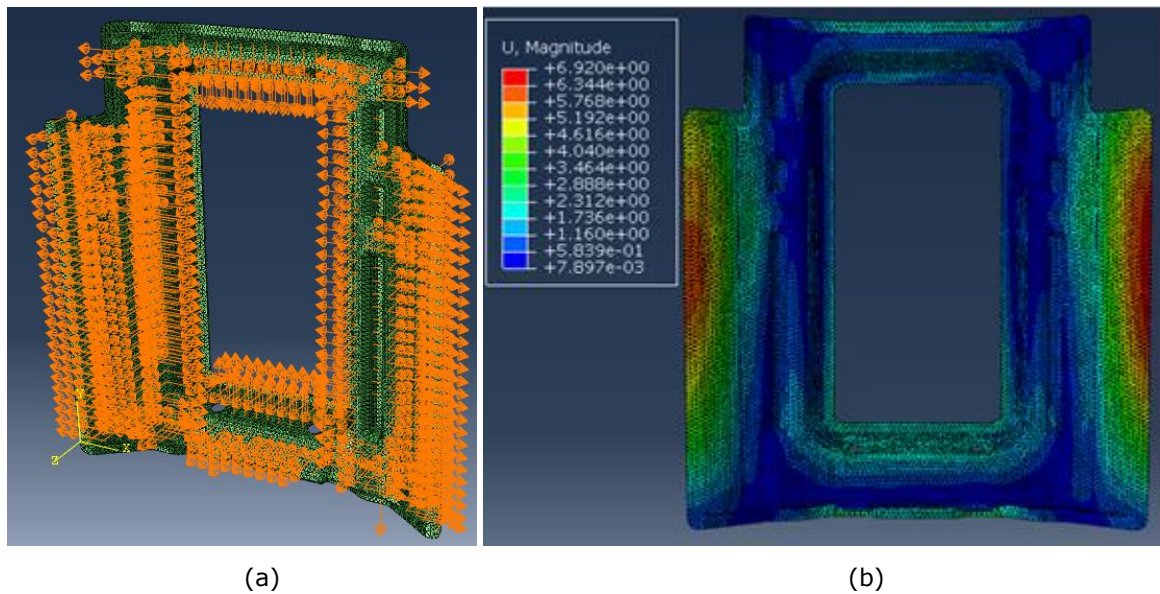


**Figure 2.10: (a) Boundary Conditions to deform SBI and (b) Resulting mesh, displacement (mm)**

Quantitatively, the previous figure presents 1268 boundary conditions (and 884 nodes selected) applied simultaneously. The resulting mesh is later exported in the STL format and its top surface extracted in HyperMesh™. The top surface is overlaid against the scanned surface in PolyWorks™ to assess how good the correspondence between deformed mesh and scanned surface is. The scanned surface employed in the comparison was the SBI replica (190524-5-1). The next figure shows the final colour map describing qualitatively the result produced.

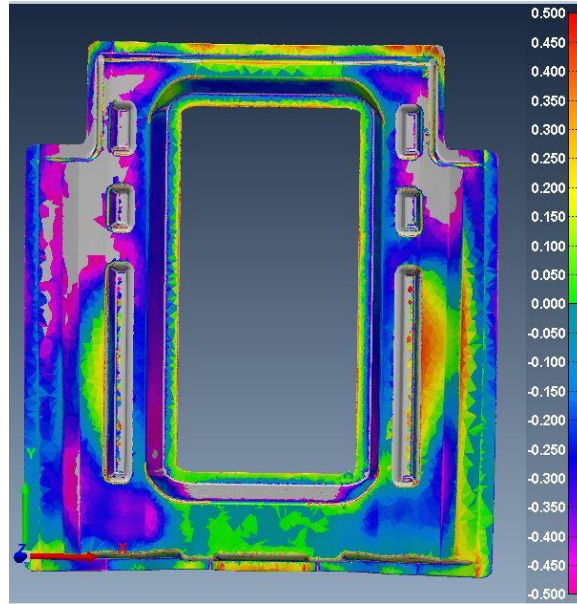


**Figure 2.11: Colour Map after deforming SBI CAD mesh – Distance in mm**

This is the initial selection of nodes. The grey regions correspond to points which the distance between Abaqus-deformed top surface and scanned data are out of range. It is always possible to add more points to the initial selection, refining further the warping method. The next table shows quantitatively the deviation still existing after the deformation.

#Points	83574
Dev Mean	-0.065
StdDev	0.256
Pts within +/- (1 * StdDev)	51867 (62.061%)
Pts within +/- (2 * StdDev)	81791 (97.867%)
Pts within +/- (3 * StdDev)	83574 (100.000%)
Pts within +/- (4 * StdDev)	83574 (100.000%)
Pts within +/- (5 * StdDev)	83574 (100.000%)
Pts within +/- (6 * StdDev)	83574 (100.000%)
Surface Out of Tol	0.000%

**Table 2.2: Resulting overlay for SBI**

The distance between nodes and warped surface initially intended was of +/-0.5 mm. Accordingly, the table shows a mean close to zero (-0.065 mm) and 97.9% of nodes inside the range of +/- 2 standard deviations, which numerically represents points at a

distance between -0.577 mm and 0.447 mm to the target surface. This is considered a good result, proper to use in the following clamping and welding simulations.

In terms of efficiency, it was selected only 1.05% of all nodes in the mesh reaching the results thus presented ( $884/83574 = 0.0105 \rightarrow 1.05\%$ ). And in terms of simulation time, the time required to conclude the whole simulation was 1 minute and 11 seconds.

## 2.6 Chapter Summary

The warping procedure described in this chapter produced meshes considered acceptable regarding a tolerance applied to local warpage. The same method was used in two different geometries selecting a small amount of all their nodes (approximately 0.7% and 1.05%, respectively). The main drawback and time-consuming process is the selection of which nodes are going to be displaced. However, once the group of nodes selected is established, the same method can be applied to different scans of real warped parts. The main advantage of this procedure is the possibility of using a real warpage profile by including an intermediate warping simulation. A limitation identified of such a process is that the thickness of real manufactured parts, and how it varies throughout each part, is not taken into account.

## Chapter 3 : Pre-Clamping Simulations

### 3.1 Overview

This chapter describes simulations using warped parts produced by the last chapter method in the pre-clamping context, in which both parts are placed initially on the fixture. It will describe the intermediate set-up of a model involving two parts only, SBO and fixture, recreating the situation in which this component is placed on the fixture. It will further describe the whole model's set-up involving three parts: SBI, SBO and fixture. Such simulations recreate both pre-clamping conditions.

### 3.2 Two-Part Simulation

The two-part simulation treats the initial condition in which SBO is placed on the fixture. Such simulation will be used later on as the initial condition for the placement of SBI over SBO. For that, SBO should be stable and in contact with the fixture. For the model's description, Abaqus' modules will be followed, and terms used on the software will be presented in bolded font.

In module Part, the geometry of the fixture should be included. The original geometry is in the Parasolid format (X\_T), which allows the directly importing into Abaqus™. Some simplifications were applied prior to importing it, ignoring some blocks, bolts and components that, in our opinion, would not jeopardize either assembly orientation (relative position between parts) or connectivity within the fixture. The settings chosen were: include the part in a 3D modeling space, discrete rigid part. The next figure shows the fixture's geometry after such simplification was applied.

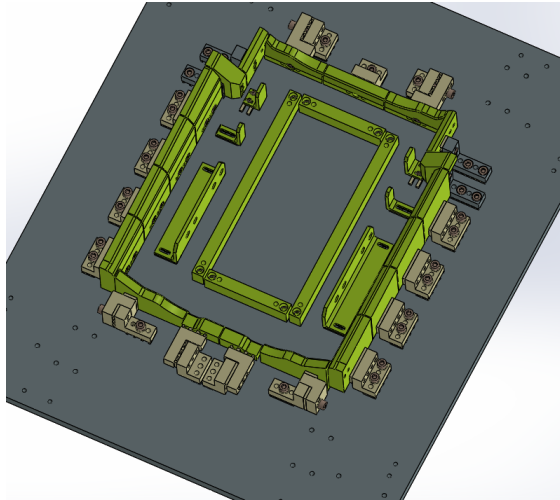


**Figure 3.1: Assembly fixture after simplification**

It is evident that, for some, the fixture could still be simplified further. However, the present state agrees with the whole model presented in this thesis. A discrete rigid part setting is applied because the geometry is, in some way, arbitrary, some features not included in Abaqus<sup>TM</sup>. Besides, the deformation will be assumed negligible and the stress under which it is submitted will not be of a matter of interest. All this is justified if we note the contact we are dealing with occurs between parts where the fixture is stiffer (metal) than the SBO (composite).

Furthermore, due to Abaqus' limitations, it is only possible to mesh a component, using rigid elements, if the original discrete rigid part contains shells or wires (or a combination of both). The simplified fixture is a solid part, being not possible to mesh it directly into rigid elements. To overcome this, the option to convert the solid to shell is chosen under the shape options. The whole fixture is selected in the visualization window, and the conversion is concluded. Once this is done, it is possible to mesh the fixture using rigid elements. Additionally, a reference point (RF) is defined in one of the fixture nodes as a requirement for a future boundary condition (encastre). The next figure shows the resulting fixture after all previous conversion and meshing.



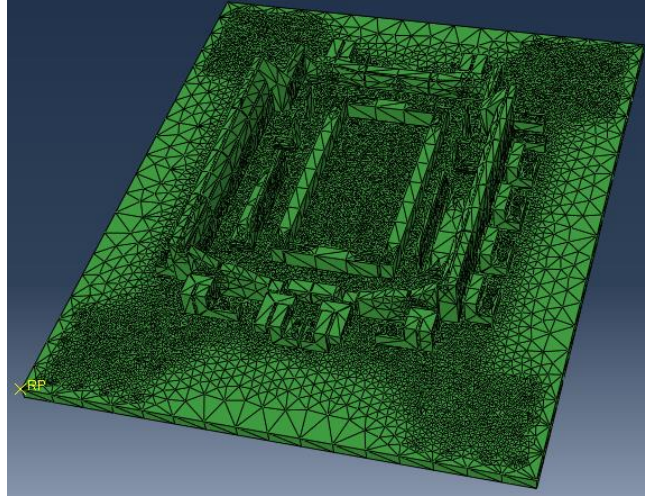


**Figure 3.2: Fixture meshed with Reference Point defined**

At this point, the surfaces involved in the contact detection and analysis will be defined. Such a definition will be done intending to reduce the computational cost. Instead of testing the contact for all elements' surfaces present in the simulation only those selected will be tested. Three surfaces were identified where the contact is more likely to occur. Each surface was defined as a mesh-type, including all adjacent element's faces. The next figure shows which surfaces were defined.

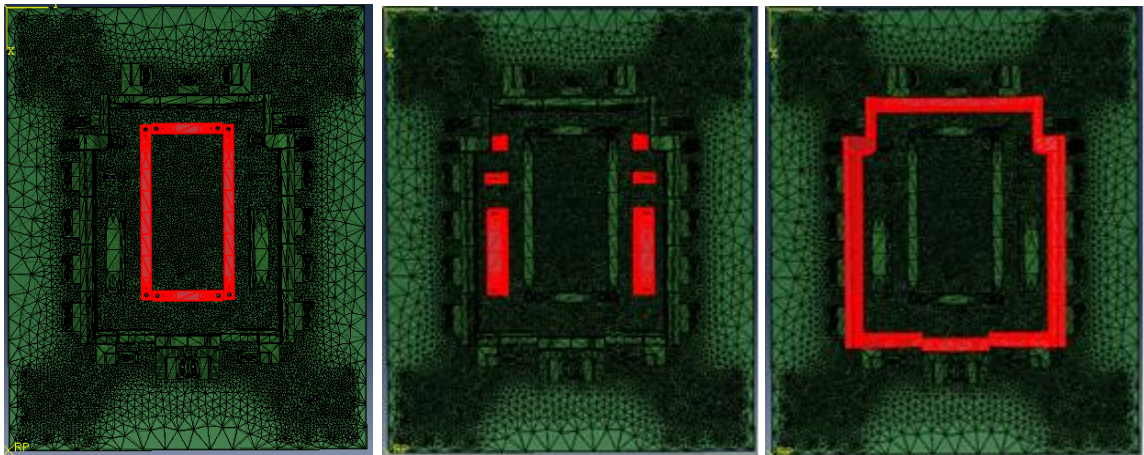


**Figure 3.3: Surfaces defined on the fixture mesh**

Still, in module part, the SBO warped by the method presented in the last chapter is imported. It is defined as a deformable part, with a homogeneous solid section and made

of the same material previously described (LFT-isotropic). Similarly, the corresponding contact surfaces should be defined in the SBO for later contact calculation and detection. The next figure shows which contact surfaces were defined.

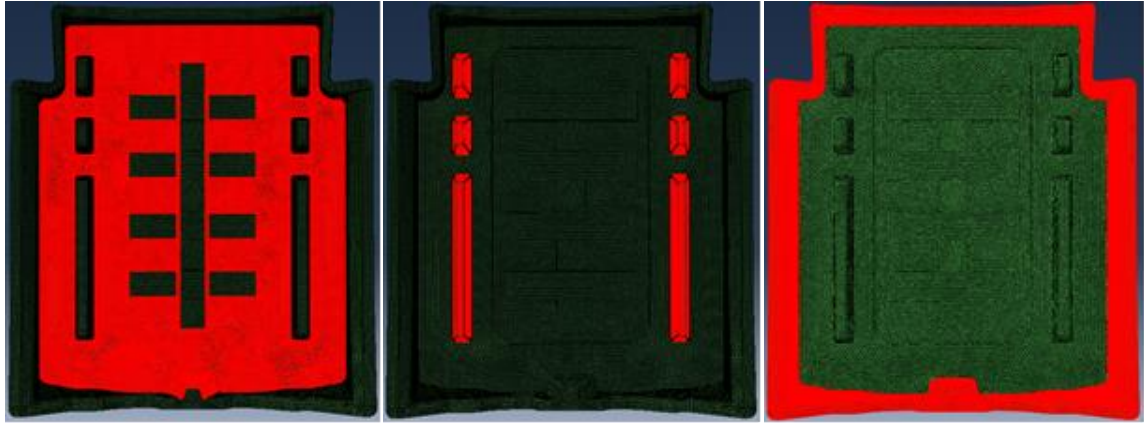


**Figure 3.4: Surfaces defined on the SBO mesh**

All previous definitions conclude the setting for this module. In the assembly, we create two instances, fixture and SBO, aligning them properly. Due to the degrees of freedom to assembly both parts, different users inevitably will place the SBO on the fixture differently. It is even understandable that visually it is not possible to detect, whatever alignment is chosen, all possible contacts or overlap of surfaces during the assembly of instances. The tool “Find Contact Pairs” in the interaction module is used to prevent any contact or surface overlap before the simulation. In its settings, it is possible to set: (i) tolerance for the separation between surfaces; and (ii) the angle under which each surface is extended. Once both are set, the tool detects (and highlights) pairs under the tolerance chosen, allowing the user to adjust the assembly. Once all contacts and overlaps are removed, the assembly is considered finished.

Next, in the interaction module, it is possible to define the fixture as a rigid body. Under the option to create constraints, of the rigid body type, the whole fixture (all elements) is selected in the visualization window. They are assigned to the whole body (elements). A reference point should be selected, as well. For this, the reference point defined previously is used (see Figure 3.2).

Then, in the module steps, it will be set the Initial conditions of this model. Under the option of Interactions, three interactions are created of the surface-to-surface contact type. For each interaction, we should define a master-slave pair. At this point, it is convenient to express all criteria pointed out by Abaqus<sup>TM</sup> User's Manual, which oriented the choices made. The following rules orient the assignment of master-slave roles:

- The master role has to be assigned to rigid analytical surfaces or rigid-element-based surfaces;
- The slave role must be assigned to deformable bodies.

Those criteria are particularly important, depending on the contact formulation assigned. Following the previous rules, it is evident that all surfaces defined in the fixture will have the master role assigned while all surfaces defined in the SBO the slave role. Thus, each surface shown in Figure 3.3 had a master role assigned to and each surface shown in Figure 3.4 had a slave role assigned, correspondently [12,13,14].

Another setting available in the definition of the contact is the discretization of contacting surfaces. Two options are available: node-to-surface or surface-to-surface discretization. In the node-to-surface discretization, the contact definitions are only applied depending on the interaction between each "slave" node (belonging to the defined slave surface) with nearby "master" nodes (belonging to the defined master surface) or the interpolations between "master" nodes. Under such a discretization method, "slave" nodes do not penetrate the master surface, not being guaranteed the other way around ("master" nodes are allowed to penetrate the slave surface).

In the surface-to-surface discretization, both master and slave geometries are accounted for around the region of contact. For this formulation, the contact definitions are applied in average terms, considering both "slave" nodes itself and the area surrounding it. In such a formulation, the "slave" nodes are the centre of its surrounding area. Some penetration may occur at individual nodes; however, extensive areas of "master" nodes penetrating the slave surface will not happen, representing an improvement when compared with the previous formulation. This formulation is preferable for the present



model. The next figure pictures the difference of both formulations when applied on a specific model.

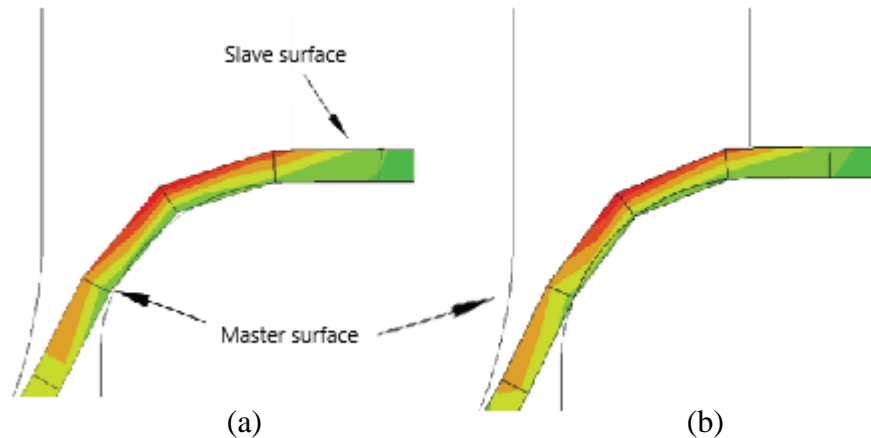


**Figure 3.5: (a) Surface-to-surface and (b) Node-to-surface discretization (adapted from Abaqus Analysis User's Guide version 6.14, Dassault Systems [12])**

Figure 3.5 shows that some penetration occurs in both formulations, but it is greater in the node-to-surface discretization. Still, in the interaction definition, all other parameters will be kept on their default options, namely: finite sliding formulation, path contact tracking, no adjustment of the slave surface, no surface smoothing and default contact controls. Finally, a property for the contact should be defined. It was assigned values used by GM when investigating the contact property between metal and LFT. For instance, the parameters defined were:

- Mechanical property - Tangential behaviour - Friction formulation: Penalty - Directionality: Isotropic - Friction coefficient: 0.3;
- Mechanical property - Normal behaviour - Pressure-Overclosure: "Hard" Contact - Constraint enforcement method: Default - Allow separation after contact: on;
- Mechanical property - Damping - Definition: Damping coefficient - Tangential fraction: use default - Linear option: on - Damping coefficient: 0.1 when Clearance is 0.0 - Damping coefficient: 0.0 when Clearance is 0.1.

Progressing further on the module steps still, the initial boundary conditions (BCs) for the fixture should have all its degrees of freedom restricted. The options selected were to create a BC, of the mechanical category, from the encastre type. The reference point created is selected as a geometric region on which the boundary condition will be applied. Finally, the option encastre is chosen, restricting all translational and rotational movements of the fixture.

Now, it is convenient to discuss which boundary condition is adequate to recreate the placement of the SBO over the fixture and where to apply it. We identified and investigated at least three options:

1. Free movement of the SBO under gravity;
2. Selection of nodes where the contact is likely, applying z-displacement to cause contact; and
3. Selection of points where the contact takes place (real assembly), applying z-displacement accordingly.

Each approach was tried which allowed to draw the following conclusions and comments. Initially, the first option was applied. It was noticed the main drawback of such an approach regards the stabilization time. Adopting a dynamic simulation was expected a fast stabilization without relevant alteration on nodes' coordinates. However, since no damping coefficient was applied to the simulation as a whole, the small damping coefficient defined (interaction) was not enough to stabilize the model in reduced time simulation (1s, 2s or 3s). If the simulation time is increased, a drastically significant amount of data will be stored for such an initial step. This line of action would be adopted, whether the alternative options be better or not in terms of accumulation of data.

Then, the second option was applied. For this case, it was assumed the likely contact would happen firstly on the lateral flanges. The second approach's main advantage is not to rely on stabilization time to reach a converging result. However, it has a drawback because it ignores at which points the contact firstly occurs. Once this approach was tried,

it was possible to note that by displacing lateral flanges and forcing them to contact, the warped part excessively deforms at the nodes where the contact first occurs.

Finally, it can be noted the third and final approach is the proposed solution after detecting all previous drawbacks and trying to work around them. However, it was necessary to measure the actual assembly placing the pair used in the simulation. Just as a reminder, for this simulation, the pair employed is: SBO (190318-4-4) and SBI (190524-5-1). Back in the mechanical laboratory, both parts were placed on the fixture in sequence, and the gap between flanges was measured. Through this approach, it was naturally impossible to measure the internal gap across both surfaces. Hence, we only rely on the smallest gap detectable on the external flanges. The next figure shows where the smallest gap was detected.

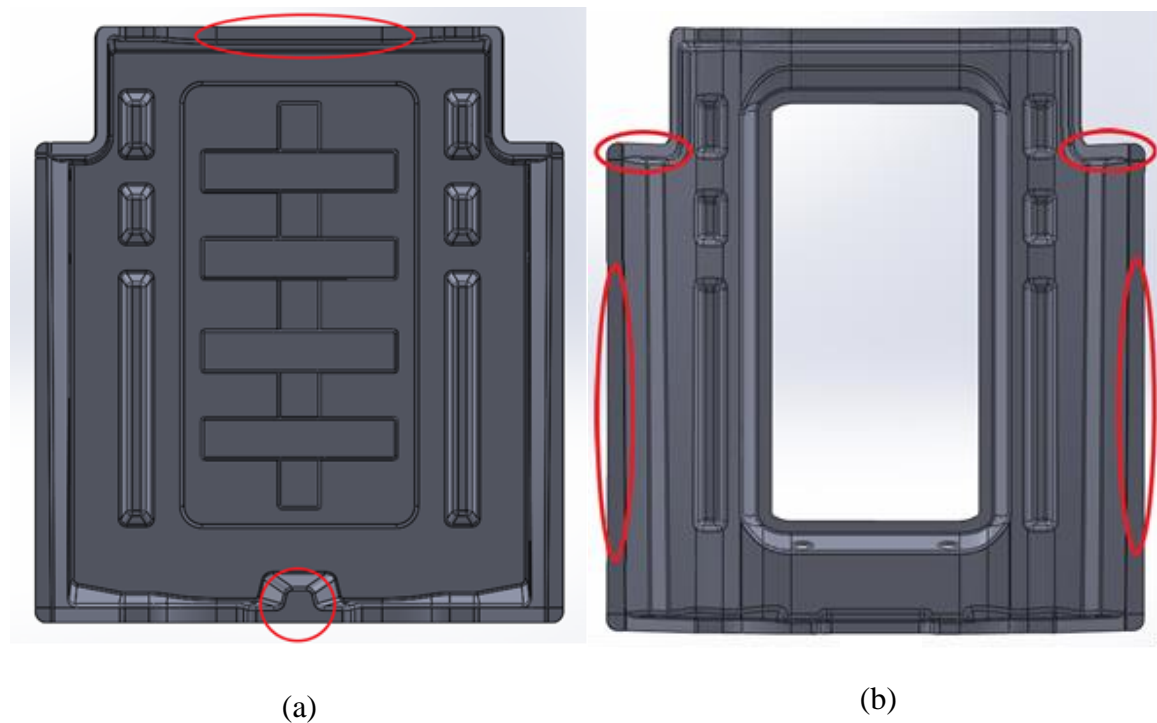


**Figure 3.6: Regions with the smallest gap in the actual assembly: (a) between SBO and fixture; (b) between SBI and SBO.**

With these regions in mind, we measured the z component of the distance between nodes of the SBO and the fixture contained on the red oblongs on Abaqus™. The value

measured will be used to displace the entire part causing the contact to occur at those nodes. Particularly for the initial positioning adopted in our model, a step (Step-1) is created as a dynamic type applying an implicit solver. A simulation time of 1s is chosen with the possibility of non-linear effect to be detected. Increments are assigned to have a maximum size of 0.05 is selected and a minimum size of 1e-8, giving more room to convergence. Further on, a mechanical boundary condition of the displacement type is created. On the visualization window, nodes contained in the red oblongs regions previously presented (Figure 3.6) are selected, applying a 6.1 mm negative displacement in the z-axis ( $U3 = -6.1$ ). The next picture shows the arrow representation of the boundary condition chosen.

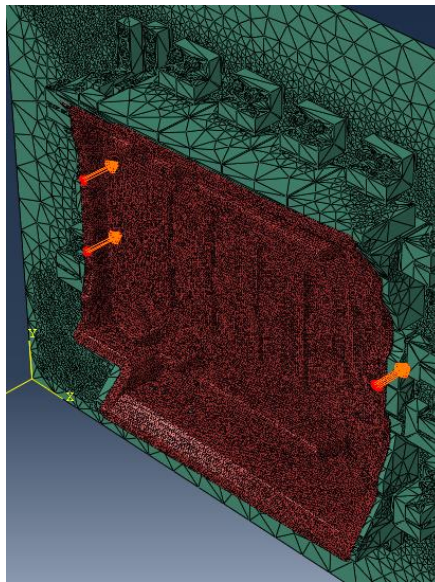


**Figure 3.7: Boundary condition for SBO placement over the fixture**

Still in the steps module, the option of using previous results is selected. This option allows to capture data from steps and use them as a starting point for the following simulation. It means that by capturing the result of the ongoing simulation, possible to use it as an input for the three-part simulation. Editing the requests, the option to capture frames with at every increment and overlaying it every time an increment is concluded.

Finally, in the steps module, one more variable is included to be calculated besides the default ones under. The additional output selected was the current nodal coordinate (COORD). Once the simulation is done, the result produced was the following.

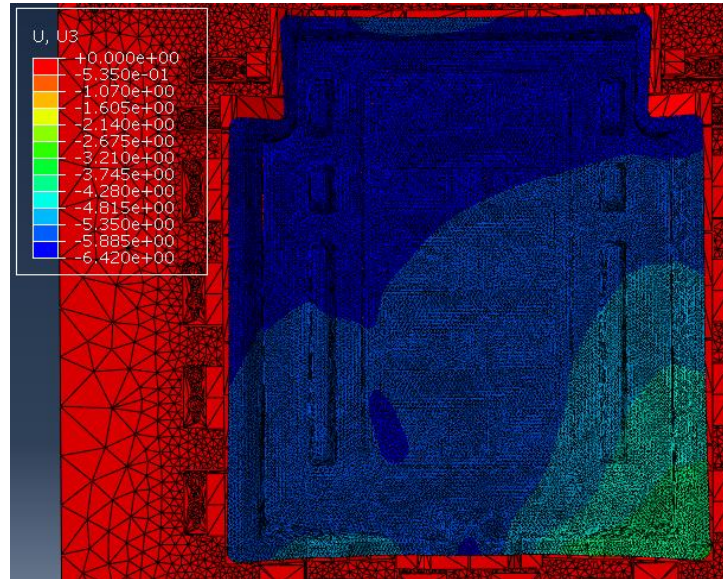


**Figure 3.8: 2-part result z-displacement (mm)**

The main observation is the asymmetrical distribution of the vertical displacement on the SBO. Possible reasons for that are the asymmetrical warpage of the part, which influences where the contact is happening, resulting in different displacement distribution; and the initial position of the SBO in the assembly, causing some points to move more than others. In terms of simulation time, the time required to conclude this simulation was close to 3 hours and 40 minutes.

### **3.3 Three-Part Simulation**

The three-part simulation treats the positioning condition in which SBI is placed over SBO already positioned. Such simulation will be used later on as the initial condition for the clamping of both parts. After SBI positioning, both parts should be stable with an initial contact occurring between SBO and fixture while SBI touches the SBO at contact points. For the model's description, Abaqus' modules will be followed, and terms used on the software will be presented in bolded font.

This new model starts by editing attributes of it to create a restart simulation. It is possible to edit options of the model. The option to read the data from a previous job is selected, writing the name chosen to previously two-part simulation. It is necessary that the name of the previous job should be consistently inserted. Finally, this set up finishes using the option to restart from the end of the step. Parallel to this, files from the two-part simulation should be inside the directory folder in which the simulation is running:

1. Simulink model (.mdl);
2. Abaqus Output (.odb);
3. Siemens Part file (.prt);
4. RES file (.res);
5. STT file (.stt).

In module part, both the warped SBO and the fixture are already present. The SBI mesh warped by the method presented in the last chapter should be imported. It is defined as a deformable part, with a homogeneous solid section and made of the same material previously described (LFT-isotropic). Similarly, surfaces where the contact between SBO and SBI is more probable should be defined. Three surfaces were defined in the SBI (bottom surfaces), and three other surfaces defined on the SBO (top surfaces). The next figure shows which contact surfaces were defined.

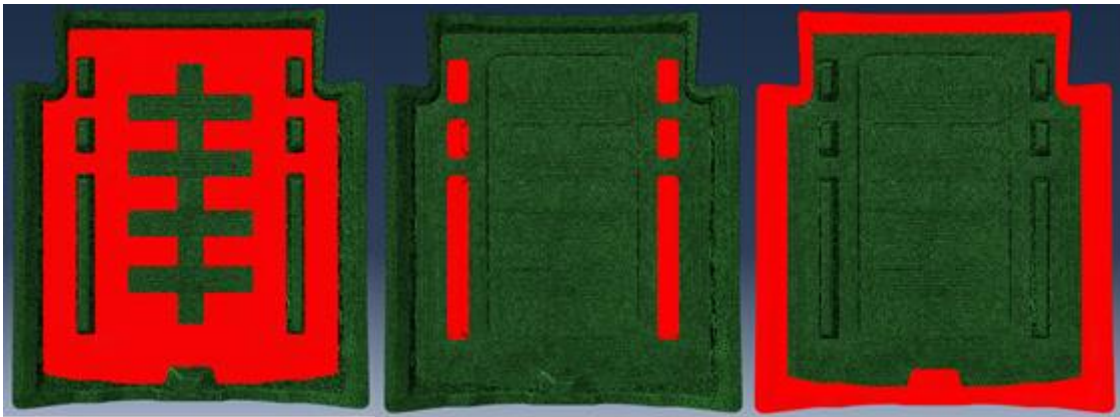


**Figure 3.9: Additional surfaces defined on the SBO mesh**

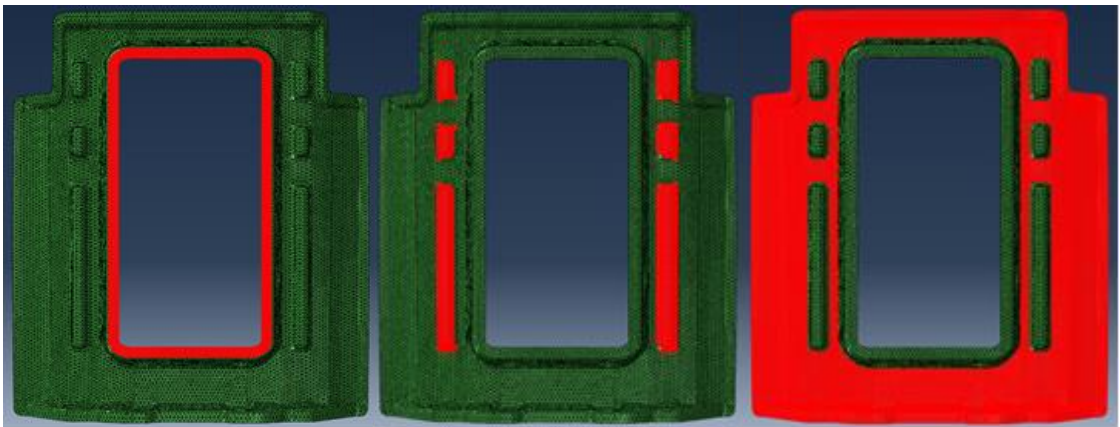


**Figure 3.10: Surfaces defined on the SBI mesh**

In the module assembly, another instance is created, SBI, aligning it correctly with the already included parts. As before, different users may place the SBI differently over SBO, but it is possible to have them minimally aligned. Again, some tools can be applied to prevent any contact or surface overlap before the simulation. Rotations and translations were used to also visually detect overlaps and contact before simulating it. Once all of them are removed, the assembly is considered finished. Three interactions using slave-master pairs corresponding surfaces presented in Figure 3.9 and Figure 3.10 were defined.

At this point, a new step (Step-2) is created, keeping the same setup adopted at Step-1. Further on, a mechanical boundary condition of Displacement\Rotation type is created.



Considering the regions at which the contact first happens in the actual assembly, presented in Figure 3.6, the boundary condition to be applied to the SBI should be defined. The amount to translate SBI is extracted from measuring the z component of the distance between nodes of the SBO and SBI. The reasoning behind is to guarantee contact between parts only, without deforming them at these nodes. In this case, a 16.1 mm negative displacement in the z-axis ( $U_3 = -16.1$ ) was applied. Displacements in x-axis and y-axis were applied as well to prevent part rotation while it is placed. In this case,  $U_1 = 0.75$  and  $U_2 = 0.5$  were chosen. The next picture shows the arrow representation of the boundary condition chosen.

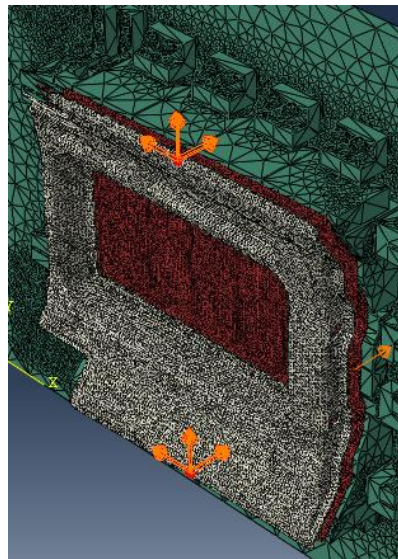


**Figure 3.11: Boundary condition for SBI placement over SBO**

In the steps module, the option of using previous results is selected. Editing the requests, the option to capture frames with at every increment and overlaying it every time an increment is concluded for Step-2. Once the simulation is done, the result produced was the following.



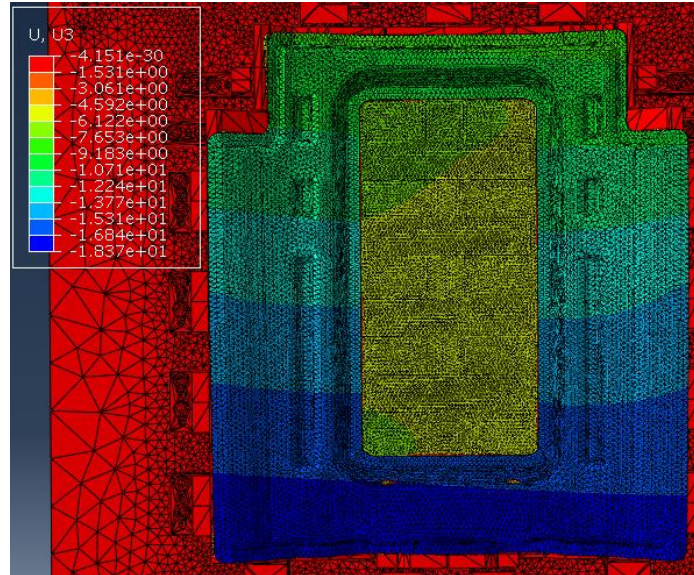


**Figure 3.12: 3-part result z-displacement (mm)**

On this result, a better symmetry in the vertical movement of the SBI is observable. This is profoundly influenced by the boundary condition chosen (allowing rotation around the horizontal axis). In terms of simulation time, the time required to conclude this simulation was 2 hours and 40 seconds.

### 3.4 Chapter Summary

This chapter extensively described how to set up the two initial simulations to place SBO and SBI over the fixture detailing hypotheses used and applying them on Abaqus<sup>TM</sup>. In both simulations, contact properties were defined, assessing how accurate each approach is and what each hypothesis could convey. Each result is used in the subsequent simulation by applied the Restart tool from Abaqus<sup>TM</sup>, and both simulations are preparations for the following clamping procedure to be discussed next chapter.

## **Chapter 4 : Clamping and Welding Simulations**

### **4.1 Overview**

This chapter describes the clamping and welding simulations using previous results produced in the last chapter. It will initially discuss the clamping pattern applied to the assembly. Next, the sequential clamping simulation will be described in all its steps, highlighting some possible pre-stress effects on both parts before welding them. Finally, the welding simulation will be described in its set up and at which points the welding is done.

### **4.2 Clamping Pattern and Sequence**

The clamping simulation intends to recreate the sequence in which the clamps are applied to a specific pair SBI and SBO, before welding. In the real assembly, the clamping is done by an operator intending to restrict any relative movement between parts and fixture.

The clamping pattern used in the simulation is an initial suggestion coming from industrial partners, regardless of process efficiency, serving as a proof case on the extent to which the clamping procedure affects or is affected by the warpage of real moulded parts. Although it is not the original intention to discuss aspects of the pre-stress state induced by clamping, the results of simulations may be used to assist such inquiry.

The clamping simulation's main interests are 1) the final relative position of both parts in relation to the fixture; and 2) the gap along flanges, which will be welded. To achieve that, the same clamping pattern employed in other research material in the same project will be digitally applied and compare the resulting gap in both cases.

In the work entitled "Method development for measuring assembly forces during the joining of D-LFT components." [15], a clamping pattern was adopted when measuring the subsequent welding force and displacement at the welding points. Such a pattern is illustrated qualitatively in the next figure.

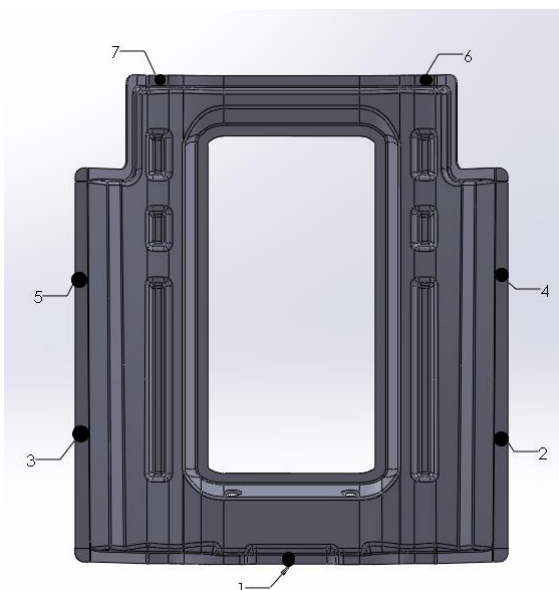


**Figure 4.1: Clamping points**

The clamping point over the SBI were chosen because they effectively take place over it. It is also possible to quantitatively identify these points using a coordinate pair (x,y) using as the origin Point 1 (mid-section) in the above figure. The following table lists such coordinates.

**Table 4.1: Clamping Points coordinates**

Clamping Point	X coordinate (mm)	Y coordinate (mm)
1 (origin)	0	0
2	232.53	144.90
3	-232.53	144.90
4	233.30	312.42
5	-233.30	312.42
6	149.19	535.24
7	-149.19	535.24

The previous coordinates were established on a front view, guaranteeing each clamping point is on the upper surface of SBI. It is not necessary to worry about the z coordinate since it will vary accordingly with the warpage along flanges of a specific replica. As a result, the z coordinate would produce different values depending on how warped the part is, and the previous table is enough to find where each clamping point is.

The discussion then shifts to the clamping sequence, namely in which order the 7 points presented should be applied. The first thought was to use the sequence clamping following the numerical tags presented in the previous figure. On the one hand, it would be possible to know how the stress develops through the clamping process and how each node moves, closing gaps and opening others. On the other hand, the amount of data generated by such an approach seemed unnecessary.

As already mentioned, the behaviour of the assembly under clamping is not one of the main interests. If that was the case, node-based boundary conditions should be more carefully applied. Nonetheless, the way the clamping simulation was set up, as it will be presented in the next sections, allows to investigate the stress induced by the clamping procedure by minor changes in the model. One of the changes would be to use a surface-based boundary condition (selection of faces or patches on the SBI) instead of the current node-based (cluster of points). That been said, the criteria that oriented it were the following:

1. At the end of clamping simulations (all 3 steps), the 7-clamps pattern should be applied;
2. The model should pass through all clamping steps without either unnecessary accumulation of data or excessive clamps being applied at once.

The expression "excessive clamps being applied" can sound subjective in some way, but it was noted that by closing all clamps at once, many boundary conditions were applied at the same time leading to a non-convergent simulation [12]. Some attempts were made, removing clamps symmetrically from the whole group, which lead to propose the following sequence:

1. First Clamping Step: Clamps 1, 2 and 3 being closed;
2. Second Clamping Step: Clamps 4 and 5 being closed; Clamps 1-3 kept closed;
3. Third Clamping Step: Clamps 6 and 7 being closed; Clamps 1-5 kept closed.

With this last sequence, the clamping pattern was determined, involving 7 points; also, at which position each clamp is closed and their order. This clamping pattern will be used as a baseline to discuss our future parametric study in later chapters. The next section describes which boundary conditions were chosen to recreate the clamping closing.

### 4.3 Clamping Simulations

The clamping simulations deal with the sequential closing of the clamps. The first of them uses the result of the three-part simulation as a starting point and so forth. They will be used later on as the initial condition for the welding of both parts. As before, Abaqus' modules will be followed to describe the setup, and terms used on the software will be presented in bolded font.

#### 4.3.1 First Clamping Simulation

Since all parts necessary for this model are already included, we should copy the previous model (three-part simulation), editing its attributes. The restart option will be used, and consequently, the prior list of files (as shown in Section 3.3) is necessary to guarantee the continuity of simulations. Following that, a new step (Step-3) is created, using the same setup adopted in previous ones (dynamic, number of increments, initial increment time, etc.).

Now, it can be discussed how to recreate the closing of each clamp. Tools were not available to measure either the pressure at the clamping head or the force required to close it. Thus, it would not be possible to estimate coherent boundary conditions for those parameters. Alternatively, it was possible to measure the vertical distance required to put both parts in contact and close the gap, either in the real assembly or in Abaqus<sup>TM</sup>. In the real assembly, the calipers could be used to measure these distances, while in Abaqus<sup>TM</sup> other tools are available to assess it. Hence, a boundary condition based on displacements

of nodes was applied. The amount of displacement to be applied was measured in the following manner.

First, having each clamping position, in Abaqus the local distance is measured between the following points: 1) a node in the back surface of SBI; and 2) a node in the vertical block of the fixture. Such a measurement produced a 3-dimension vector, but the most relevant information is the z-component of it. For instance, consider the measure done locally at clamping 1 position pictured in the next figure.

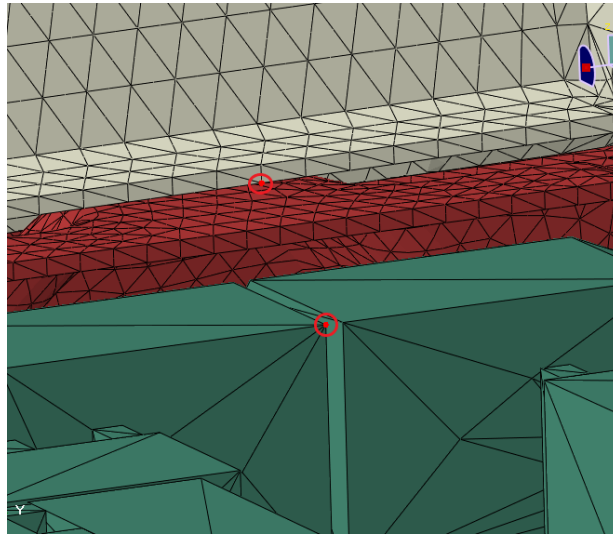


**Figure 4.2: Measurement locally done at Clamp 1 position**

The z-component measured was 25 mm in this example. It is assumed that since the clamp has a bumper made of rubber material, the clamp's head should not compress the parts across the thickness (material compression). The nominal thickness for both parts, at external flanges, is 2 mm. For this reason, and taking into account the measured z-component, a z-displacement should be applied discounting SBO thickness. In this example, the boundary condition was  $U3 = -23$  mm, but it should be applied to nodes on the top surface of SBI. This procedure was adopted in all clamping simulation, at each clamping location, to determine the amount of vertical displacement to be applied.

After the previous procedure is applied to all three clamping points, we list measurements and boundary conditions used in the following table.

**Table 4.2: Measures and BC for Clamps 1, 2, and 3**

	Z-measurement (mm)	BC to be applied (mm)
Clamp 1	18.95	$U3 = -16.95$
Clamp 2	21.02	$U3 = -19.02$
Clamp 3	16.84	$U3 = -14.84$

The first point to be noted is the difference between BC's applied to symmetrical clamps (namely, clamps 2 and 3). Since the SBI is not uniformly warped along the flanges, and even its initial position is not perfectly parallel to the fixture (relying mainly on the operator's skill to position it in the Assembly in Abaqus), it should not be expected equal values for symmetrically positioned points.

Once all this is done, three boundary conditions in Step-3 are created. For each of them, six to ten nodes are selected at each clamping position. Additionally, the boundary conditions related to part placement should be "turned off" because, in the restart option, they are active in subsequent steps (Step-3 forward). Previous BC's can be made inactive using the manager tool available, selecting which BC should be deactivated and at which step.

Similar to previous simulations, in the steps module, the option of using previous results is selected. Editing the requests, the option to capture frames with at every increment and overlaying it every time an increment is concluded for Step-3. Once the simulation is done, the result produced was the following. The next figure shows the arrow representation of all three clamps closing on the first simulation.

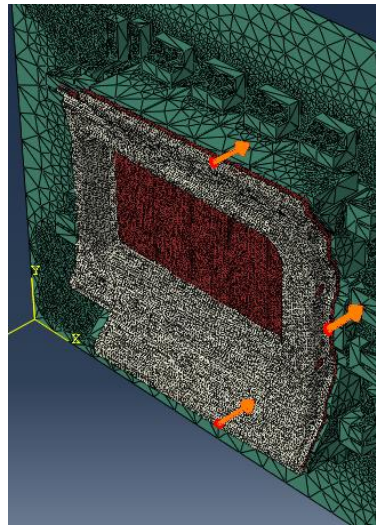
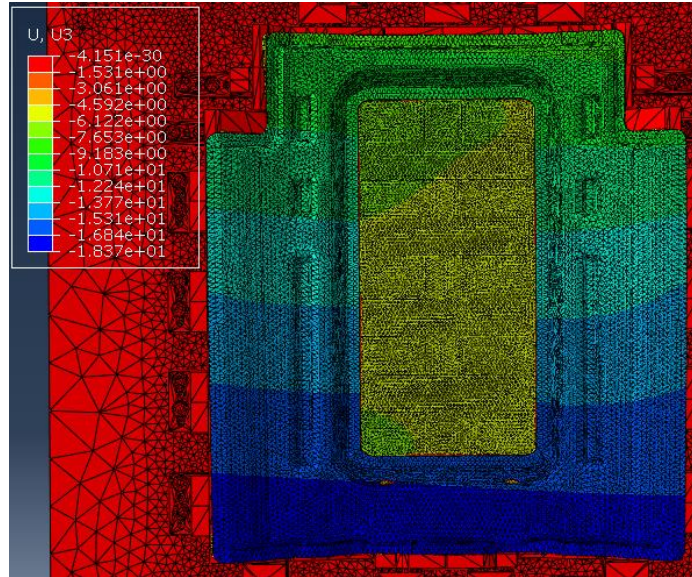


**Figure 4.3: BC for Clamps 1, 2 and 3**

Once the simulation is completed for the first three clamps, the following stress distribution (von Mises) is presented in the Visualization module.



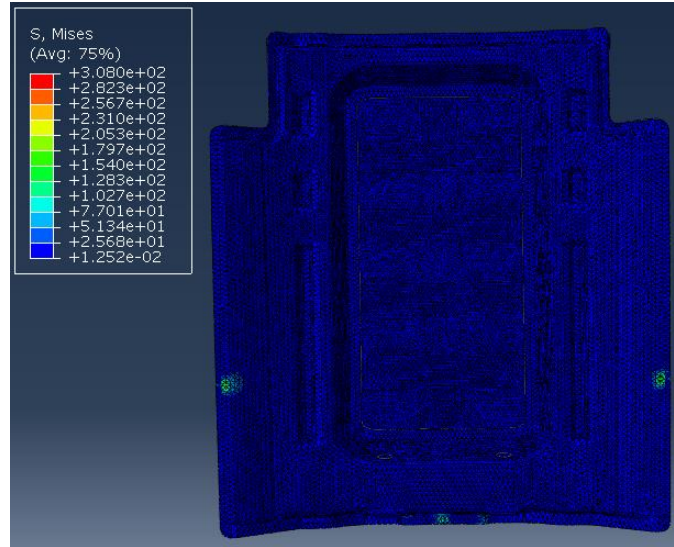


**Figure 4.4: Stress distribution after Clamps 1, 2, and 3 – (MPa)**

Overall, most of the surface of SBI and SBO are not subjected to high stress levels after closing the first three clamps (visually, between 0.012 and 25.68 MPa). The maximum stress level reached after clamp closing is 308.0 MPa, which is a considerable value in thermosetting materials. A possible explanation for this is that nodes (points) were selected at which the displacement is applied. With it, concentrated forces are imposed at each selected node, drastically increasing the stress level at these points. About the fixture, since the model was set as a rigid body, the stress level experienced by it is neither calculated nor an object of interest. For these reasons, the fixture was not chosen to show it in the last figure. In terms of simulation time, the time required to conclude this simulation was 3 hours 43 minutes and 3 seconds.

#### *4.3.2 Second Clamping Simulation*

The previous model (first clamping simulation) is copied, editing its attributes to use the output from the first clamping simulation. The restart option is used, and consequently, files should be available in the working directory (as shown in Section 3.3) being necessary to guarantee the continuity of simulations. Finally, a new step (Step-4) is created, using the same characteristics adopted in previous ones (dynamic, number of increments, initial increment time, etc.).

As before, local measures of the distance between SBI and the fixture is made to determine the z-displacement enough to close the gap (clamps 4 and 5). Again, the SBO flange thickness (nominally 2.0 mm) is subtracted. The following table was produced with the measurements made and boundary conditions defined.

**Table 4.3: Measures and BC for Clamps 4 and 5**

	Z-measurement (mm)	BC to be applied (mm)
Clamp 4	20.79	$U3 = -18.79$
Clamp 5	16.61	$U3 = -14.61$

With this, two boundary conditions in Step-4 were created. Again, 6 nodes were selected to which the boundary conditions are applied. Accessing the manager of BC's, all previous clamps (1, 2, and 3) were kept active. Finally, in the steps module, the option of using previous results is selected. Editing the requests, the option to capture frames with at every increment and overlaying it every time an increment is concluded for Step-4. Once the simulation is done, the result produced was the following. The next figure shows the arrow representation of all three clamps closing on the first simulation.

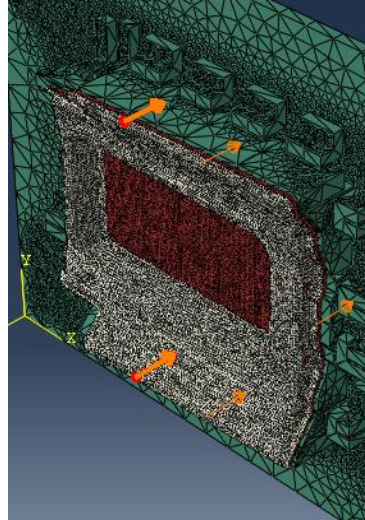


**Figure 4.5: BC for Clamps 1 through 5 (Clamps 4 and 5 highlighted)**

Once the simulation is completed, the following stress distribution (von Mises) is presented in the Visualization module.

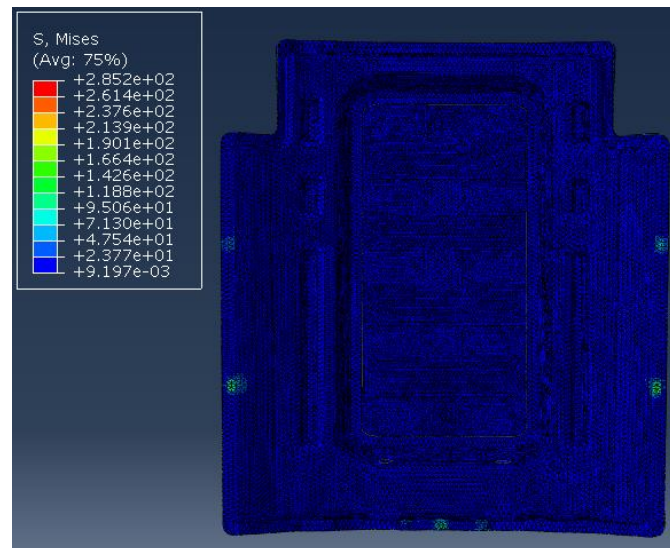


**Figure 4.6: Stress Distribution after Clamps 4 and 5 – (MPa)**

Again, most of the SBI and SBO are not subjected to high stress levels after closing the subsequent clamps (visually, between 0.009 and 23.77 MPa). The maximum stress level reached after the fifth clamp's closing is 285.20 MPa, considerable for a thermoset matrix. The same previous explanation applies here because the same boundary condition

are still applied of node selection (resulting in concentrated forces). In terms of simulation time, the time required to conclude this simulation was 4 hours 29 minutes and 11 seconds.

#### 4.3.3 Third Clamping Simulation

The previous model (second clamping simulation) is copied, editing its attributes to use the output from the second clamping simulation. The restart option is kept, putting all files necessary in the working directory to guarantee the continuity of simulations. Then, a new step (Step-5) is created with the same characteristics (dynamic, number of increments, initial increment time, etc.).

Again, local measures are done for the distance between SBI and the fixture to determine the z-displacement enough to close the gap (clamps 6 and 7). The SBO flange thickness (nominally 2.0 mm) is subtracted to determine the z-displacement to be applied at nodes on the top surface of SBI. The following table is produced with the measurement made and boundary conditions to be defined.

**Table 4.4: Measures and BC for Clamps 6 and 7**

	Z-measurement (mm)	BC to be applied (mm)
Clamp 6	20.20	U3 = -18.20
Clamp 7	17.74	U3 = -15.74

As before, two boundary conditions in Step-5 were created. As previously, 6 nodes were selected to which the boundary conditions are applied. Accessing the manager, all previous clamps (1 through 5) are kept active. Finally, in the steps module, the option of using previous results is selected. Editing the requests, the option to capture frames with at every increment and overlaying it every time an increment is concluded for Step-5. Once the simulation is done, the result produced was the following. The next figure shows the arrow representation of all three clamps closing on the first simulation.

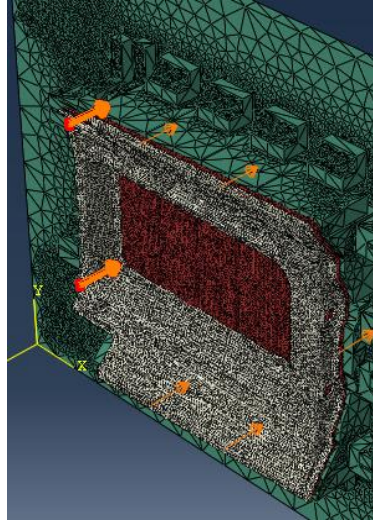


**Figure 4.7: BC for Clamps 1 through 7 (Clamps 6 and 7 highlighted)**

Once this simulation is completed, the following stress distribution (von Mises) is presented in the Visualization module.

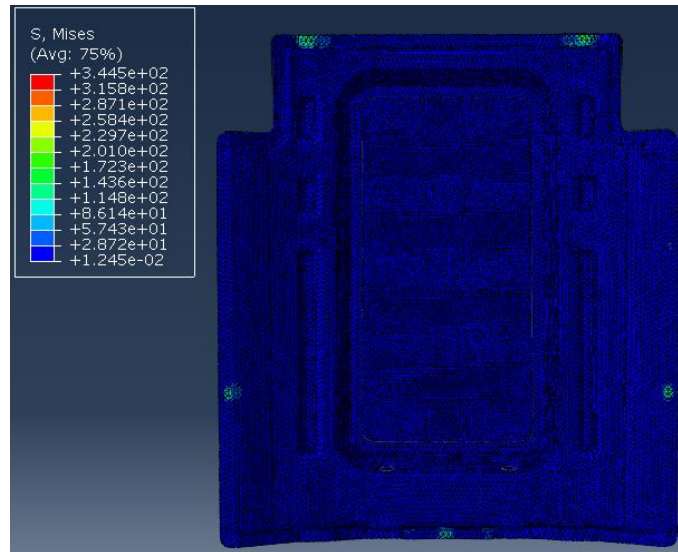


**Figure 4.8: Stress distribution after Clamps 6 and 7 – (MPa)**

As before, most SBI and SBO are not subjected to high stress levels after closing the subsequent clamps (visually, between 0.012 and 28.72 MPa). The maximum stress level reached after the seventh clamp's closing is 344.5 MPa, considerable for a thermoset

matrix. In terms of simulation time, the time required to conclude this simulation was 3 hours 15 minutes and 18 seconds.

#### 4.3.4 Gap Comparison after Clamping

As an intermediate stage, it was decided to measure the SBI and fixture gap after all clamps were closed to assess how close the simulation result is to the real assembly. In the real assembly, the same pair used in the simulations (SBO: 190318-4-4, SBI 190524-5-1) is positioned on the fixture and have the gap measured from the top surface of each block of the fixture to the bottom surface of SBI using a calliper. This procedure was repeated to all accessible points of the next figure (external flanges only). The reference used was the fixture and its blocks. In Abaqus<sup>TM</sup>, the corresponding vertical distance was measured at the same locations.

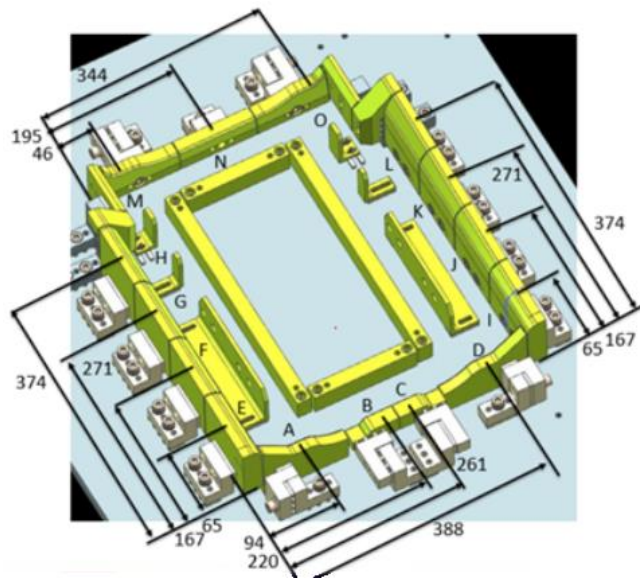


**Figure 4.9: Gap Measuring Points**

All values measured were registered on the next table, using as a reference the previous figure.

**Table 4.5: Gap Measurements**

<b>SBO</b>	<b>190318-4-4</b>			
<b>SBI</b>	<b>190524-5-1</b>			
	<b>Real Assembly</b>	<b>Simulation</b>		
<b>Points</b>	After 7th Clamp (mm)	After 7th Clamp (mm)	Difference (mm)	Difference (%)
<b>A</b>	4.71	4.48	-0.23	-5%
<b>B</b>	SBO Thickness	SBO Thickness	-	-
<b>C</b>	SBO Thickness	SBO Thickness	-	-
<b>D</b>	4.84	4.88	0.04	1%
<b>E</b>	4.06	3.95	-0.11	-3%
<b>F</b>	SBO Thickness	SBO Thickness	-	-
<b>G</b>	2.70	2.72	0.02	1%
<b>H</b>	2.59	2.53	-0.06	-2%
<b>I</b>	3.86	3.84	-0.02	-1%
<b>J</b>	SBO Thickness	SBO Thickness	-	-
<b>K</b>	2.34	2.40	0.06	2%
<b>L</b>	2.51	2.38	-0.13	-5%
<b>M</b>	SBO Thickness	SBO Thickness	-	-
<b>N</b>	5.18	5.05	-0.13	-3%
<b>O</b>	SBO Thickness	SBO Thickness	-	-

Initially, it can be noted that some measuring points coincide with clamp positions (points B, C, F, J, M and, O). At each of those locations, the gap SBI and fixture was assumed to be the SBO thickness since all clamps were active. As a consequence, no difference was calculated, either absolute or relative. For all the other points, the relative differences not greater than 5% (five percent) were registered. It becomes quantitatively clear how close the simulation and its results are to the real setup allowing us to proceed to the welding simulations.

## 4.4 Welding Simulations

The welding simulations deal with the next assembly step after the clamps are closed, which is the welding of both parts at a specific location. This section starts by presenting



all possible welding points, and it is discussed which points will be the object of analysis. Following that, briefly comment are made on which effects were tried to account for. Finally, the simulation setup is described using Abaqus<sup>TM</sup> modules as guide. As before, specific terms used on the software will be presented in bolded font.

#### 4.4.1 Possible Welding Points

Initially, without any elaborate thought, the welding can occur at a whole set of locations. Some of these points are identified in the next figure.

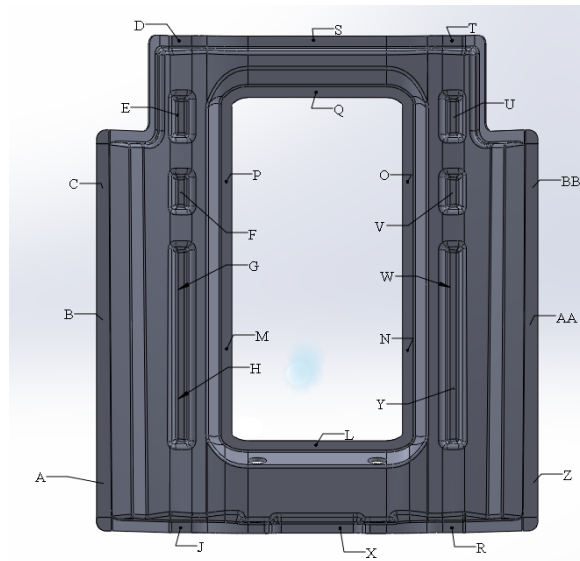


**Figure 4.10: Possible welding points**

As can be noted, using the SBI as a reference, the welding can be done either on the external flanges (A, B, C, D, S, T, AA, BB, Z, R, X, J) or on internal flanges (L, M, N, O, P, Q) or on internal features, sometimes named "pockets" (E, F, G, H, U, V, W, Y). To create a simulation for each of these welding points has its value; however, it also represents a repetitive process. The main objective, on this research, is to choose points relevant to the real welding process from which relevant information can be extracted for external flanges. The following discussion will focus on points A (bottom left flange), AA (middle right flange) and S (middle top flange).

All simulation descriptions presented so far are possible to be applied to any of these points; the following descriptions, applied to chosen points, can be altered and adapted if



any further investigation is intended at different locations. Just an additional note: the welding points presented in the last picture sometimes do not correspond to points where the gap measurement was done. For the welding simulation section and descriptions, we will be referring to points contained in the last picture (points over SBI).

#### *4.4.2 Welding Simulation Set-up*

As before, the previous model (third clamping simulation) is copied, editing its attributes to use the output from it (third clamp). The continuity of simulations will be kept, putting all files necessary in the working directory. Then, a new step (Step-6) is created with the same characteristics (dynamic, number of increments, initial increment time, etc.) as the previous ones.

It is not necessary anymore to overlay results for a following step on the step module because the welding simulation is the final one. Thus, on the restart option, it can be toggle off in the current option. Specifically, on the Step-6, the variable requested is edited, including the pressure loads output for the model. Still, on Step-6, discussing how to apply a boundary condition to recreate the welding condition.

The boundary condition should, at the same time, promote the contact between both parts (SBO and SBI) at the welding points and cause the same force (or pressure) on the area in contact with the welding head (welding machine). As noted in previous simulations, concentrated forces are induced to appear by applying displacements to nodes. It does not correspond to the situation when the welding head is used because of its geometry. Those concentrated forces were admissible in the clamps simulations because results were not extracted (force, stress or pressure). Hence, an alternative path should be pursued.

The next figure presents the welding head model, used in an experiment with real assembly parts.

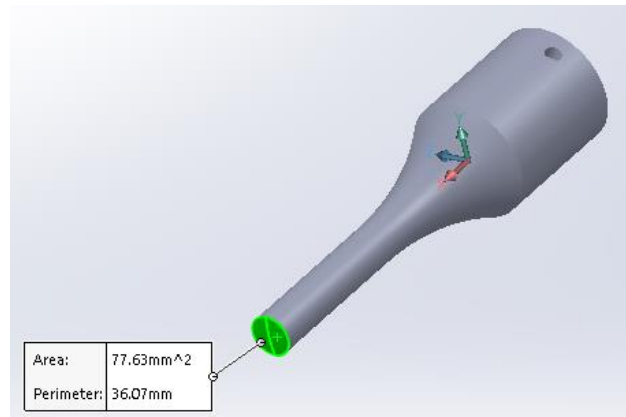


**Figure 4.11: Welding Head model (touching surface highlighted)**

As could be noted, the mesh generated for the SBI does not contain pre-drawn patches at the welding points to help us select a region over which the force (or pressure) is applied. As an alternative way, faces of neighbouring elements were selected forming a hexagon with a measured area close to the area highlighted above. The next figure presents how these elements were selected.

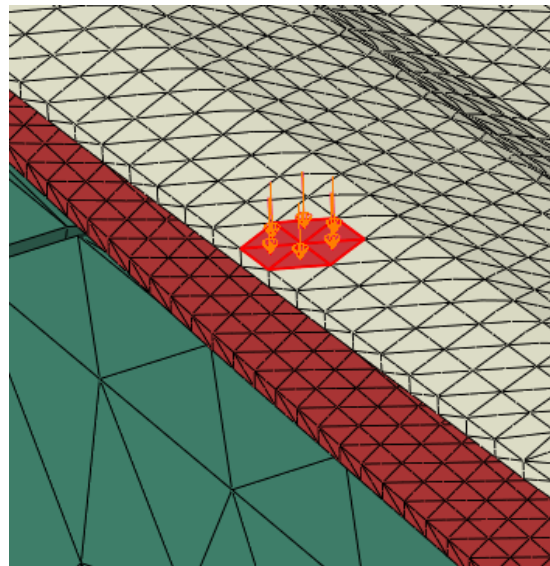


**Figure 4.12: Area selected**

With this in mind, a load in Step-6 is set of a pressure type. The region on which the pressure will be applied is some elements of the mesh, and on the visualization window, selecting the corresponding elements. Such a load is distributed, assigning a total force

over the selected faces with a magnitude equal to the one measured on the experiment. Since the welding of points A, AA and S are simulated, the maximum force values applied are presented in the next table.

**Table 4.6: Maximum Force Measured at Welding Points**

Points	Maximum Force Measured (N)
A	1127.66
AA	1561.82
S	1150.43

As a result, the next figure presents an overview when the welding boundary condition is applied at the same time all clamps are active.

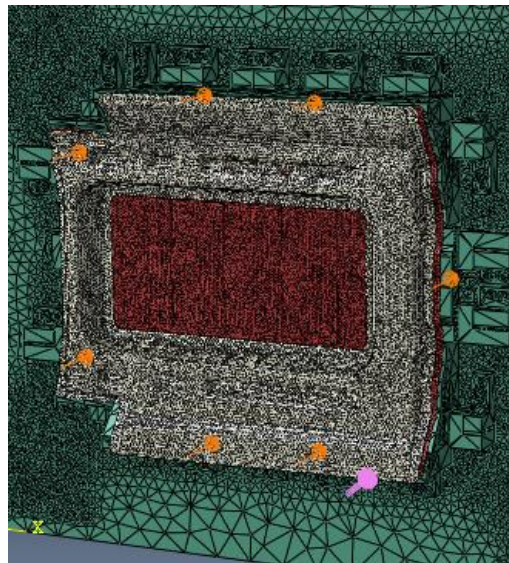


**Figure 4.13: Welding boundary condition (purple arrow) and clamps**

Once the simulation is done, curves are extracted, correlating pressure measured at the surface regions with the same points' displacement. In terms of simulation time, the time required to conclude all previous simulations is presented in the next table.

**Table 4.7: Welding Simulation Time**

Welding Point	Simulation time (hh:mm:ss)
A	1:39:04
AA	1:14:53
S	1:02:55

The next chapter discusses conclusions drawn from these curves and how they compare with the real assembly experiment.

## 4.5 Chapter Summary

This chapter described, firstly, the clamping pattern chosen to be applied to the simulation and in which sequence the clamps should be closed. Secondly, it detailed how to set sequential simulations, recovering output from previous ones, to recreate the clamping sequence, and, at the same occasion, extracted some information about the stress imposed by the boundary conditions applied. Finally, this chapter presented possible welding points, which of them were chosen to analyze deeper in this work, and how to set up boundary conditions to coherently later compare with the experimental data produced.

## Chapter 5 : Analysis of Welding Measurements

### 5.1 Overview

This chapter presents the pressure versus displacement curves extracted from three main welding points. It further dissects a single curve, proposing explanations about what is happening in each section. Later on, experimental results are compared with simulation results after all seven clamps were closed, during welding. Finally, experimental and simulation pressure-displacement curves are compared.

### 5.2 Pressure vs. Displacement curves

This section starts by presenting the graphs extracted from the simulations, combining the pressure on the welding regions' surface with the displacement of nodes contained in these elements. The next picture shows the pressure versus displacement curve for welding point A.

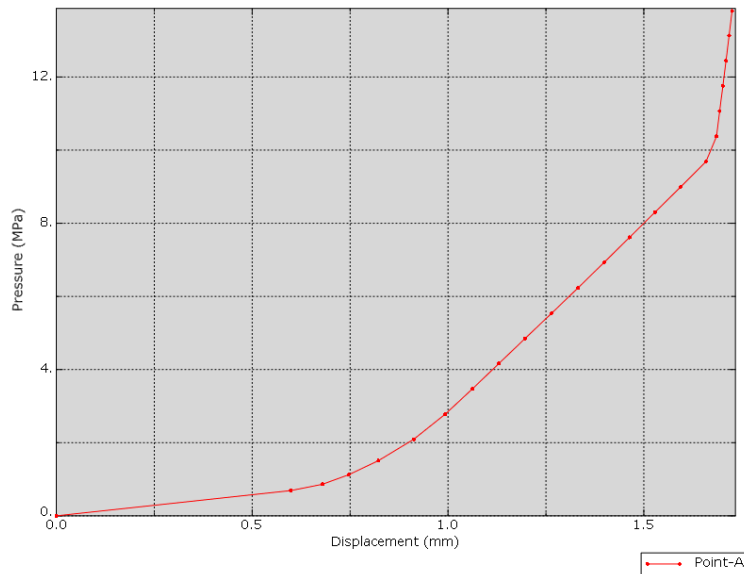


**Figure 5.1: Pressure vs. Displacement plot for welding point A**

The next picture shows the pressure versus displacement curve for welding point AA.

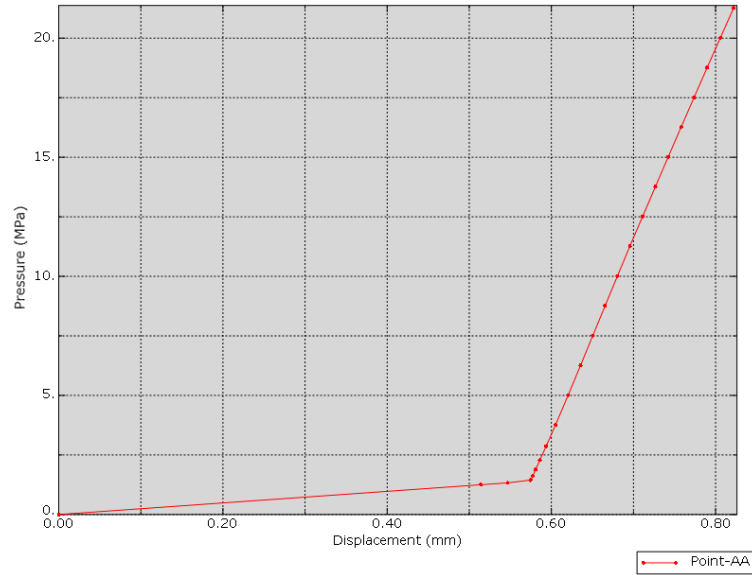


**Figure 5.2: Pressure vs. Displacement plot for welding point AA**

The next picture shows the pressure versus displacement curve for welding point S.

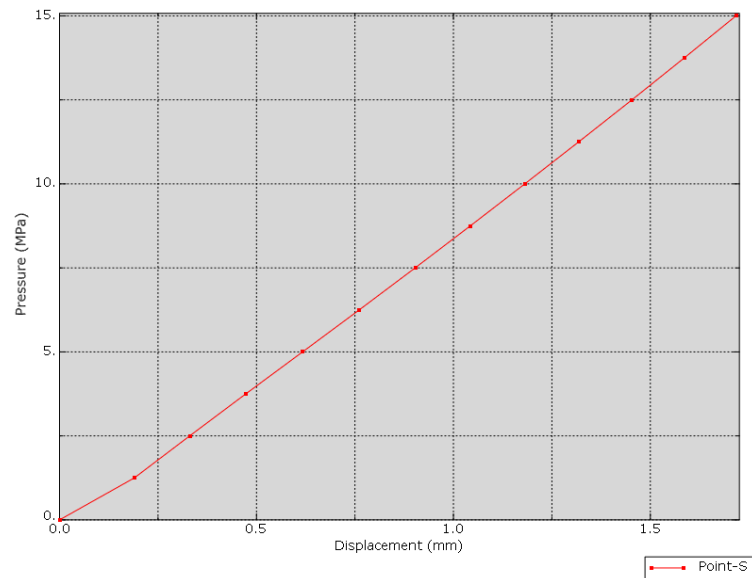


**Figure 5.3: Pressure vs. Displacement plot for welding point S**

The first observation is about the x-axis range. The displacement of selected nodes was registered only during the welding simulation, in a manner that the starting point (origin) corresponds to the moment after all seven clamps are closed. The different ranges in all plots depend on how locally warped is the SBI around the welding point; the more

upwardly warped the SBI surface is, the greater is the range presented on the plot. If we refer back to the table containing the gap measured between SBI and fixture in the simulation (table 4.5) and creating a correspondence between points, it can be concluded that: point A (gap measurement) corresponds to welding point A; point K (gap measurement) corresponds to welding point AA; point N (gap measurement) corresponds to welding point S. The following table presents an estimation of vertical displacement required to close local gaps during welding for the cited points, subtracting the nominal SBO thickness (2.00 mm) in the estimate.

**Table 5.1: Estimate of vertical displacement required**

Gap Measurement	Welding Point	Vertical Gap (mm)	Displacement Required (mm)
A	A	4.48	2.48
K	AA	2.40	0.40
N	S	5.05	3.05

With those estimates, it is possible to grasp how the distance traveled varies at those welding locations. Some nodes required a larger displacement (A and S), others a smaller one (AA). By exposing those nodes to the maximum force measured in the experiment, it is detectable the distance travelled. If the force imposed is more than enough to close the gap, it will start to compress both parts. This last observation suggests to investigate each section noted in the plots above because possibly compression was taking place at some of them.

Not only that, but there is other possible behaviour can be evidenced in the number of sections present in each pressure plot. In the pressure plot for welding point A, it can be clearly noted three sections with considerably different slopes. Parallely, for welding point AA, it is possible to identify only two sections with a sharp transition of slopes. Finally, for welding point S, it is recognizable only two slopes with a more smooth

transition. So, there is a difference not only in the number of slopes but in their shift as well.

In the next subsection, the discussion dives deeper into the plot of welding point A, trying to understand better possible causes for all changes of slopes. It is expectable that conclusions drawn at this point can be extended to the other pressure plots.

### 5.2.1 Sections of Pressure vs. Displacement Curves

In this section, the hypothesis that the main factor influencing the slopes in the previous plots is the occurrence of contact is pursued, either between SBI and SBO or between SBO and fixture, affecting the resulting stiffness of the model. As a starting point, the contact distribution is presented throughout the bottom surface of the SBI and the bottom surface of the SBO. The next figure pictures both distributions.

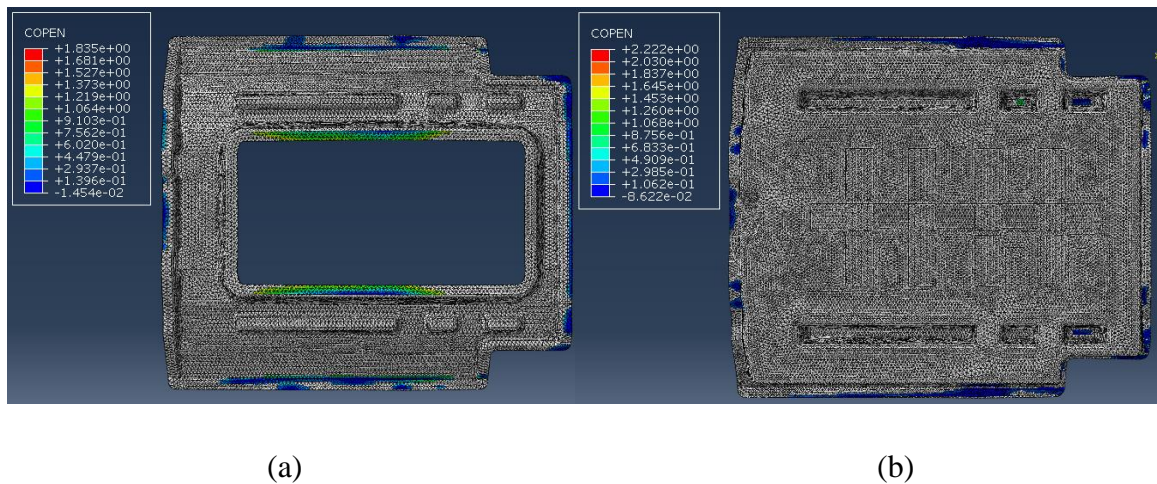


**Figure 5.4: Contact distribution before welding point A (mm): (a) SBI and SBO; (b) SBO and fixture**

Elements under pressure at A will be detailed, trying to see how the contact evolves at each increment calculated. The pressure versus displacement graph are presented for the welding point A for the sake of reference, with each increment numbered.



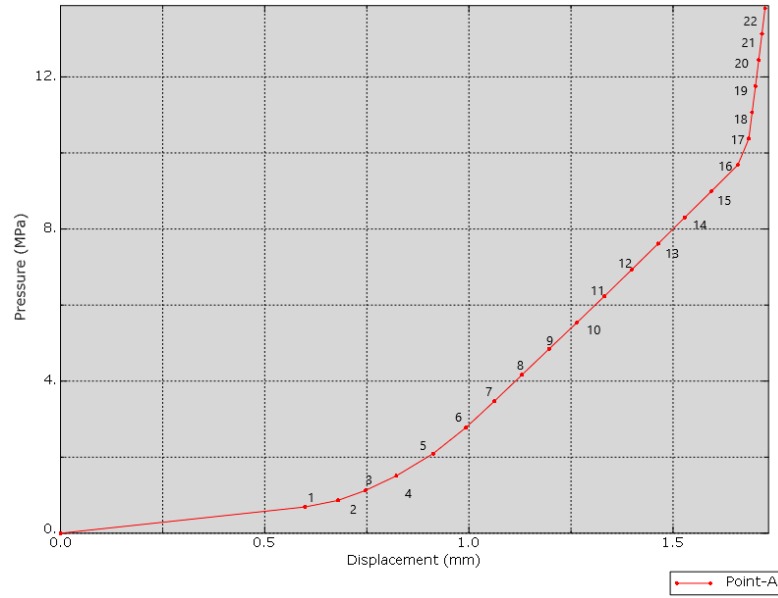


**Figure 5.5: Pressure versus Displacement for welding point A (increments numbered)**

The first increment ( $U3 = 0.598579$  mm,  $P = 0.69028$  MPa) marks the ending point of a linear section on the plot. From the second increment ( $U3 = 0.6793$  mm,  $P = 0.86285$  MPa) to the fifth increment ( $U3 = 0.912369$  mm,  $P = 2.092411$  MPa) there is a transition between two slopes. Investigating the contact on those increments visually on the SBI and SBO, we produced the following pictures in which we note the expansion of the region under contact between parts.

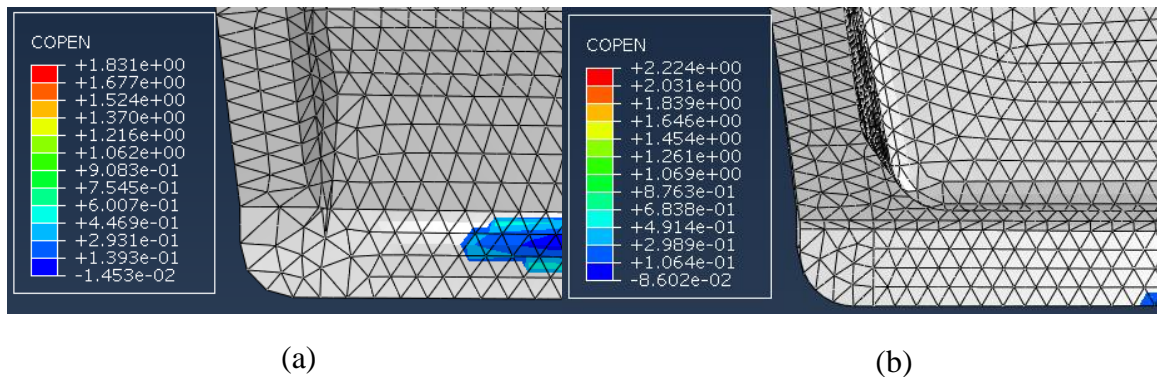


**Figure 5.6: Contact closure at welding point A during Increment 2 (mm): (a) SBI and SBO; (b) SBO and fixture**

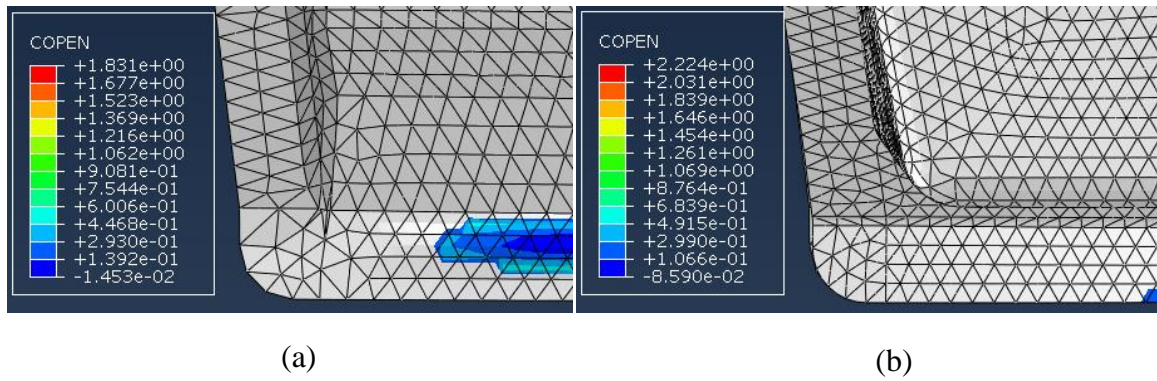


**Figure 5.7: Contact closure at welding point A during Increment 7 (mm): (a) SBI and SBO; (b) SBO and fixture**

Comparing Figures 5.6 and 5.7, it is possible to note that not much changes in the contact between the bottom surface of SBO and the fixture (pictures b). However, at the same time, the contact between the bottom surface of SBI and the upper surface of SBO progresses (pictures a). In the next picture, the evolution only for this contact is compared to help visualize it, identifying in which elements the pressure was applied on the opposite side.

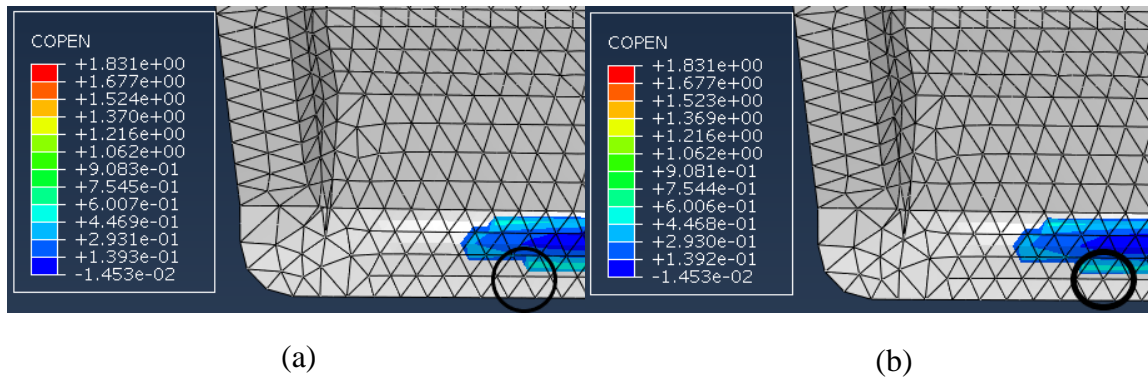


**Figure 5.8: Contact closure at welding point A between SBI and SBO (mm): (a) Increment 2; (b) Increment 7**

Thus, it is possible to affirm that before Increment 2, the elements exposed directly to the pressure did not have a well-developed contact (Figure 5.8 (a)). As a consequence, in the first two increments (1 and 2), a linear relationship between pressure and displacement is

still expected, following the stiffness of the SBI only. Once the contact is detected and spread on a larger surface exposed directly to the pressure above (Increment 6, 7 and onward), it can be noted that the contact is distributed over a larger area signifying that from that moment on, both parts will move together, explaining the change of slope in the graph.

Another comment can be done about how smooth is the slope change. It could identified six increments (increments 2 to 7) on the graph required to shift from a less stiff movement to a stiffer one. It completely agrees with the case in which two warped flanges are contacting each other, and the contact region becomes larger and larger. As the contact increases, the effective part resisting the pressure becomes stiffer. Initially, the resisting part was SBI only, with the contact, a combination of SBI and SBO progressively starts to resist the imposed pressure.

Now, the discussion is directed to the next slope transition between Increments 16 ( $U_3 = 1.65863$  mm,  $P = 9.685492$  MPa) and 18 ( $U_3 = 1.693563$  mm,  $P = 11.06605$  MPa). As before, the following pictures are produced to visualize the contact in both increments, initial and final.

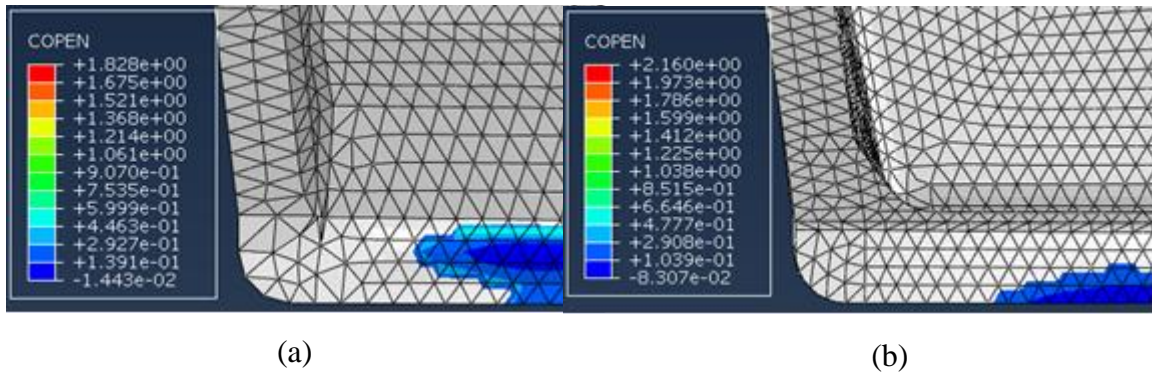


**Figure 5.9: Contact closure at welding point A during Increment 16 (mm): (a) SBI and SBO; (b) SBO and fixture**

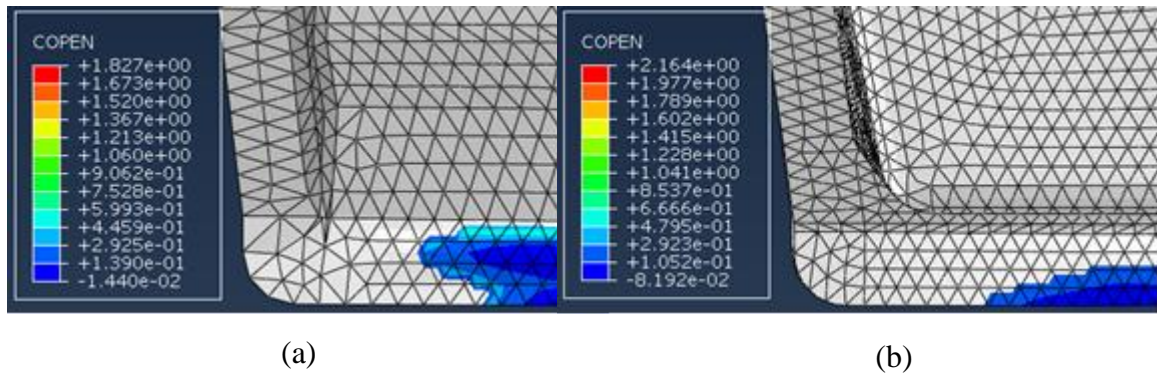


**Figure 5.10: Contact closure at welding point A during Increment 18 (mm): (a) SBI and SBO; (b) SBO and fixture**

Comparing Figures 5.9 and 5.10, it is possible to note that not much changes in the contact between the bottom surface of SBI and the upper surface of SBO (pictures a). However, at the same time, the contact between the bottom surface of SBO and the fixture progresses (pictures b). In the next picture, the evolution only for this contact is compared (SBO and fixture) to help visualize it, identifying in which elements the pressure was applied on the opposite side.

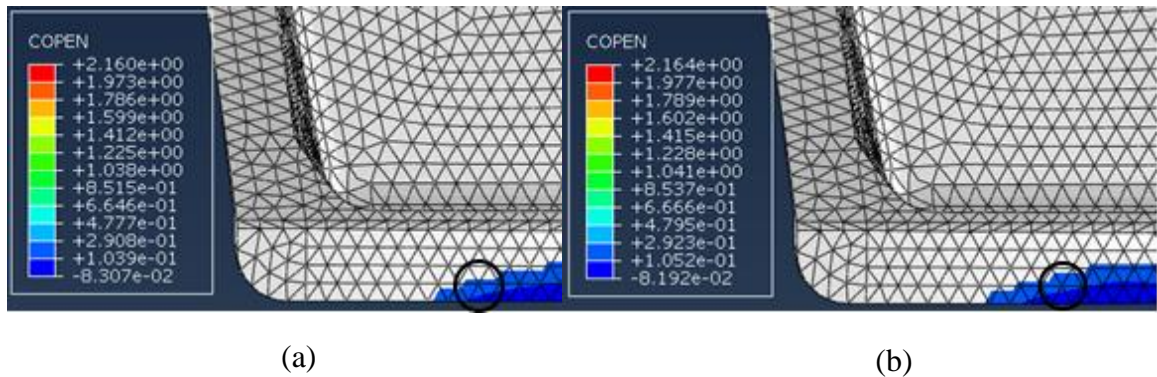


**Figure 5.11: Contact closure at welding point A between SBO and fixture (mm): (a) Increment 16; (b) Increment 18**

Hence, at Increment 16, the identified elements exposed directly to the pressure did not have a well-developed contact (Figure 5.11 (a)). In dark blue, the region extends only in some bottom elements. Consequently, in increment 16, the plot presents a less stiff



material, but still a combination of SBI and SBO. Once the contact is spread on a larger surface (dark blue) exposed directly to the pressure above (Increment 18 and onward), the contact is distributed over a larger area signifying that the SBO has a bigger area of contact with the fixture. With this, the material compression of both parts takes place.

It is worthy of note the transition of slopes. Three increments (increments 16 to 18) can be identified on the graph required to shift from the second region to a stiffer region. It agrees with the case in which material compression is occurring.

By considering how smooth the transitions are, it can be hypothesized that for the welding point AA, at which a sharp transition occurs, both parts were already in contact during the first section while the pressure was initially being applied. Consequently, the only transition detectable would be from the combined movement of SBO and SBI to material compression. On the other hand, the smooth transition detected at the welding point S suggests that the pressure applied was not enough to close the gap with the fixture. So, the only transition represents the contact between SBI and SBO. It becomes evident when we check the final gap between SBI and fixture. The next figure pictures the measurement taken after the simulation of point S is completed.

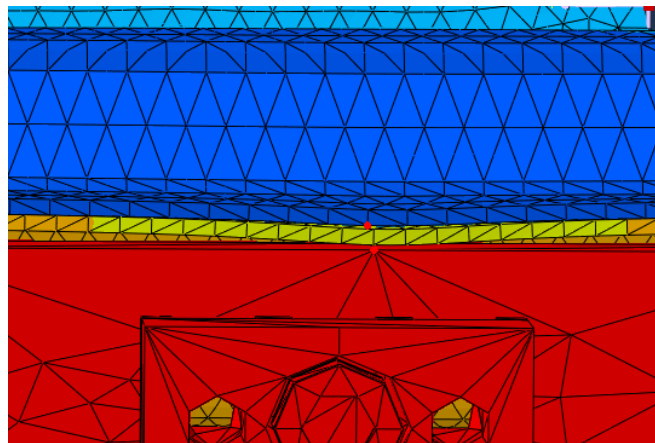


**Figure 5.12: Gap measurement at welding point S**

The vertical component of the distance between points selected was  $U3 = 2.486$  mm. Since the nominal thickness of SBO at the upper flange is 2.00 mm, it confirms the previous supposition that the total force applied at welding point S was not enough to

entirely close the gap locally. Differently from the experiment, it can be noted that even applying the same total force on equivalent areas, mainly for point S and other points not investigated, and it would be possible that the closure at the welding points was not reached.

For welding point AA, only two sections can be noted and not only that. By checking the simulation's final increment, the pressure curve's final section corresponds to the compression stage in which the gap is closed. Thus, three possibilities can be listed for the initial section of the original curve:

1. It may correspond to SBI independent movement. If that is the case, the sharp inflection point represents the combined movement (SBI + SBO), and final contact collapsed, happening at the same time;
2. Alternatively, it may correspond to the combined movement (SBI + SBO) since the beginning of welding simulation. As a consequence, it corresponds to a section with the SBI independent movement;
3. Finally, the first section may correspond to a smooth transition from one situation to another. So, the curve would represent the SBI independent movement at its initial increment. At some point along the same line, the transition to a combined movement occurs without a sudden stiffness change.

It is possible to eliminate the second hypothesis by measuring the gap between SBI and SBO at the initial position before welding AA. Being different from zero, as is the case, we can ignore it, leaving us with the remaining two possibilities. The third hypothesis is admissible only if another contact is occurring close to the AA location, capable of influencing the first increments' stiffness. We will put this discussion on hold because we will alter parts' geometry later when we conduct our parametric study (warping). This change will help us eliminate possible contact between SBI and SBO that may influence the first section of the pressure plot.

Thus, it is convenient to compare how far off the simulation is regarding stiffness and gap closure, specifically for the three points discussed so far. The next section brings the

experimental data produced and compares them with the data produced by the simulations.

## **5.3 Experimental Data and Comparisons**

This section brings data produced along the same project, using a experimental set up, in which both the force applied to close gaps and the displacement suffered as a consequence of its application were tracked. This research used a different approach regarding the gap measurement, but such information will be adapted for our purpose. The final gap measurement will be compared with simulation gaps; and the pressure versus displacement curves produced experimentally and numerically will be compared as well.

### *5.3.1 Comparison of Pressure vs. Displacement curves*

This section starts by presenting the pressure displacement plots produced by the experiment and imported to Abaqus<sup>TM</sup>. The next figures show the graphs for welding points A, AA and S.

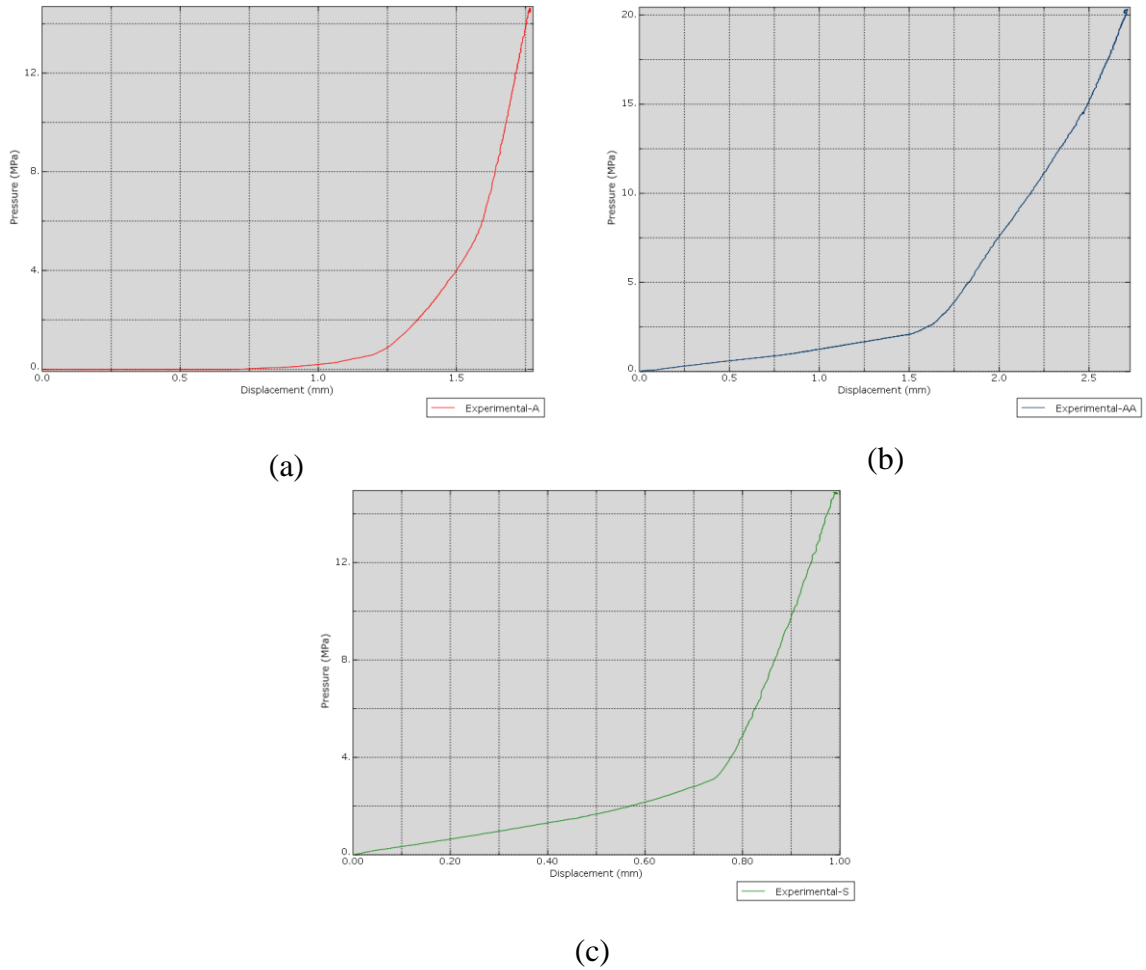


**Figure 5.13: Experimental Pressure versus Displacement plot: (a) welding point A, (b) welding point AA, (c) welding point S**

The previous plots were produced by translating the data horizontally to guarantee that the starting point of the curve is placed as soon as a force different from zero is measured (origin). The plots produced were imported into Abaqus superposing them to each simulations curves for each welding point. The next figures show the resulting graphs.



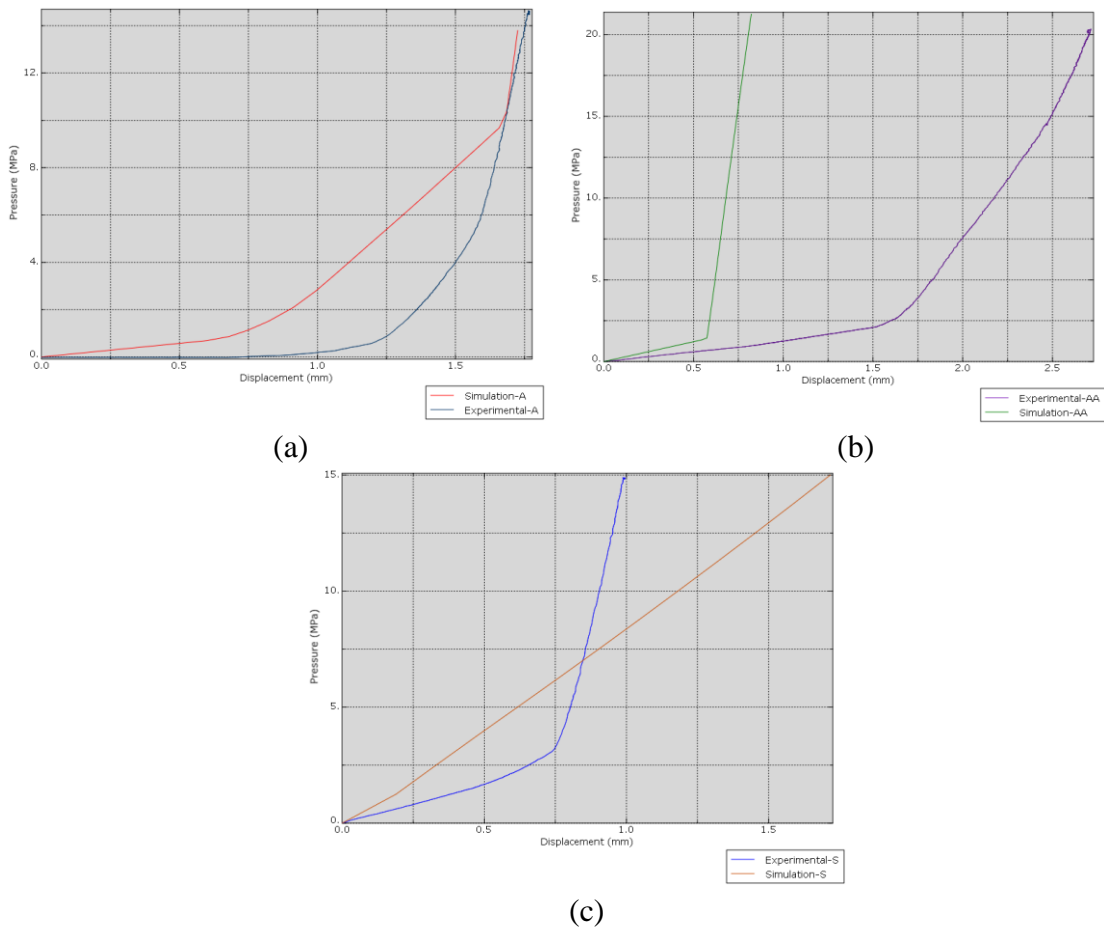


**Figure 5.14: Comparison plots: (a) welding point A, (b) welding point AA, (c) welding point S**

Initially, the primary factors can be listed and where they mainly influence the behaviour of both curves, namely:

1. SBI warpage: directly influences the horizontal length of the initial section and the maximum pressure measured at the final point of it;
2. SBO warpage: its relation with SBI warpage directly influences the initial section of the plot but primarily affects the second section horizontal length and its maximum pressure reached in its final point;
3. Stiffness of both parts: affects the slope of all sections;

4. Boundary condition selected: it can somehow contribute to the model's resulting stiffness during welding since it locks some nodes' vertical movement, interfering in the sliding and sideways movements.

With regards to the similarity, it is evident that better agreement occurs at welding point A. Considering the three sections of the plot (a), it is notable that SBI in the simulation is stiffer than the experimental SBI in the initial section. Not only that, in the experiment, it takes longer for the contact to occur between SBI and SBO. It can be due to the combination of SBI and SBO warpage, that is, the distance between surfaces is greater in the experiment. The curves seem to shift once the contact takes place, but both curves' slopes are somewhat parallel in the second section.

It becomes evident the SBO warpage in the second section. In the experiment, we note a smaller displacement required to cause the gap closure when compared with the simulation one. In the final section, we compare both slopes and once again, the simulation is stiffer than the real assembly, probably because of stiffer model and the boundary conditions selected. As a summary, from our previous list, the main factor influencing the response at point A is the warpage of both parts locally, which acts shifting one curve to another.

Regarding graph (b), for welding point AA, the main difference is the occurrence of all two contacts sequentially in the experiment, dividing the plot into three sections, as expected. The same did not happen with the simulation data. It seems that, in the simulation, both contacts (SBI+SBO and SBO+fixture) happen at the same time, explaining the initial smooth slope (SBI movement only) transitioning suddenly at one point only to a steeper slope (compression of parts).

Another evident difference is the horizontal length of both cases. The simulation seems to agree better with which we measured at the laboratory and in Abaqus<sup>TM</sup>. Since the experiment was done before the scanning, it is possible that the real parts may have suffered additional deformation, altering the warpage profile at that local. The cause of this additional deformation may be the experiment itself, by applying loads cyclically at the clamps and the welding points, or another one not identified by us. Such speculations

do not justify the model being stiffer, but such behaviour is similar to what occurred at point A.

About graph (c), for welding point S, again, the main difference is the contact being evident in the experiment. As we already showed in the simulation, the final contact between SBO and fixture did not happen. We can also identify the disparity of vertical displacement required to close the gap at it. Another big difference is the horizontal length of the second section of the graph, whose cause is presumably the relation between both parts' warpage. It makes evident how different is the SBI gap in both cases, experimentally and numerically.

A possible conclusion drawn from all previous observations is the influence of welding positions to clamp positions. Welding happening in-between clamp locations (points AA and S) produces stiffer models and curves not containing all three sections, sometimes only the contact of parts, sometimes only between part and fixture. Not only that, but there is a great difference in warpage at these locations after clamping boundary conditions are applied. Consequently, the displacement required to close the gaps at welding points is decreased, altering the slope at each curve.

In regards to points A, not located perfectly in-between clamps, the influence is dampened. A stiffer model still can be resulted but not at the same rate. Thus, it is possible to conclude that a more rigid model is produced as closer a welding point gets to clamping positions because of the boundary condition chosen. Finally, for cases in which compression was detected (points A and AA), the slopes of both experiment and simulation are similar, except for the point AA case at which it probably still has the influence of boundary condition making it more rigid.

## 5.4 Chapter Summary

In this chapter, the resulting pressure-displacement curves produced were presented by the simulation setup in previous chapters. Two types of curves were noted: one divided into three sections for the welding point not located in-between clamps, and another divided into two sections for welding points perfectly aligned between clamps. Initially, it

could be hypothesized about what caused such regions and changes of slopes. Later on, the numerical result were compared with experimental data, pointing out possible influences for differences on results.

## **Chapter 6 : Parametric Studies**

### **6.1 Overview**

This chapter presents the parametric study conducted in the simulation, varying the following parameters: material, parts warped and clamping pattern. An initial description of how the study was conducted is presented followed by the main results and interpretation for each of them. At each category, the impact of changing each parameter is discussed.

### **6.2 Parametric Studies Description**

Previous chapters have described the setup of a simulation that involved a specific chosen material (LFT, supposed isotropic) applied to numerically warped parts (SBI and SBO) been assembled using a pre-established clamping pattern. These three main characteristics, namely, materials, use of non-use of warped parts and clamping pattern, are going to be varied, objecting to seeing how influential each of them are.

In the material simulations, three different materials will be adopted, two supposed isotropic and one with some anisotropy included with all remaining variables (clamping pattern and warped) kept constant. One of these options is commercially known as Tepex™, which consists of a polyamide matrix containing roved glass fibres woven randomly. In this work, it will be referred to under the name GMT – isotropic. The second option will be referred to as LFT- Anisotropic.

In the use of no use of warped parts, all possible combinations of warped and non-warped SBI and SBO is compared, keeping the remaining factors unaltered (isotropic material and clamping pattern). Finally, we suggested two additional clamping sequences for the clamping pattern simulations, involving not seven clamps as in the base-case, but five-clamp and three-clamp setups. As expected, the remaining factors (materials and warped parts) were fixed.

The next table summarizes the parametric study, with parameters involved and which simulations are or not required.

**Table 6.1: Parametric Study summarized**

		Simulations			
		Warping	Positioning	Clamping	Welding
Material	Base-line:  1) Warped SBI + Warped SBO; 2) LFT – Isotropic; 3) Standard Clamping (7).	X	X	X	X
	LFT – Anisotropic (1 and 3 fixed)	X	X	X	X
	GMT – Isotropic (1 and 3 fixed)		X	X	X
Warped Parts	Warped SBI + Undeformed SBO		X	X	X
	Undef. SBI + Warped SBO		X	X	X
	Underf. SBI + Undef. SBO		X	X	X
Clamping Pattern	Non-Standard Clamping (5)			X	X
	Non-Standard Clamping (3)			X	X

Some observations can be made. Firstly, since the new anisotropic material is applied to both parts' undeformed mesh, it is necessary to re-run the warping procedure (as described in Chapter 2) to transfer the geometry to those parts. As a consequence, all the following simulation should be executed again. For the GMT - Isotropic material, the

warping simulations are unnecessary because the deformed state is assumed free from stress. Only at the positioning stage, we allow the stress to be measured.

For the warped parts, all possible combinations between warped and not deformed meshes were applied. Since the previous warped meshes were used, the warping simulations were unnecessary. However, in every substitution (removal of a warped part to include an undeformed one), a new positioning simulation is required. That is why they were marked. Finally, for the change in clamping pattern, the simulation starts from the previous positioning, altering the clamping simulation onwards.

The next section describes the setup for the material change and discusses its results compared with experimental and numerical data.

### **6.3 Change in Material Properties**

With regards to materials, two new options for materials were chosen, and the main properties adopted for the numerical simulation of GMT – Isotropic were:

1. Young's module: 19000 MPa;
2. Density: 1.80 g/cm<sup>3</sup>;
3. Poisson's ratio: 0.35 (the same assumed for the LFT isotropic case);

Alternatively, the second material option was numerically established. By using the moulding simulation performed in Moldex<sup>TM</sup> by another contributor, a mapping procedure build-in the software was used. Through this mapping procedure, the orientation of fibres and its local weight percentage are mapped into the not deformed mesh of Abaqus<sup>TM</sup>. As a consequence, elements' properties (density, Young's module, and Poisson's ratio) are affected. The software automatically groups together elements with the same mechanical properties on a second step, creating a new not deformed mesh with some anisotropy defined.

Once this mesh is defined and imported in Abaqus<sup>TM</sup>, previous simulations (warping, placing and clamping simulations) need to be re-run to put both parts in their initial stage for welding. This work will refer to this material as anisotropic, even though it is

recognizable that it does not correspond to the real anisotropic LFT material. The objective of using this material is to assess the model's results when even some anisotropy is inserted into it. The next table summarizes all material properties applied.

**Table 6.2: Material Properties for parametric study**

Material	Young's Module (MPa)	Density (g/cm <sup>3</sup> )	Poisson's ratio
LFT – Isotropic (baseline)	14300	1.45	0.35
LFT – Anisotropic	Moldex <sup>TM</sup>	Moldex <sup>TM</sup>	Moldex <sup>TM</sup>
GMT - Isotropic	19000	1.80	0.35

It is possible to interpret the results for the LFT - Anisotropic welding simulations. Once the welding simulations are done, the pressure versus displacement curves were extracted and superposed with the results from the base-case. The next figure shows the superposition for welding point A between LFT – Isotropic and LFT - Anisotropic.

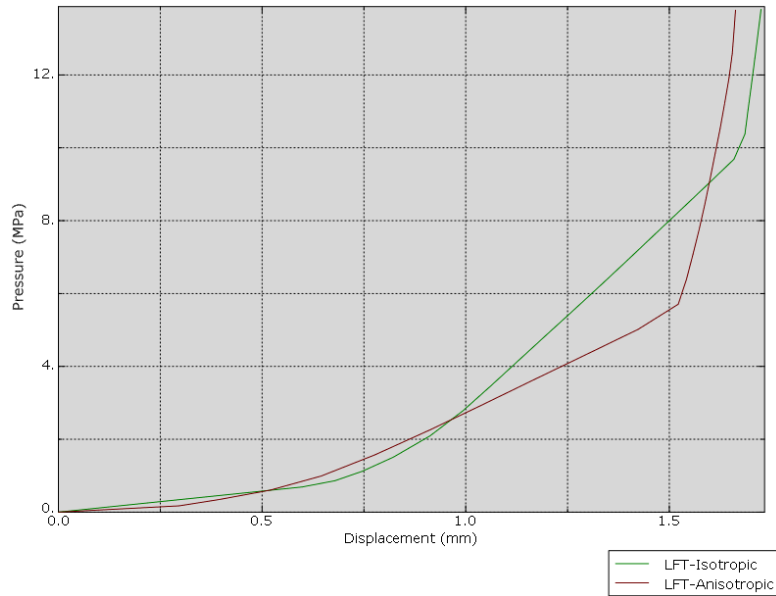


**Figure 6.1: Pressure-displacement curve comparing Isotropic and Anisotropic LFT – point A**



Some differences in the stiffness of both materials are clearly noted. At every section, as expected, the anisotropic material is less stiff than the supposed isotropic one, the only exception being at the third and final section, at which material compression is taking place and some parallelism between curves. Another point is the similarity between the displacements required to close the gap at this location. It takes roughly 1.6 mm for the isotropic case to close it (second transition, green curve), whereas it takes nearly 1.5 mm for the anisotropic case (second transition, brown curve). It can be assumed that the difference is due to clamping a less stiff material since we did not change the clamping position or pattern before welding A. It allows the anisotropic parts to better conform to each other, reducing the gap between them and between parts and fixture.

Comparing, then, the anisotropic simulations with the experimental data, the following superposing plot was produced.

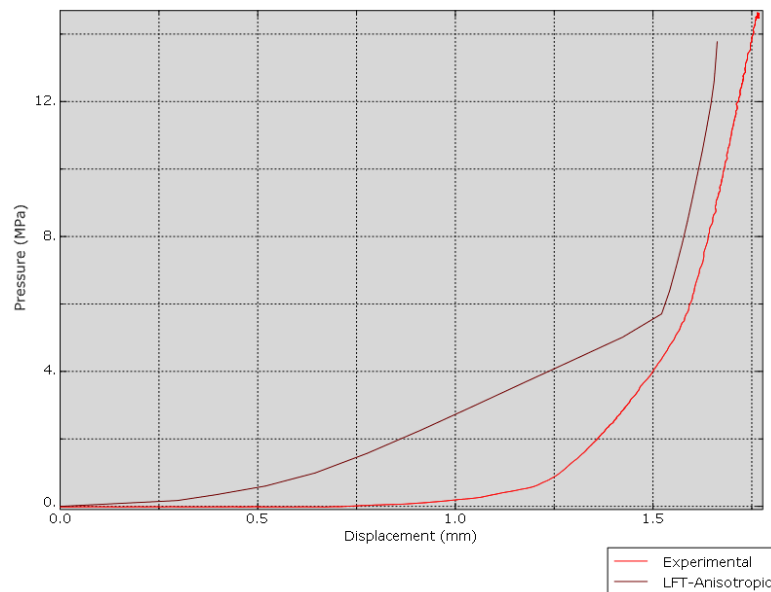


**Figure 6.2: Pressure-displacement curve comparing Experimental and Anisotropic LFT – point A**

Regarding the displacement required to close the gap, a smaller distance (second transition) than the previous plot is noted. Again, a good approximation is found between slopes at two sections (namely, in the first section, SBI movement and in the third section, compression against the fixture). However, in the second section, at which there

is a combined stiffness of SBI and SBO, two effects take place: 1) the displacement in which both parts are moving, and 2) a less inclined slope, indicating a smoother material than the experimental one.

Moving to the other welding points, now the comparison between isotropic and anisotropic for welding point AA is presented.

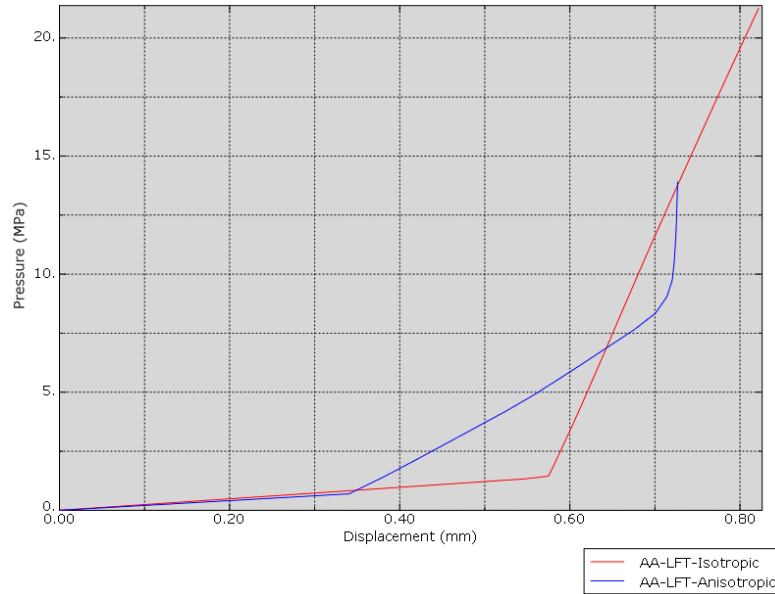


**Figure 6.3: Pressure-displacement curve comparing Isotropic and Anisotropic LFT – point AA**

The more striking difference is the presence of all three sections in the anisotropic curve, while two sections were produced in the isotropic one. It suggests the anisotropic simulation, even with the same clamping boundary conditions, better compares with the experimental data. The isotropic case and its stiffness (combining material property and nearby clamps) heavily interfere in the curve behaviour. Both curves start with a close inclination, with the anisotropic case being slightly smaller, as expected. In both cases, gap closure and some compression occur. However, the stiffness in the isotropic case overshadows the distinction supposed to occur between the last two sections, whereas in the anisotropic case, it is clearer the distinction.

Superposing the anisotropic case with the experimental data, the following plot was produced.

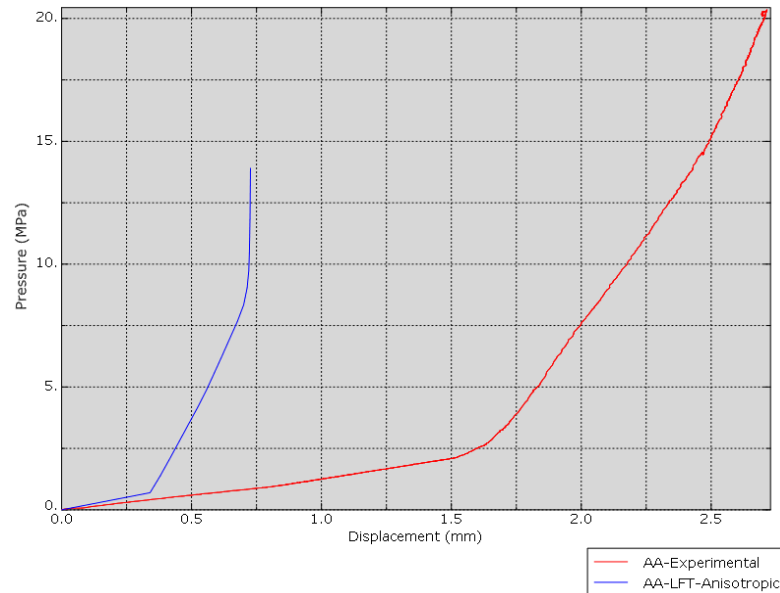


**Figure 6.4: Pressure-displacement curve comparing Experimental and Anisotropic LFT – point AA**

Initially, a great difference between the vertical displacements required to close the gap in both cases is evident. Added to that, even applying an anisotropic material, a stiffer model than the experimental data is produced in all sections. This comparison makes more evident the influence of the fact point AA located between two clamping's boundary conditions, making a more rigid model than at welding point A, latter compared.

Moving to the next welding point, now the comparison between isotropic and anisotropic for welding point S is presented.

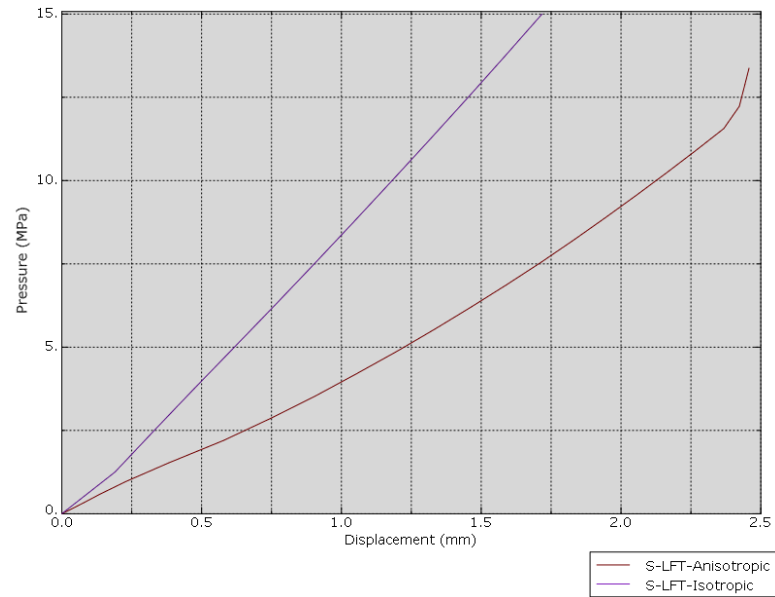


**Figure 6.5: Pressure-displacement curve comparing Isotropic and Anisotropic LFT  
– point S**

All three sections were produced for the anisotropic simulation (gap closure), evident by the second transition and the occurrence of some compression. By the plot, it can be estimated that the vertical displacement required to close the gap was 2.25mm for this location. Comparing with the isotropic case, the anisotropic one produced a less stiff model, as expected.

Superposing the anisotropic case with the experimental data, the following plot for welding point S was produced.

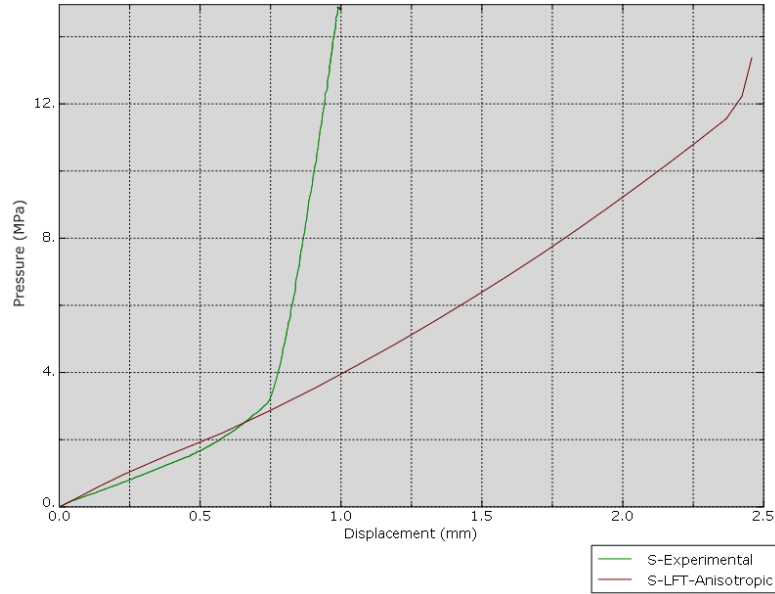


**Figure 6.6: Pressure-displacement curve comparing Experimental and Anisotropic LFT – point S**

A great difference between the vertical displacements in the second section of both curves (SBI and SBO in contact, combined) can be pointed out. Even applying an anisotropic material, a slightly stiffer model than the experimental data in the same section is produced. There is some parallelism between curves in the third section (compression), but the experimental data presents a less stiff material.

At this point, partial conclusions can be drawn. Firstly, the definition of an anisotropic material did not alter the displacements required to close gaps. As a consequence, the horizontal length of each curve section is either not altered or slightly changed because we did not act upon the geometric aspect of all parts compared. Another conclusion is the anisotropic inserted, producing a less stiff model. We can identify that the model's whole stiffness is due to a combination of: 1) stiffness induced by the boundary conditions selected and 2) the stiffness defined for the part's material. In the anisotropic case, the material stiffness was reduced, as a whole, so the boundary condition brings the model to a stiffness close to that measured experimentally. To finish our comparison, we present the next table comparing the simulation time for the base-case and the LFT-Anisotropic

case. All simulation times presented here after correspond to the time required to finish the simulation using a machine with the following specifications:

- Processor: Intel<sup>R</sup> Core<sup>TM</sup> i7-6700 CPU@ 4.00GHz
- RAM: 32 GB
- 64-bit operating system, x64-based processor
- 10 Abaqus' tokens (6 CPU cores, without concurrent jobs)

**Table 6.3: Comparison Simulation Time (LFT-Anisotropic)**

		Simulation time (hh:mm:ss)	
		LFT-Isotropic	LFT-Anisotropic
Clamping Simulations	1 <sup>st</sup> -2 <sup>nd</sup> -3 <sup>rd</sup>	3:43:03	3:07:02
	4 <sup>th</sup> -5 <sup>th</sup>	4:29:11	1:53:46
	6 <sup>th</sup> -7 <sup>th</sup>	3:15:18	5:00:52
Welding Point	A	1:39:04	1:13:03
	AA	1:14:53	0:54:47
	S	1:02:55	1:01:51

With the exception of the second clamping simulation, all simulation time required to conclude them reduces.

We can now turn our attention to the definition of a new material, namely, GMT - Isotropic. For this case, we only redefined some parameters in the Material tab. In the next figure, we superposed pressure-displacement curves, comparing LFT - Isotropic and GMT – Isotropic for welding point A.

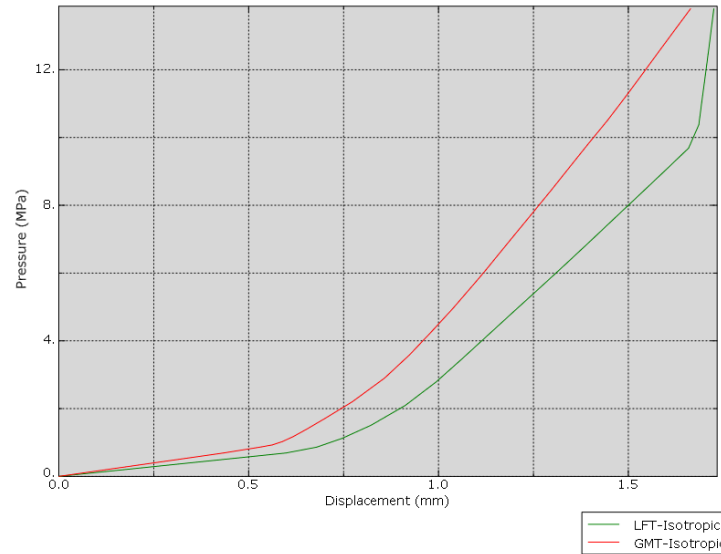


**Figure 6.7: Pressure-displacement curve comparing LFT-Isotropic and GMT-Isotropic – point A**

Since we all occasions the force applied to the welding surface is the same; we note that the total force applied was not enough to bring both parts to compression (third section) and close the gap. As we have defined a stiffer material (GMT-Isotropic), such a curve's behaviour is expected. In the first and second sections, we note a more inclined slope confirming the effect of introducing a stiffer material.

Comparing, then, the GMT-Isotropic simulations with the experimental data, we produced the following superposing plot.

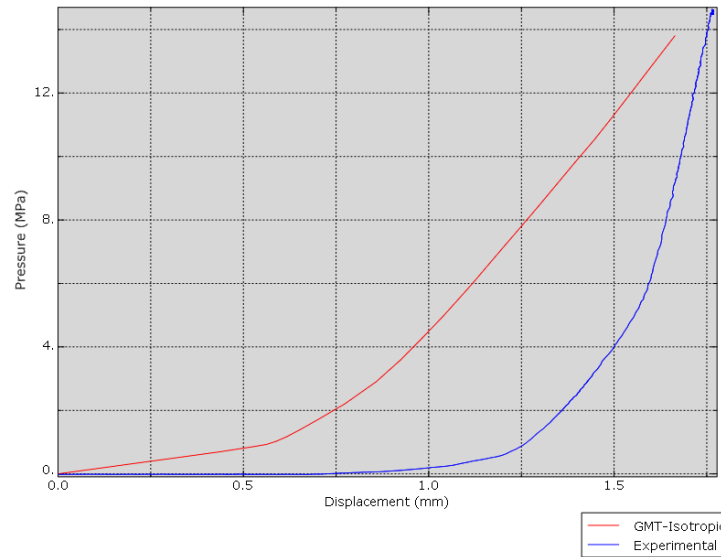


**Figure 6.8: Pressure-displacement curve comparing Experimental data and GMT-Isotropic – point A**

As expected, the GMT-Isotropic curve has a more inclined slope indicating a stiffer material than the real components. Individually, in the first section, it is evident how much the SBI (GMT) is stiffer than the real part. Superposing the LFT – Isotropic with GMT – Isotropic for welding point AA, we produced the following plot.

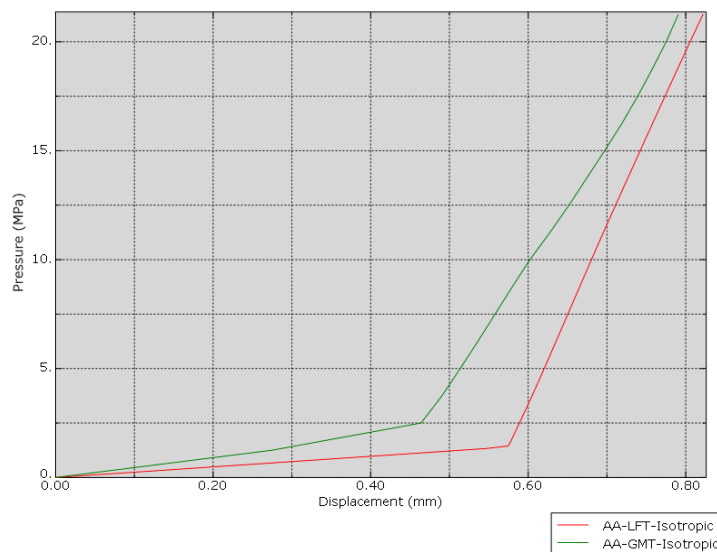


**Figure 6.9: Pressure-displacement curve comparing LFT-Isotropic and GMT-Isotropic – point AA**



The first section of both curves corresponds to an expected behaviour for a stiffer material, the GMT material presenting a higher slope. Besides that, we note a difference in the vertical displacement required to contact between SBI and SBO. However, the last section for both curves presents the stiffer material with a less inclined slope. This last result is counter-intuitive to what was expected.

Comparing the experimental data with the GMT-Isotropic curves at the same welding point, we produced the following graph.

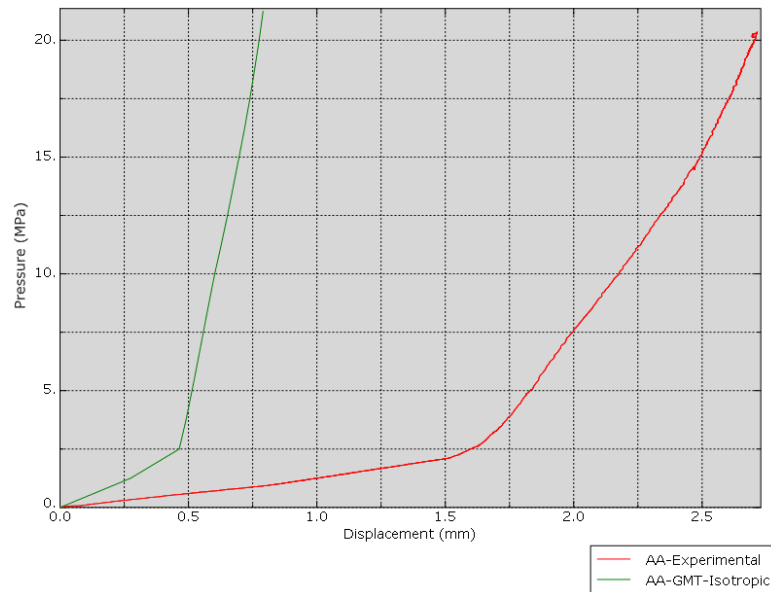


**Figure 6.10: Pressure-displacement curve comparing Experimental data and GMT-Isotropic – point AA**

This graph shows how much stiffer the GMT-isotropic material is compared with the experimental data. This behaviour in all sections was expected since the GMT material is numerically stiffer when defined.

Now we turn our attention to welding point S, comparing the data produced with material GMT-isotropic and our base-case. We produced the following graph.

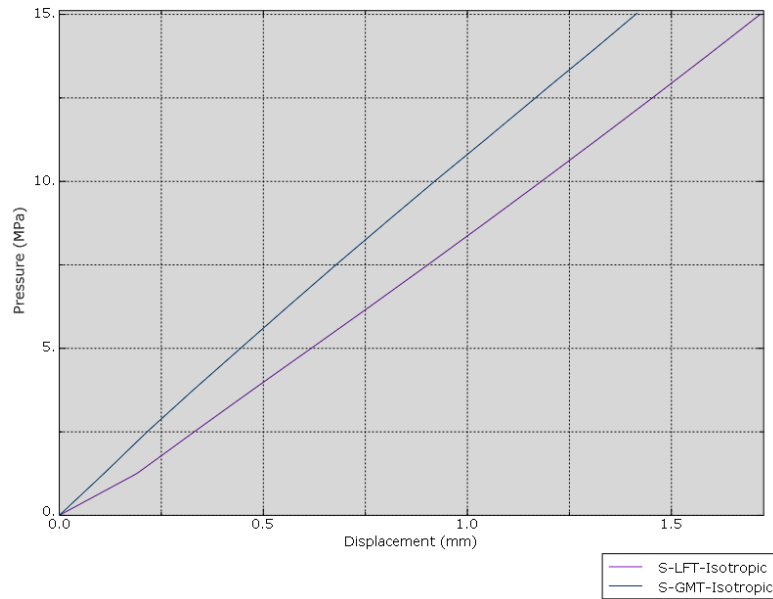


**Figure 6.11: Pressure-displacement curve comparing LFT-Isotropic and GMT-Isotropic – point S**

Since we deal only with the first two sections at welding point S and the GMT material is evidently stiffer, the plot shows an expected behaviour. Another consequence, the total force applied was not enough to close the gap either, keeping the plot on the first two sections without compression.

Comparing the experimental data with the GMT-Isotropic curves at the same welding point, we produced the following graph.

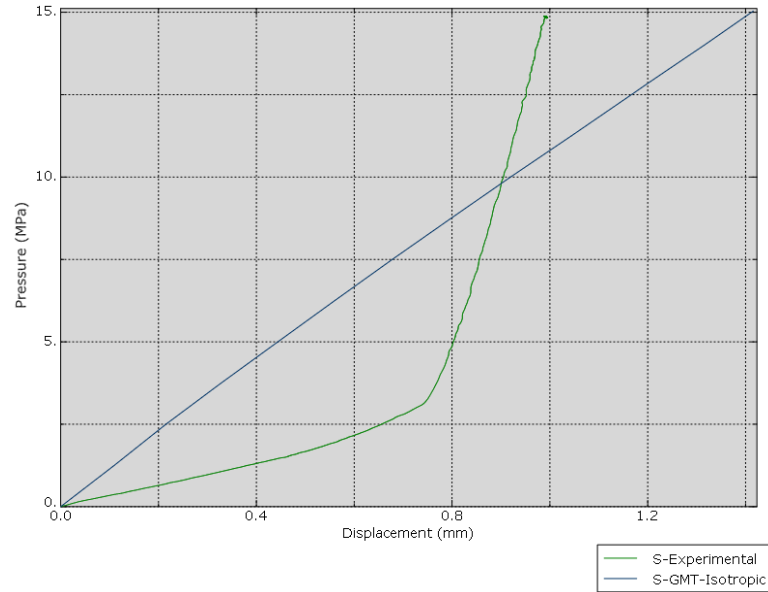


**Figure 6.12: Pressure-displacement curve comparing Experimental data and GMT-Isotropic – point S**

As presented before, the use of a stiffer material (GMT-Isotropic) did not allow the gap closure. So, when comparing the experimental data, it only makes sense to compare the first two sections of the experimental data with the corresponding section of the simulation. Consequently, the behaviour of the GMT material is stiffer than the experimental one, as expected. To finish our comparison, we present the next table comparing the simulation time for the base-case and the GMT-Isotropic case.

**Table 6.4: Comparison Simulation Time (GMT-Isotropic)**

		Simulation time (hh:mm:ss)	
		LFT-Isotropic	GMT-Isotropic
Clamping Simulations	1 <sup>st</sup> -2 <sup>nd</sup> -3 <sup>rd</sup>	3:43:03	6:03:29
	4 <sup>th</sup> -5 <sup>th</sup>	4:29:11	2:56:20
	6 <sup>th</sup> -7 <sup>th</sup>	3:15:18	4:10:52
Welding Point	A	1:39:04	2:17:14
	AA	1:14:53	1:47:35
	S	1:02:55	1:37:46

With the exception of the second clamping simulation (4<sup>th</sup> and 5<sup>th</sup> clamps), all simulation time required to conclude them increased.

In summary, the partial conclusions draw only by changing the material properties are:

1. The use of Moldex<sup>TM</sup>-defined anisotropic material reduced the stiffness of all sections. When compared with experimental data, it became less stiff in the first two sections, and with comparable stiffness in the third section (comparison);
2. The use of GMT-isotropic material created a stiffer model as a whole. It affected all section of the pressure curve, as expected. Such material was even stiffer than the experimental data;
3. Since we kept the same force applied over the same area for stiffer materials, the force was not enough to close the local gap and make the simulation reach the compression stage.

This section altered only the material properties trying to visualize which sections of the pressure-displacement curve would be affected by it. The next section alters the warpage

of each part, alternatively, and for both parts at the same time. It tries to make evident the geometric influence of gaps into the pressure curve.

## 6.4 Change in Warped and Not Warped Parts

In this section, it is intended to assess the model (with proposed BC's) in terms of geometric influence due to each part's warpage. By altering each part's geometry (warpage), the vertical displacement required to contact to occur will be changed and gaps to be locally close. To summarize the content of this section, the next table is presented.

**Table 6.5: Summary of Warpage Change**

	SBI	SBO
Base-Case	Warped	Warped
1 <sup>st</sup> Case	Warped	Undeformed
2 <sup>nd</sup> Case	Underfomed	Warped
3 <sup>rd</sup> Case	Undeformed	Undeformed

For clarification purposes, each case will be compared with the experimental data because it was noted how different the local gaps are at the considered welding points. Instead, it will be compared the base-case against each change and point out where the main effects are.

The next plots compare the effects of using an undeformed SBO at all welding points. Starting with welding point A, the following plot was produced.

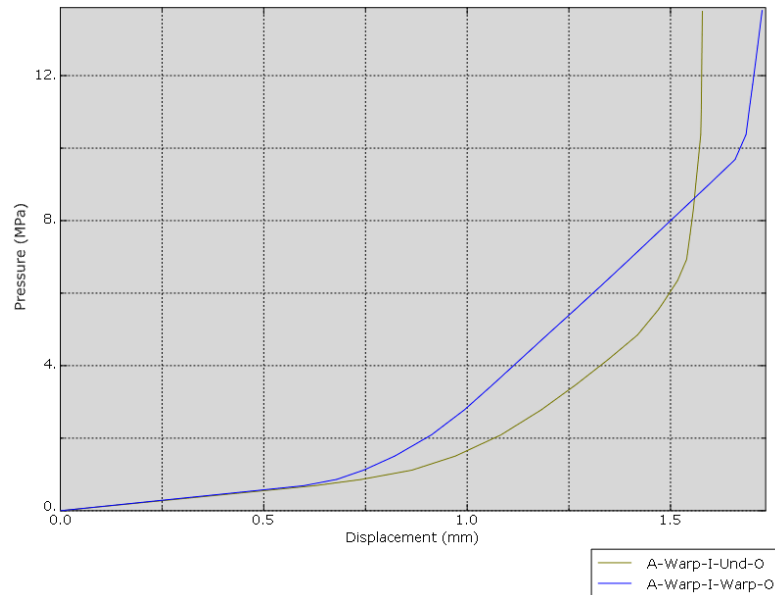


**Figure 6.13: Pressure-displacement comparing the base-case with 1st Case - point A**

As expected, since a warped SBI is used, the first section of both curves coincide. They start to move apart at the inflection point, at which, as shown before, the contact with SBO starts to occur and spread locally. Since a geometrically different SBO is used, with and without vertical warpage, the moment of contact is different, explaining the curves apart. From that point on, different slopes can be seen even though either material properties or clamping positions were changed. The explanation proposed is the geometry (warpage) of SBO affecting its stiffness, in a way that warped SBO is stiffer than the undeformed version, producing a stiffer when combined with the same SBI (second section). Later on, the difference on the second inflection point is noted as a direct consequence of a geometric change in SBO. Naturally, if an SBO as-designed is used, the gap between it and the fixture is either zero or close to it, requiring a smaller displacement to close it and cause the final contact. Finally, a stiffer model is noted with the undeformed part.

The next plot compares the pressure curves for welding point AA.

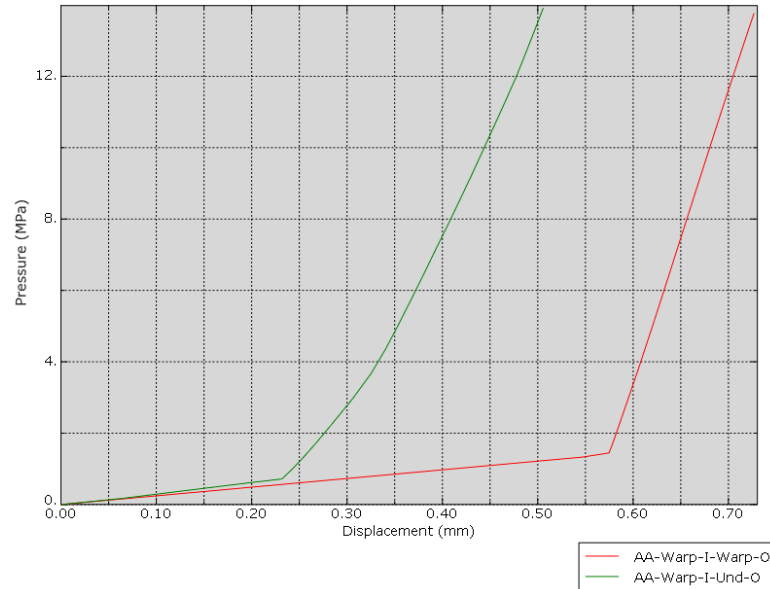


**Figure 6.14: Pressure-displacement comparing the base-case with 1st Case - point AA**

Three sections are evident in the green curve (with undeformed part). An intermediate line segment for the second section, corresponding to the combined movement, appears when a sufficient gap between SBI and SBO is inserted in the original model, which was done by changing one of the parts' geometry. For the final section, the undeformed part caused the whole model to be less stiff. For the final section, the undeformed part caused the whole model to be less stiff. As with the previous plot, a drastic change in the vertical displacement required to close contact is found, evident mainly on the first inflection point.

Moving forward, the next plot compares the pressure curves for welding point S.

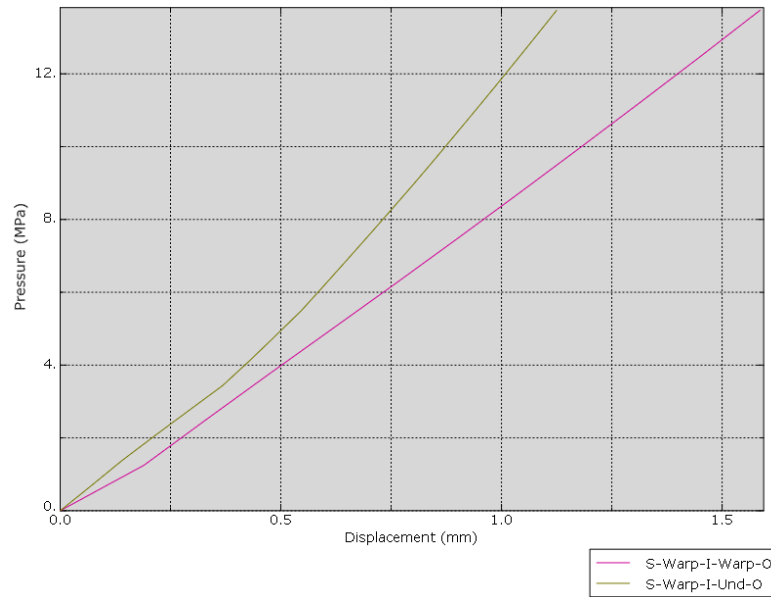


**Figure 6.15: Pressure-displacement comparing the base-case with 1st Case - point S**

Again, as it has been the case for welding point S where only sections are evident in the pressure curve, the use of an undeformed part affect the model in two ways: firstly, in the inflection point between the sections presented, and secondly, on the stiffness of model when SBO is involved. Both aspects are evident in the last plot, in which the inflection point is more pronounced in the light green plot and occurring later than the warped version. It represents that warpage of SBO cause contact with SBI to occur earlier. To finish our comparison, the next table is presented comparing the simulation time for the base-case and the 1<sup>st</sup> Case.



**Table 6.6: Comparison Simulation Time (1st Case-WIO)**

		Simulation time (hh:mm:ss)	
		Base-case	1 <sup>st</sup> Case (WIO)
Clamping Simulations	1 <sup>st</sup> -2 <sup>nd</sup> -3 <sup>rd</sup>	3:43:03	2:50:25
	4 <sup>th</sup> -5 <sup>th</sup>	4:29:11	1:26:32
	6 <sup>th</sup> -7 <sup>th</sup>	3:15:18	2:48:16
Welding Point	A	1:39:04	0:55:41
	AA	1:14:53	1:35:08
	S	1:02:55	0:46:00

Most of the simulations had the time required reduced, with exception of welding point AA. Then, the next step is to change SBI only, substituting the warped part for the undeformed version. The next plot pictures the effect on welding point A.

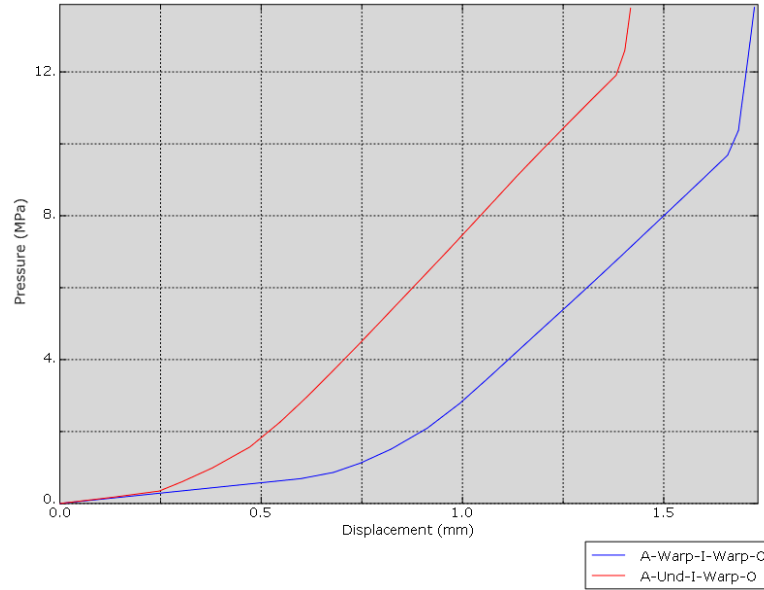


**Figure 6.16: Pressure-displacement comparing the base-case with 2nd Case - point**

**A**

The last plot comparison shows the effect when we act on the SBI geometry. Using an undeformed version of SBI, the model's stiffness was almost not changed but it directly influenced the inflection point where the contact between parts occurs. Since any other factor (clamping positions, for example), the change can be inferred to be a result of geometry. Some influence was expected in the second section, in which the stiffness of SBI and SBO is combined. As it can be seen, the combined stiffness increases. Finally, when the gap is closed, and compression starts to take place, both parts are compressed through the combined thickness, and the resulting stiffness does not seem to change, being an expected result since this section is influenced directly by material properties.

The next plot compares the pressure curves for welding point AA for the second case.

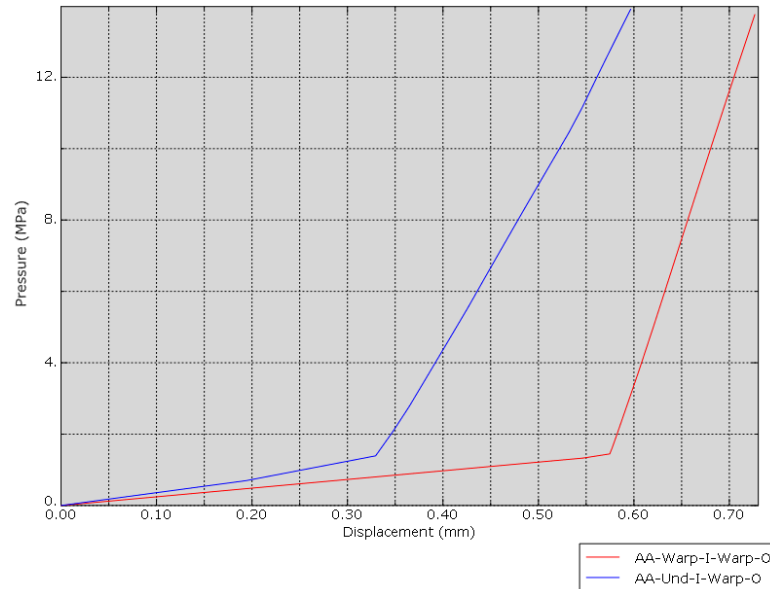


**Figure 6.17: Pressure-displacement comparing the base-case with 2nd Case - point AA**

The last effects pointed previously are seen here as well. The displacement required to close the contact between SBI and SBO is changed. However, for welding point AA, contradicting what was seen for welding point A, the stiffness was decreased for the compression section (third). It happened for the individual movement of SBI an increase of the stiffness. Since we did not change the geometry of SBO, the same behaviour in the collapse of the second section is expected because both contacts should happen at the same time. Once the SBI contact it, SBO is too close to the fixture causing the contact between SBO and fixture to occur.

Moving forward, the next plot compares the pressure curves for welding point S for the second case.

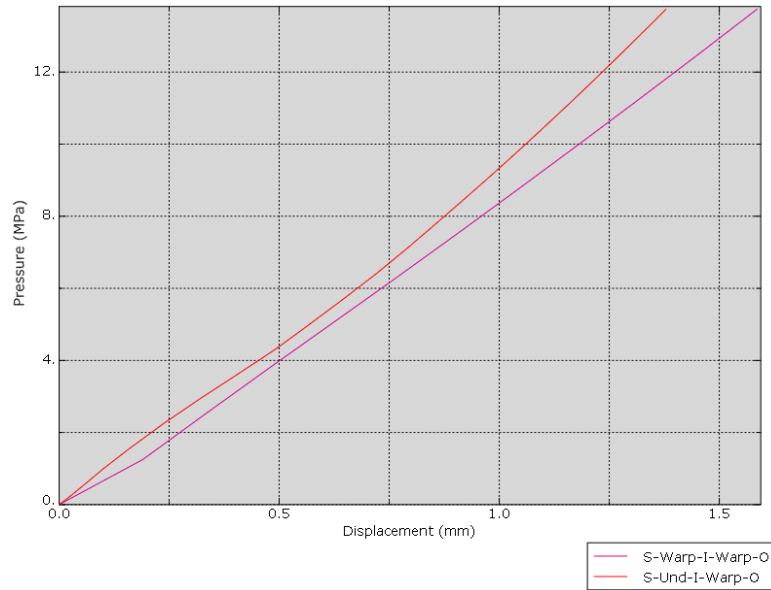


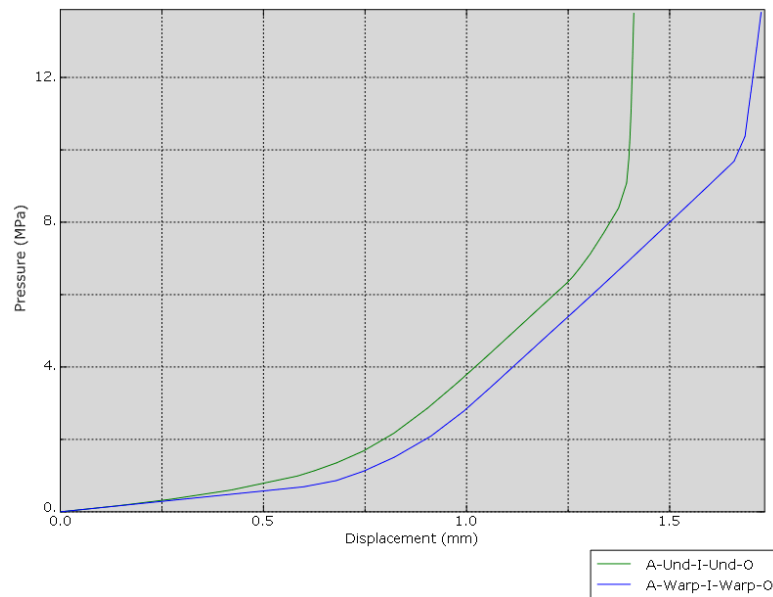
**Figure 6.18: Pressure-displacement comparing the base-case with 2nd Case - point S**

Again, the inflection points between the sections presented are different between curves. Initially, the second sections seem to be parallel, but the final portion of the curve reveals the existing difference. For point S, the stiffness on these sections was increased when using an undeformed part. To finish our comparison, we present the next table comparing the simulation time for the base-case and the 2<sup>nd</sup> Case.

**Table 6.7: Comparison Simulation Time (2nd Case-IWO)**

		Simulation time (hh:mm:ss)	
		Base-case	2 <sup>nd</sup> Case (IWO)
Clamping Simulations	1 <sup>st</sup> -2 <sup>nd</sup> -3 <sup>rd</sup>	3:43:03	4:20:56
	4 <sup>th</sup> -5 <sup>th</sup>	4:29:11	1:56:24
	6 <sup>th</sup> -7 <sup>th</sup>	3:15:18	3:40:07
Welding Point	A	1:39:04	1:22:39
	AA	1:14:53	1:06:34
	S	1:02:55	1:09:39

Here, it is not possible to find a consistency among these simulations. Finally, we move into the change of SBI and SBO, substituting both warped parts for the undeformed versions. The next plot pictures the effect on welding point A.

**Figure 6.19: Pressure-displacement comparing the base-case with 3rd Case - point A**

Again, the undeformed model produced a curve stiffer in its first section, when only SBI influences the slope. Once the inflection point occurs (first contact), the stiffnesses are much more similar, producing parallel lines. As expected, there is a change in the displacement required to close the whole gap. It becomes evident on the second inflection point. Finally, the model produced with undeformed parts presents a stiffer pair under compression locally at A.

The next plot compares the pressure curves for welding point AA for the third case.

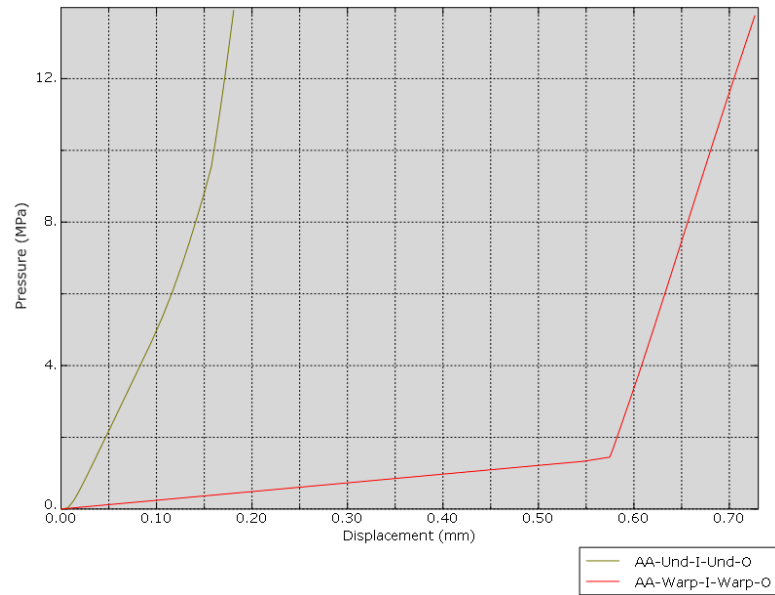


**Figure 6.20: Pressure-displacement comparing the base-case with 3rd Case - point AA**

When both parts used are as-designed, the displacement required to close the gap is drastically decreased. Consequently, the force applied closes the gap rapidly, and it is visible the resulting stiffness in the process. Similar to the welding point A, all sections present stiffer behaviour for the undeformed pair.

Moving forward, the next plot compares the pressure curves for welding point S for the third case.

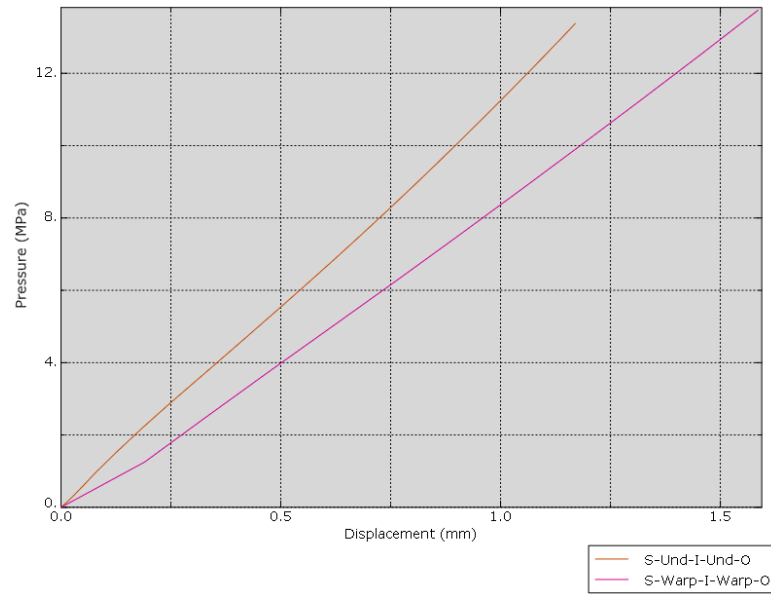


**Figure 6.21: Pressure-displacement comparing the base-case with 3rd Case - point S**

With both parts not deformed, the stiffness for all sections increased, and the same as in all other cases for welding point S, it was not possible to close the gap at this location. To finish our comparison, we present the next table comparing the simulation time for the base-case and the 3<sup>rd</sup> Case.

**Table 6.8: Comparison Simulation Time (3rd Case-IO)**

		Simulation time (hh:mm:ss)	
		Base-case	3 <sup>rd</sup> Case (IO)
Clamping Simulations	1 <sup>st</sup> -2 <sup>nd</sup> -3 <sup>rd</sup>	3:43:03	5:09:57
	4 <sup>th</sup> -5 <sup>th</sup>	4:29:11	2:10:54
	6 <sup>th</sup> -7 <sup>th</sup>	3:15:18	4:13:16
Welding Point	A	1:39:04	1:43:25
	AA	1:14:53	1:47:12
	S	1:02:55	0:53:47

It possible to note that, when involving parts not deformed, the time required drastically increases in the first three clamps. Once this step is concluded, the following times start to decrease.

In summary, the partial conclusions draw only by the use of warped and not warped parts are:

1. Even though we did not change material properties, every curve section influenced by some undeformed part the slope increased, behaving as a stiffer material;
2. The use of undeformed parts changed the displacement required for contacts to happen or gap closure;
3. The "collapse" of the second section for the pressure curve in welding point AA became evident. On the base-case, it was not possible to detect the sharp transition. Changing the SBO made it possible to see that the contact between SBI and SBO occurs simultaneously when the gap between SBO and fixture is closed.



This section altered which warped and not warped were used, trying to visualize which sections of the pressure-displacement curve would be affected by it. The next section alters the clamping pattern, with the same objective. It tries to make evident the stiffness induced by the adopted clamping boundary condition.

## 6.5 Change in Clamping Pattern

Regarding clamping pattern, we suggested two new patterns intending to assess how the clamping boundary conditions interfere with the whole model stiffness. The next figure pictures the new position where the clamps are applied.

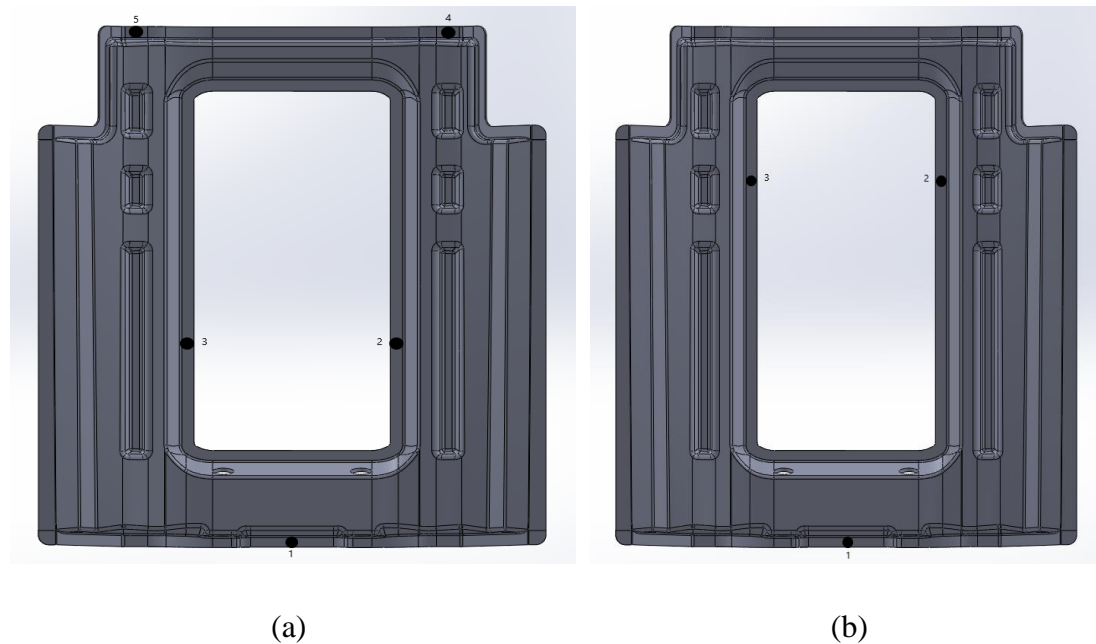


**Figure 6.22: New Clamping Patterns: (a) 5 clamps, (b) 3 clamps**

By removing clamps and altering the position of some of them in the second clamping pattern, we expect to interfere in the aspect of pressure curves for welding points A and AA. We still expect to cause some interference in the behaviour for welding point S. The initial comparison plots will help us to assess how much the clamping boundary conditions affect the pressure detected at welding points. Besides that, we will not be

comparing the second pattern with experimental data since the experimental data uses seven clamps, being not that relevant.

Initially, we superposed the curves for point A, comparing the original clamping pattern with the 5-clamp pattern.

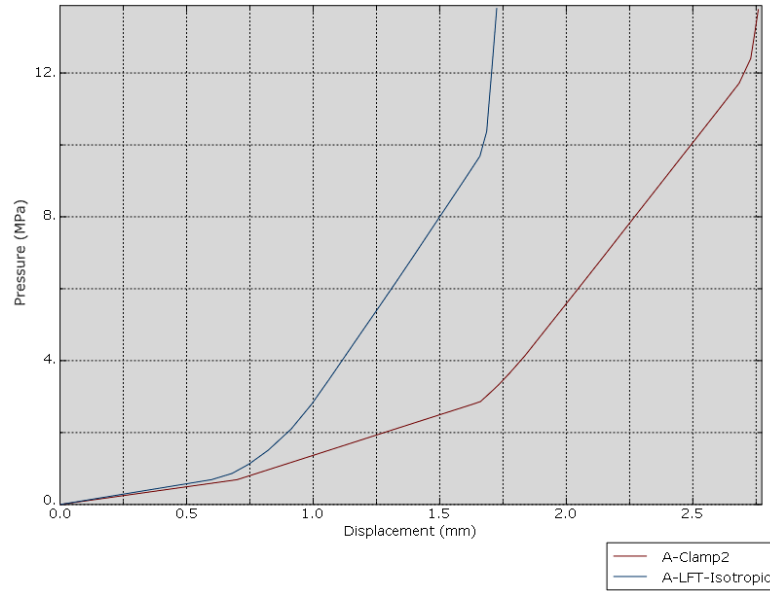


**Figure 6.23: Pressure-displacement plot comparing LFT-Isotropic (base-case) with 2nd clamping pattern – point A**

The most striking feature is the apparent four sections in the new clamping pattern curve. The reason for that was the time increment on the first step. For being excessive for a smooth initial line, it caused an inflection point to be formed, and the SBI movement altered. A solution to such behaviour is to reduce the initial time increment, allowing the SBI to receive the force which acts upon it without drastic increases. Analytically, we can interpolate all increments, up to the second inflection point, producing a more representative line.

Besides that, we note an increase in the total gap. The gap is closed between 1.5-1.75 mm for the standard clamping pattern, whereas, for the 5-clamp pattern, it is closed with 2.75mm. It shows us that applying clamps on the internal flanges combined with the removal of one clamp causes the external flanges to rise, increasing the distance required

to close gaps. Additionally, since the clamping boundary conditions are more distant to the welding point in the second pattern, there is a reduction in the model's whole stiffness in the second section of the curve, even though we did not alter the material used. This last conclusion shows how the relative position between clamps and welding points interferes with the stiffness detected on pressure-displacement graphs, mainly in the first and second section of the curve, but not in the third section when material compression takes place.

We produced the following plot comparing the base-case with the second clamping pattern moving forward to welding point AA.

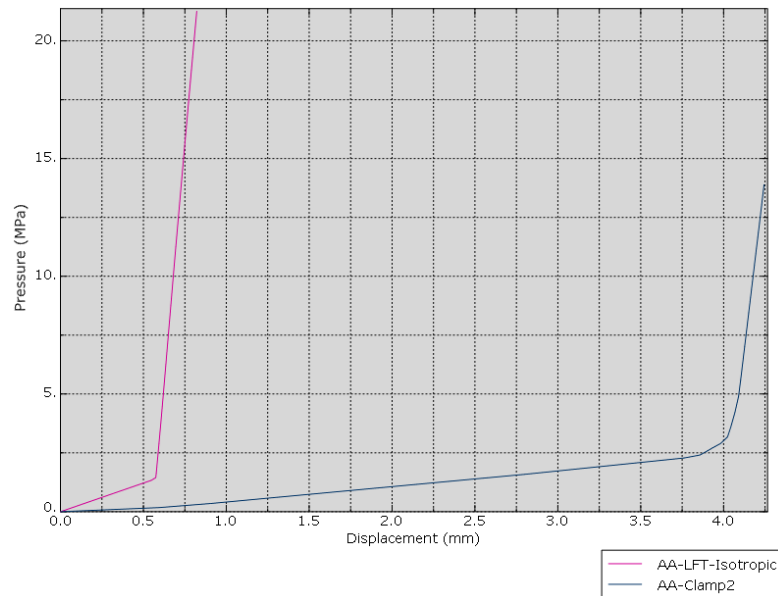


**Figure 6.24: Pressure-displacement plot comparing LFT-Isotropic (base-case) with 2nd clamping pattern – point AA**

In the last plot, our previous observation became even more evident. The fact of having applied clamps in internal flanges rose the external flanges, increasing the distance required to close the total gap at AA. Not only that, the combined effect of removal of close clamps (clamps BC's) and making the relative position greater caused the whole model stiffness to decrease in the first and second sections, producing curves with less inclined slopes even without material change. Additionally, in the changed pattern, it becomes clearer the three sections of the pressure curve. The second section (SBI + SBO

movement) collapsed on the original curve, resulting in a two-section curve because the gap between SBO and fixture is not big enough to be registered in the standard setup.

We expected that the third section of the curve (material compression) could be influenced by nearby clamping boundary conditions and material properties. This last comparison shows that the clamping BC's does not heavily influence the final section but represents a noise included in previous sections in the same curve.

We proceed to the following plot comparing the base-case with the second clamping pattern at the welding point S.

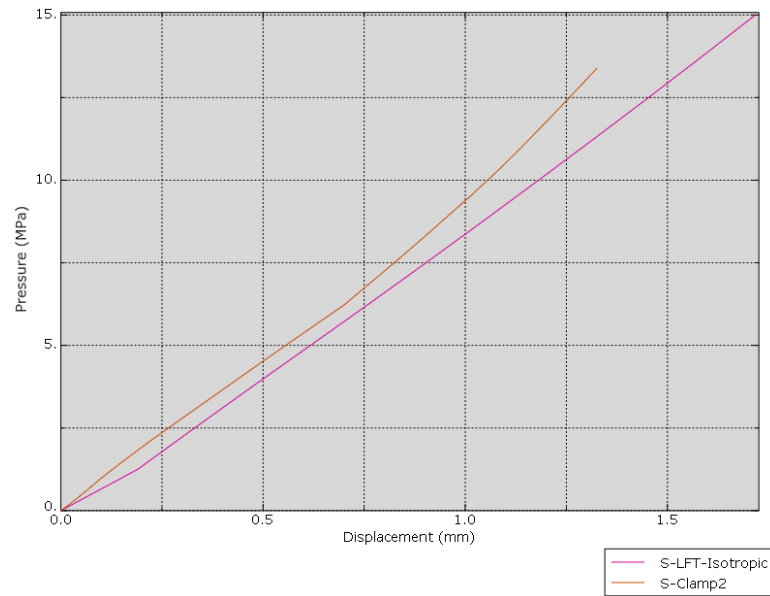


**Figure 6.25: Pressure-displacement plot comparing LFT-Isotropic (base-case) with 2nd clamping pattern – point S**

We would not expect much change between curves in the last plot since the second clamping pattern did not alter the welding point's clamps. With the reduction of clamping BC's, it would be counter-intuitive to expect an increase in whole model stiffness. The previous figure confirms the first suspicion and hit us as well with the prospect of a counter-intuitive result. We could detect an increase in the slope representing a resulting stiffer model. Consequently, since the curve at this location presents only the first two sections, its behaviour is more influenced by stiffness induced by clamping BC's.

Additionally, since we kept the same amount of force acting over the same area and the second pattern being even stiffer, the new pattern did not allow the gap closure at S too.

Now, we move forward comparing the third clamping pattern with the original one and the second pattern. The next figure brings the comparison between the third pattern (3-clamp) with the first one while welding point A.

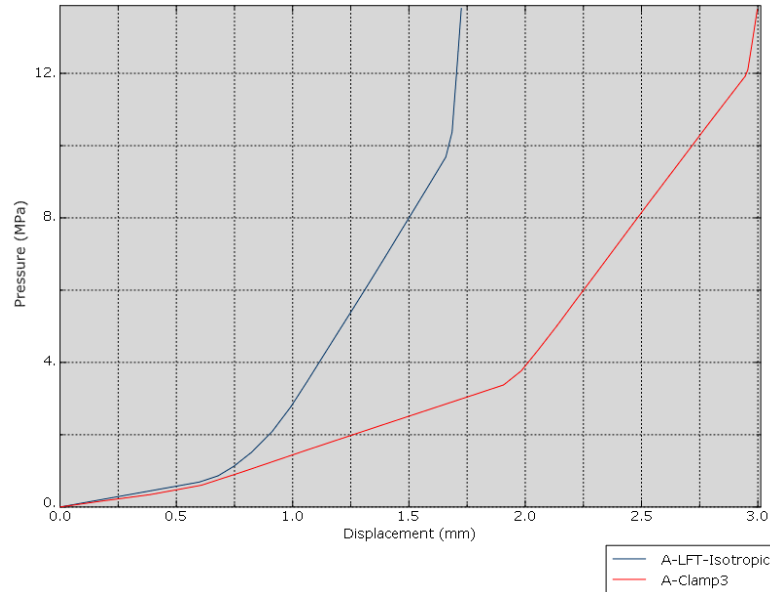


**Figure 6.26: Pressure-displacement plot comparing LFT-Isotropic (base-case) with 3rd clamping pattern – point A**

Again, the apparent fourth section in the new clamping pattern curve shows up. The reason for that is the same as presented before, the time increment on the first step. Additionally, we note an increase in the total gap. The gap is closed between 1.5-1.75 mm for the standard clamping pattern, whereas, for the 3-clamp pattern, it is closed almost 3.0mm. In this simulation, we confirm the previous observation that the change in clamping position to the internal flange causes the external flange to rise. The last plot still presents a reduction in the model's whole stiffness in the second section of the curve, even though we did not alter its material, showing the effect of change of clamping BC's mainly on the initial sections of the curve.

Next, we produced a comparing plot the second and third clamping patterns moving at the same welding point A.

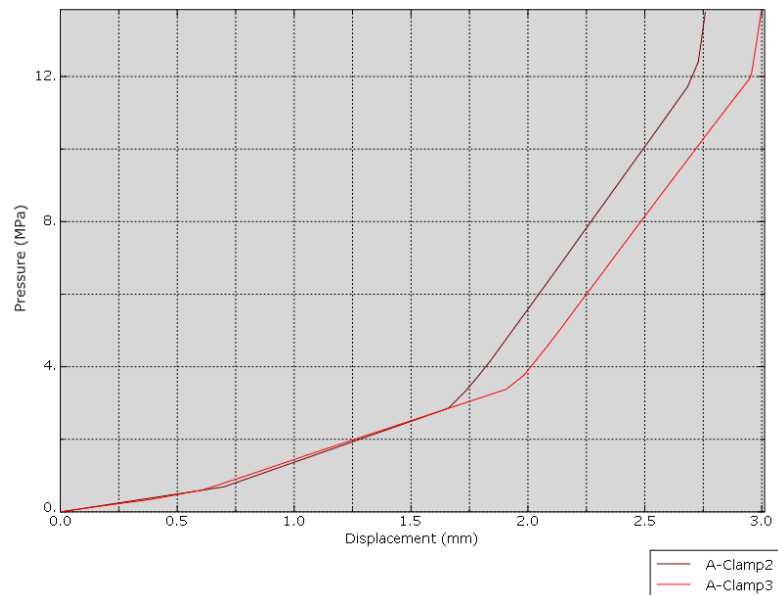


**Figure 6.27: Pressure-displacement plot comparing 2nd with 3rd clamping patterns – point A**

We can note the difference in the transition from the first section to the second section representing how the gap between SBI and fixture is increased from the second to third clamping pattern. This change seems to shift the whole curve sideways since the whole stiffness is almost kept the same. We can conclude the first alteration in the clamping caused the main change in the stiffness of the model.

We move forward comparing the third clamping pattern with the original one and the second pattern. The next figure brings the comparison between the third pattern (3-clamp) with the first one while welding point AA.

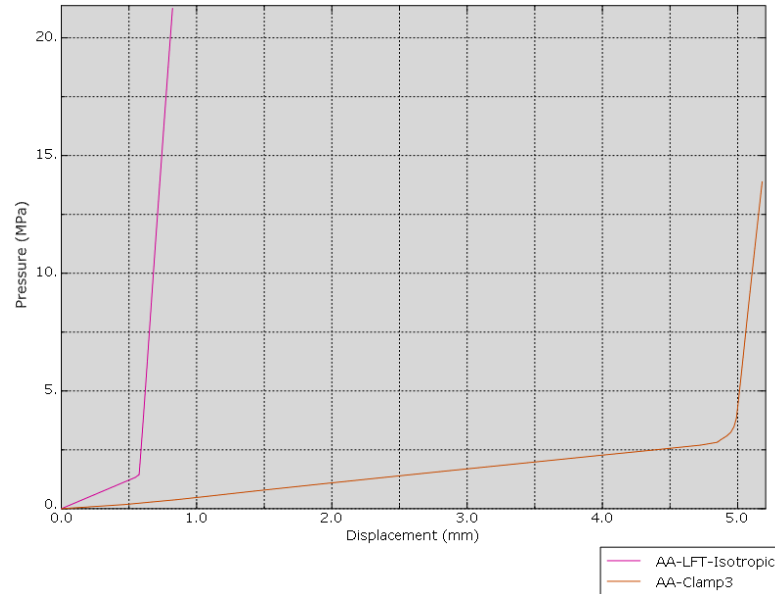


**Figure 6.28: Pressure-displacement plot comparing LFT-Isotropic (base-case) with 3rd clamping pattern – point AA**

The first observation is the huge difference for the gap closure, mainly because of the external flange being moved upward due to internal clamping. In terms of model stiffness, the first section is less stiff for the 3-clamps than for the base-case, making evident the clamping BC's influence in the whole model stiffness. The only section in which the change of clamping pattern does not seem to affect the third section (compression).

Comparing then the plot the second and third clamping patterns at the same welding point AA.

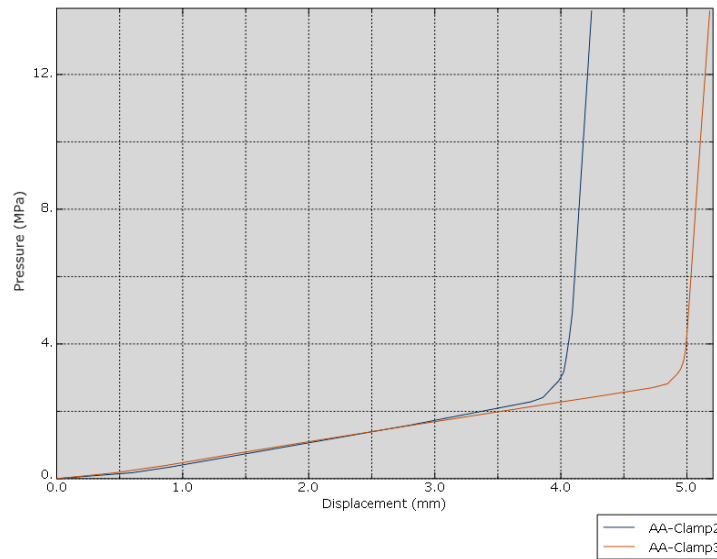


**Figure 6.29: Pressure-displacement plot comparing 2nd with 3rd clamping patterns  
– point AA**

The last plot pictures that further changes in the clamping pattern, reducing from five to three clamps, does not induce any additional change regarding model stiffness. However, the displacement required to close the gap between SBI and fixture increases as we reduce the number of clamps and their positions.

Finally, comparing the pressure plots between the original clamping pattern and the third one at welding point S.



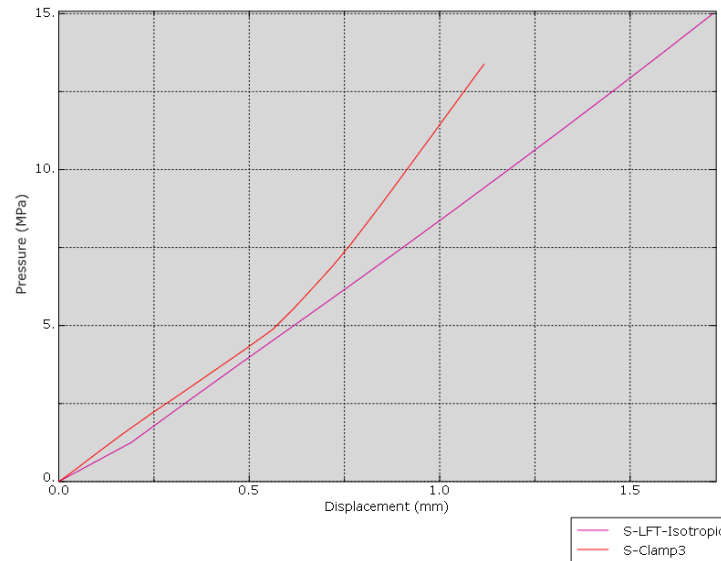


**Figure 6.30: Pressure-displacement plot comparing LFT-Isotropic (base-case) with 3rd clamping pattern – point S**

In the third clamping pattern, we finally moved the clamping points to the internal flange in a way that the welding point S is not between them. The conclusion is that the way the pattern was changed, we actually induced a stiffer model. Since the only sections presented are the first two, they are the most affected by the change of clamping BC's.

Then, we compare the plot for the second and third clamping patterns at the same welding point S.

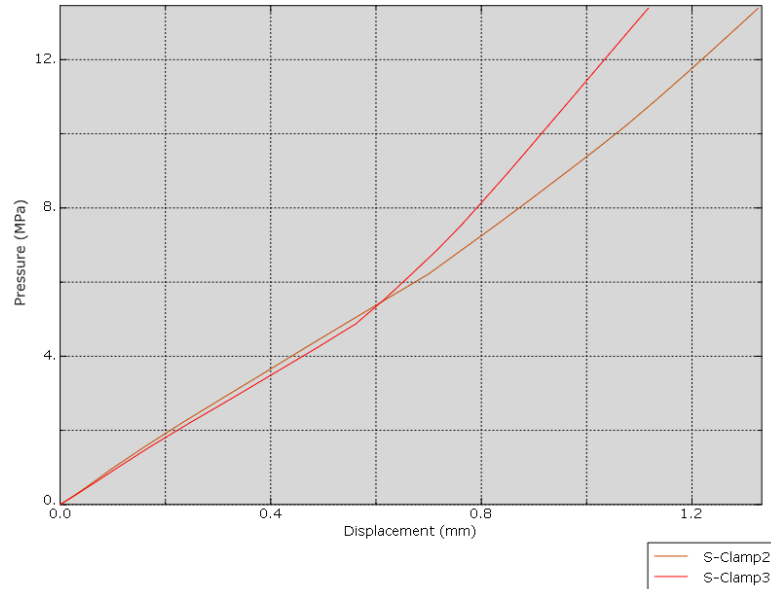


**Figure 6.31: Pressure-displacement plot comparing 2nd with 3rd clamping patterns – point S**

It makes evident the conclusion drawn in the last comparison, increasing the whole model stiffness by the change of clamping positions. It consequently shows that, for the upper flange (point S), the whole model stiffness increases by moving the clamps to the internal clamp. The change does not affect the first section of the curve (SBI only); however, it affects the second section (SBI and SBO movement).

In summary, the partial conclusions draw only by changing the clamping pattern are:

1. The drastic change promoted at welding points A and AA showed us that we have at least two factors influencing the whole model stiffness: material properties and clamping BC's (effected by relative position between clamping point and welding point);
2. The clamping BC's factor influences the first two sections of the pressure-displacement curve, namely, in the movement of SBI only and the combined movement of SBI and SBO;
3. Since the third sections of all curve (when reached) were visually parallel, then it is estimated a small influence of the clamping BC's in the stiffness of the model, once it reaches this stage;

4. Even with a considerable relative distance between welding point S and clamps altered, a stiffer model can be produced by removing clamps, being a counter-intuitive result;
5. The resultant stiffness is reduced for welding points on lateral flanges by clamping the internal flange while it increases for welding points on the upper flange.

In this section, it was possible to see the influence of the clamping boundary condition on the pressure curve: how the proximity with the welding points and the number of clamps influence the stiffness at the welding point.

## **6.6 Chapter Summary**

In this chapter, the parametric study was conducted in the digital interface, varying three parameters mainly (materials, warped parts, clamping pattern). The influence of each of these parameters was analyzed using the resulting pressure-displacement curves. The conclusions drawn in this section will outline the conclusions of this work.

## Chapter 7 : Conclusion and Future Work

### 7.1 Conclusions

Initially, we discussed which types of elements were available in Abaqus<sup>TM</sup> and what they produced when used in the simulation. The output required and the contact between parts limited the use of tetrahedral elements in their regular formulation.

Later on, a mapping method for the warpage was described, using the warpage pattern extracted through scanning and producing warped meshes. It was presented a cumbersome step necessary to select nodes manually from the CAD-mesh. However, once such a step was done and a proper set of nodes is established, the warping simulation was rapidly concluded as was presented in Chapter 2. Quantitatively, a relatively small number of nodes was selected, producing warped meshes that reached initial tolerance.

Regarding the pre-welding stage (clamping), boundary conditions were suggested and used with the data available. The case was to use vertical displacement at the clamping locations. This written work presented stresses at these locations. Using the same simulation proposed and changing output requests in Abaqus<sup>TM</sup>, it is possible to assess the amount of force applied at each location.

The welding simulations were then performed at different locations, measuring the pressure applied as a function of the local displacement. On this correlation, three sections were identified directly related to three various movements happening: i) SBI only, ii) SBI and SBO combined, and iii) SBI and SBO compression. Such behaviour was expected; however, two main issues showed up:

1. When comparing the pressure-displacement experimental data, all sections presented a stiffer model than the real assembly;
2. At some locations, not all curve sections were evident.

Consequently, it was decided to investigate what was causing these. At this point, the parametric study was suggested, altering three possible parameters: i) materials each part was made from, ii) warped and not warped parts, and iii) clamping pattern. The material change tried to decrease and increase the whole model stiffness to see another factor influencing the slopes of pressure-displacement curves. The use of not warped parts tried to change the vertical displacement required to close gaps to influence the moment of contact, to identify better contact points and curve sections. The clamping pattern change tried to detect clamping BC's influence on the whole model stiffness.

As shown, the conclusions extracted from the parametric study were:

1. It was noted that the experimental data is placed between the isotropic and anisotropic materials in terms of stiffness. It became evident the behaviour during contact at welding locations where the pressure-displacement curve was originally assumed incomplete;
2. By using undeformed parts, it was possible to note stiffer models and confirm the section of the same curve, not evident otherwise;
3. By changing the position of clamping BC's, it was possible to note that those BC's (locking vertical displacement) play some role during SBI and SBO movement while welding.

However, it was chosen not to quantify such effect of boundary conditions. Instead, it seems better to alter the BC's applied during the clamping simulations on later works. The next section presents possible modifications or lines of investigation for further developments to reach the objective to measure the pressure (force) required to close gaps right before welding.

## 7.2 Future Work

In terms of the elements used to mesh the parts, it was possible to mesh them with tetrahedral elements during our investigation. Not much time was available to discuss and compare the effect when meshing using a different element, for example, wedges or hexahedra. Thus, it may represent a relevant line of investigation. In terms of the warping field and warping simulations, at a later stage, it was possible to identify that such a method can represent a good avenue to assess, digitally, how warped each part is using energy as a comparison parameter. Potentially, it may be used as a metric to assess the warpage of non-conventional parts, for example, by measuring the external energy required to deform a CAD geometry into a warped part.

A difficulty found for clamping and welding simulations was selecting the area on which the boundary condition was going to be applied. For consistency and comparison reasons, it is advisable to determine split regions to be further used on those occasions, either for clamps or welding locations. In terms of the welding simulation and creation of pressure-displacement curves, an obstacle was found to select a proper area on which the total force was to be applied because the area of elements selected was not controllable. An option was made to select these areas keeping the geometric symmetry. A further improvement would be to keep the geometric symmetry at the same time guarantee the consistency of the area selected. Hence, before even meshing the original CAD file, split lines should be added in the healed geometry.

Deeper in the clamping simulations, it was noted how the locking of the vertical displacement at a final position interferes with the stiffness of the whole model. An alternative way to define clamping BC's would be to determine pressure (force) during clamping experimentally. Such data was not available when the simulations presented started, but it can be in the future if it is interesting to pursue this line of thought.

Finally, it was noted that only one warping pattern was used throughout this thesis. If the influence of the pressure (force) required to welding parts is analyzed, new warping

patterns should be used either between parts of the same batch or between parts belonging to different batches.

## References

- [1] Mallick, P.K: Materials, design and manufacturing for lightweight vehicles, Woodhead Publishing, 2010.
- [2] Song, Y.; Gandhi, U.; Koziel, A.: Effect of the initial fiber alignment on the mechanical properties for GMT composite materials. *Journal of Thermoplastic Composite Materials*, Volume 31, Issue 1, 91-109.
- [3] Ketabchi, M. R.; Khalid, M.; Hoque, M. E.: Critical concerns on Manufacturing Processes of Natural Fibre Reinforced Polymer Composites, Chapter 6.
- [4] Kalas, V. J.; Roos, L.: Welding of thermoplastic composites. Faculty of Engineering Technologies (CTW), University of Twente.
- [5] Young, S. S.; Youn, J. R.; Gutowski, T. G.: Life cycle energy analysis of fiber-reinforced composites. *Composites Part A: Applied Science and Manufacturing*, Volume 40, Issue 8, August 2008, 1257-1265.
- [6] Rajak, D.K.; Pagar, D.D.; Menezes, P.L.; Linul, E: Fiber-Reinforced Polymer Composites: Manufacturing, Properties, and Applications. *Polymers* 2019, 11, 1667.
- [7] Song, Y.; Gandhi, U. et al: Method to account for the fiber orientation of the initial charge on the fiber orientation of finished part in compression molding simulation. *Composites Part A: Applied Science and Manufacturing*, Volume 100, September 2017, 244-254.
- [8] Villegas, I. F.: In situ monitoring of ultrasonic welding of thermoplastic composites through power and displacement data. *Journal of Thermoplastic Composite Materials*, Volume 28, Issue 1, 66-85.
- [9] Cifuentes, A. O.; Kalbag, A.: A performance study of tetrahedral and hexahedral elements in 3D finite element structural analysis. *Finite elements in Analysis and Design*, Volume 12, Issues 3-4, December 1992, 313-318.



- [10] Danielson, K. T.: Fifteen node tetrahedral elements for explicit methods in nonlinear solid dynamics. *Computer Methods in Applied Mechanics and Engineering*, Volume 272, April 2014, 160-180.
- [11] Kaick, O.; Zhang, H.; Hamarneh, G.; Cohen-Or, D.: A survey on shape Correspondence. *Computer Graphics Forum*, Volume 30, Issue 6, September 2011, 1681-1707.
- [12] Dassault Systèmes (2010). *Abaqus Analysis User's Manual*. Providence, RI, USA, 32.3.1-32.3.5.
- [13] Boulbes, R.J.: *Troubleshooting Finite-Element Modeling with Abaqus*. Springer 2019.
- [14] Dassault Systèmes (2016). *Abaqus Theory Guide*. Providence, RI, USA, Section 5 – Interface Modeling.
- [15] Nicolini, M.: Method development for measuring assembly forces during the joining of LFT-D components. *Karlsruher Institute of Technology (KIT)*. April 2020.

## Appendices

### Appendix A: Mid-surface Meshing Method

#### *Mid-surface Simplification*

The mid-surface simplification uses both the upper surface and the bottom surface of the CAD model to define a middle surface, capturing all geometrical features of the original model. This middle surface is used as a base to determine wedge elements during the meshing process. However, the main limitation of this process occurs when dealing with models of varying thickness. When that is the case, the middle surface defined does not properly capture the geometrical features because of non-constant thickness.

Consequently, when the method is carried further and the mesh is produced, severe disagreements are visualized at each corner connecting two regions with different thicknesses. The next figure presents an example of a cross-section extracted in HyperMesh™, evidencing disagreements.



**A 1: Cross section of mid-surface meshing method**

### Appendix B: Top-surface Meshing Method

#### *Top-surface Simplification*

The top-surface meshing method is similar to the previous one. Instead of the middle section, the top surface is used as a base to determine wedge elements during the meshing process. Alternatively, the bottom surface can also be used in the meshing process. In

both cases, disagreements and connectivity problems occur between elements because of varying thickness.

## Appendix C: MATLAB scripts

This section presents scripts produced in MATLAB in the warping simulation, adding some comments about functions employed in them.

### *C.1 - TxtWork.m script*

```
clear; clc;
```

```
fidi = fopen('SBI-wGroup.txt','r');
```

```
Datac = textscan(fidi,'%f %f %f %f', 'HeaderLines',12, 'CollectOutput',1,'Delimiter','');
```

```
Data = Datac{ 1};
```

```
filename = 'nodesMar10.xlsx';
```

```
writematrix(Data,filename,'Sheet',1,'Range','A1');
```

Comments:

- “fidi” receives the written content of the file SBI-wGroup.txt. Of course, the name of the file can be altered. Additionally, the opening of the file occurs only to read it;
- “textscan”, as the name suggests, scans the text file “fidi” applying some settings and excluding the header lines (in our case, 12 lines of the INP file). Additionally, “%f” sets the format of the numbers to be stored in ‘Datac’, namely, floating points (real numbers). Finally, ‘Datac’ stores nodes’ identification and respective coordinates;
- ‘filename’ creates an Excel file with the name chosen;
- ‘writematrix’, again as its name suggests, writes the table contained in Data (from ‘Datac’) in the ‘filename’. At the end, the file *nodesMar10.xlsx* will contain a

table in first sheet, starting at A1 cell, with all nodes' numbers and respective coordinates (4 columns).

### *C.2 - Nset.m script*

```
clear; clc;
```

```
fidi = fopen('NsetMar10.txt','r');
```

```
Datac = textscan(fidi,'%d %d %d %d %d %d %d %d', 'CollectOutput',1,'Delimiter',' ');
```

```
Data = Datac{1};
```

```
Nodeset = reshape(Data, [2176,1]);
```

```
filename = 'nodesMar10.xlsx';
```

```
writematrix(Nodeset,filename,'Sheet',2,'Range','A1');
```

Comments:

- “fidi” receives the written content of the file *NsetMar10.txt*. Specifically, *NsetMar10.txt* contains the nodes' number selected to belong to each group (x, y, and z). This file is 8-column text, delimited by commas;
- “textscan” scans the text file “fidi”. Accordingly, ‘%d’ sets the format of the numbers read to be stored in ‘Datac’, namely, integers. Finally, ‘Datac’ stores nodes' identification;
- ‘reshape’ function, as the name suggests, receives the ‘Data’ matrix and reshapes it in a new matrix with number of lines and columns chosen by the user. In the example, a matrix with 2176 lines and 1 column. ‘Nodeset’ receives the reshaped matrix;
- ‘writematrix’ writes the table contained in Data (from ‘Datac’) in the file *nodesMar10.xlsx* already created. At the end, the file *nodesMar10.xlsx* will contain a second table in the second sheet, starting at A1 cell, with all nodes' numbers from ‘Nodeset’ (1 column).

### C.3 - *CompCopy.m* script

```
clear; clc;

A = xlsread('nodesMar10.xlsx',1);

B = xlsread('nodesMar10.xlsx',2);

[i j] = size(B);

[m n] = size(A);

C = zeros(i,4);

for k=1:m

    for q=1:i

        if A(k,1)==B(q,1)

            C(q,:)=A(k,:);

        end

    end

end

filename = 'nodesMar10.xlsx';

writematrix(C,filename,'Sheet',2,'Range','A1');

Comments:
```

- “A” and “B” receive the tables of the file *nodesMar10.xlsx*. Specifically, “A” receives a 4-column matrix (all nodes of the mesh and respective coordinates) and “B” receives a 1-column matrix (only nodes’ number of nodes contained in the groups defined);

- The ‘for’ loop makes a comparison between lines of both matrices. Every time a node number in “B” is found in the first column of “A”, the whole line of “A” is copied in “C”. At the end, “C” will be stored, in the second sheet of *nodesMar10.xlsx*, as a 4-column matrix of nodes contained in the initial group of nodes (nodes’ numbers and respective coordinates).

#### *C.4 - WriteNset.m script*

```
clear; clc;
```

```
A = xlsread(nodesMar10.xlsx',2);
```

```
[n m] = size(A);
```

```
fid = fopen('Nset.txt','wt');
```

```
fprintf(fid,'%d, %4.6f, %4.6f, %4.6f\n',A);
```

```
fclose(fid);
```

Comments:

- “A” receive the second table of *nodesMar10.xlsx* (only nodes’ number of nodes contained in the group defined);
- ‘fid’ opens and creates a new text file which will further write the 4-column matrix (group only) to be used in Polyworks™;
- ‘fprintf’ writes the matrix “A” in the proper text format.

#### *C.5 - BcWrite.m script*

```
clear; clc;
```

```
A = xlsread('20200330-Workflow.xlsx',1);
```

```
[n m] = size(A);
```

```
for i=1:n
```

```

J(i)=i;

Set(i) = A(i,1);

X(i) = A(i,2);

end

FID = [J; Set];

FID2 = [J;J;X;J;Y;J;Z];

formatspec = '*Nset, nset=_PickedSet%d, internal, instance=Part-1-1\n %7d,\n';

fid = fopen('SetsMar30.txt','wt');

fprintf(fid,formatspec,FID);

fclose(fid);

```

```

formatspec2      =      '**      Name:      BC-%d      Type:
Displacement/Rotation\n*Boundary\n_PickedSet%d, 1, 1, %f\n_PickedSet%d, 2, 2,
%f\n_PickedSet%d, 3, 3, %f\n';

```

```

fid2 = fopen('BCMar30.txt','wt');

fprintf(fid,formatspec2,FID2);

fclose(fid);

```

Comments:

- “A” receive the table of *20200330-Workflow.xlsx* (2-column matrix: nodes’ number in the group defined and distance measured in PolyWorks™);
- The ‘for’ loop creates 3 separate columns matrices: J, a matrix ordering elements; Set, nodes’ number only; X, distance measured only (displacement);

- ‘FID’ and ‘FID2’ are used together with ‘formatspec’ and ‘formatspec2’. Each ‘formatspec’ specifies the text-format to be written agreeing with the INP text format. For that, there is a sequence of numbers to be included. Either ‘FID’ or ‘FID2’ contain the correct sequence. ‘FID’ writes for the *SetsMar30.txt*. ‘FID2’ writes for the *BCMar30.txt*.



## Curriculum Vitae

**Name:** Theogenes Maia

**Post-secondary Education and Degrees:** Military Institute of Engineering  
Rio de Janeiro, Rio de Janeiro, Brazil  
2008-2012 B.E.

The University of Western Ontario  
London, Ontario, Canada  
2018-Present M.E.Sc.

**Honours and Awards:** 3<sup>rd</sup> CREA-RJ Oscar Niemeyer Award for Scientific and Technological Works  
2013

Western Engineering Scholarship  
2019-2020

**Related Work Experience** Teaching Assistant  
The University of Western Ontario  
2019-2020

Research Assistant  
The University of Western Ontario  
2019-Present